AD-A265 390

・ｲ ‐

①

Fall Sem 1992   THESIS

Rainfall-Runoff Estimation Using Digital Radar

Captain Russell A. Kutzman

S DTIC
ELECTE
JUN 0 4 1993
A D

93 6 03 018

93-12507

100

RAINFALL-RUNOFF ESTIMATION USING DIGITAL RADAR

Name: Russell A. Kutzman
Department: Meteorology
Major Professor: Peter S. Ray, Ph.D.
Degree: Master of Science
Term Degree Awarded: Fall, 1992

Storm runoff is a critical concern to meteorologists and hydrological forecasters. A runoff algorithm, part of a series of tropical weather algorithms developed for the NEXRAD (Next Generation Weather Radar) radar system, is presented. The algorithm is based on the relationship between the rainfall over the basi. and the discharge response at the gauge station. The algorithm is designed to provide runoff as a function of time for a given input(s) of rainfall excess. With known overflow levels, flood potential can also be evaluated. The runoff algorithm examined outflow at five basins within the operating scope of the Pittsburgh National Weather Service (NWS) radar. A comparison of the actual runoff was made with the algorithm generated discharge. In general, hydrograph accuracies improved with increasing rainfall excess.

THE FLORIDA STATE UNIVERSITY

COLLEGE OF ARTS AND SCIENCES

RAINFALL-RUNOFF ESTIMATION
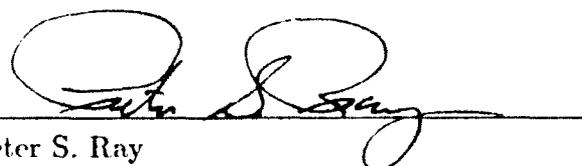# USING DIGITAL RADAR

by

RUSSELL A. KUTZMAN

A Thesis submitted to the Department
of Meteorology in partial fulfillment
of the requirements for the degree of
Master of Science

Degree Awarded:
Fall Semester, 1992

The members of the Committee approve the Thesis of Russell A. Kutzman defended on September 17, 1992.

Peter S. Ray
Professor Directing Thesis

Kevin A. Kloesel
Committee Member
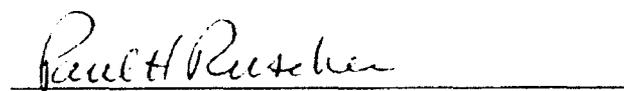
Paul H. Ruscher
Committee Member

I dedicate this to my wife, my strength and inspiration.

ACKNOWLEDGEMENTS

TABLE OF CONTENTS

LIST OF TABLES

LIST OF FIGURES

LIST OF SYMBOLS

A	cross-sectional area of flow
A	empirical constant
A_d	drainage area
D	rainfall duration
D	dropsize diameter
D_D	drainage density
Δh	difference in head
Δl	distance between measuring points
E	evaporation
F	field capacity of soil
G	antenna gain factor
K	constant
K	hydraulic conductivity
$|K|^2$	dielectric factor
L	lag to peak
L	total length of streams
N	number of drops
NWS	National Weather Service
P_e	accumulated rainfall excess
P_r	back-scattered power
P_t	power output
Q	rate of flow
Q	surface runoff
R	hydraulic radius
R	rainfall rate
$RADAP\ II$	radar data processor, version II
S	energy gradient
S_d	total depression storage capacity
S_D	soil moisture deficiency
T_b	time base

T_R	time of rise
V	average velocity
V_s	depression storage
V_t	terminal velocity
Z	reflectivity factor
a	empirical constant
b	empirical constant
e_a	vapor pressure above the water surface
e_o	vapor pressure at the water surface
f	infiltration rate
f_c	steady state infiltration rate
f_o	initial infiltration rate
h	pulse length
h	response function
i	rainfall intensity
λ	radar wavelength
n	Manning resistance coefficient
r	distance to target
t	time
θ	beamwidth of antenna
u	wind speed
u	mean flow velocity
w	width of flow
x	length of flow
y	depth of flow

ABSTRACT

Storm runoff is a critical concern to meteorologists and hydrological forecasters. A runoff algorithm, part of a series of tropical weather algorithms developed for the NEXRAD (*Next Generation Weather Radar*) radar system, is presented. The algorithm is based on the relationship between the rainfall over the basin and the discharge response at the gauge station. The algorithm is designed to provide runoff as a function of time for a given input(s) of rainfall. With known overflow levels, flood potential can also be evaluated. The runoff algorithm examined outflow at five basins within the operating scope of the Pittsburgh National Weather Service (NWS) radar. A comparison of the observed runoff was made with the algorithm generated discharge. In general, hydrograph accuracies improved with increasing rainfall excess.

CHAPTER 1

INTRODUCTION

1. Prologue

Devastation and loss of life document the nature of floods. The impact is often magnified due to population centers being situated near water. As a result, the need for hydrological forecasting and flood control systems are necessary to minimize the effects of these natural disasters.

Over the past three decades, flood prediction studies centered around the modeling of runoff in watersheds. The advent of computer technology enabled researchers to approach this problem using several methods. Hydrological systems can be deterministic or stochastic, linear or nonlinear, time invariant or time dependent, lumped or distributed (Delleur and Rao, 1973).

The runoff algorithm inputs actual or forecasted reflectivities or precipitation accumulations and computes storm runoff as a function of time for each basin. With predetermined river threshold values, the algorithm also evaluates flood potential and the time the river's capacity will be exceeded. A forecast will be made at each basin within the operating range of the radar site. The runoff algorithm is just one of a series of Tropical Weather Hazard algorithms, each designed to estimate specific aspects of threatening hurricanes and typhoons.

1

2. Physical Overview

To fully understand the runoff process, all factors influencing the hydrological cycle must be considered. These are (1) precipitation, (2) interception, (3) infiltration, (4) evaporation, (5) transpiration, (6) groundwater flow, (7) surface runoff and (8) channel flow.

a. Hydrological Cycle and Its Role in Storm Runoff

The hydrological cycle is a continuous process describing the ways in which water moves within, on, and above the earth's surface. Surface runoff is just one component of the hydrological cycle. The movement of water through various phases of the hydrological cycle is erratic in time and space, giving rise to extremes of floods or drought (Bedient and Huber, 1988). If elementary assumptions are made about the hydrological cycle, surface runoff at a basin can be estimated from the rainfall rate. Figure 1.1 shows a schematic diagram of the hydrological cycle.
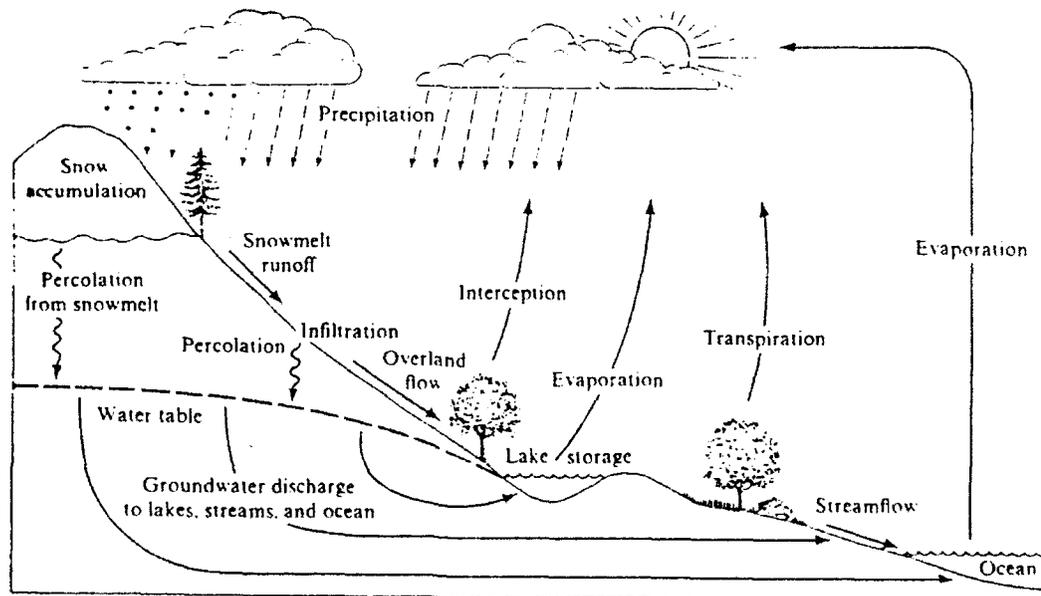
FIG. 1.1.   Schematic diagram of the hydrological cycle (Dunne and Leopold, 1978).

1) PRECIPITATION

Precipitation is considered the controlling input to the hydrological cycle and is the major cause of floods. Whether in the form of rain, snow, or hail, it is derived from atmospheric moisture. The moisture must undergo lifting and resultant cooling, condensation, and growth before precipitation can occur. Precipitation is often classified according to conditions that generate vertical air motions: (1) convective, due to intense heating of air at the ground; (2) cyclonic, associated with the movement of large air mass systems; and (3) orographic, due to mechanical lifting of moist air masses over mountain ranges (Bedient and Huber, 1988).

Flooding most often results from precipitation events of high intensity or long duration or a combination of both. Rainfall intensity has a direct bearing on runoff since once the infiltration capacity is exceeded all the excess rain is available and flows to the surface water-courses. Because intensity represents, depth/time, it cannot be considered separately from duration. The same depth of rainfall delivered over two different durations will produce different runoff rates (Wilson, 1990).

2) INTERCEPTION

When precipitation finally reaches the surface, it will either be retained where it falls, pass through the soil surface as infiltration or find its way into channel flow as surface runoff (Linsley *et al.*, 1949). Interception by vegetal cover constitutes the first loss to the total precipitation budget. The quantity of interception depends on the characteristics of the precipitation and the nature of the cover (Dunne and Leopold, 1978). The effect of vegetal cover in reducing the amount of precipitation reaching the ground is usually insignificant in studies of major floods. However, areas where storms yield only small amounts of precipitation, interception by forest or dense cover commonly amounts to 25 percent of the annual precipitation (Linsley *et al.*, 1949).

Net interception can be measured by subtracting the net rainfall entering the soil from the total gross rain. Several studies by Patric (1965) and Leyton *et al.* (1967) examined the interception of deciduous and coniferous trees (see Table 1.1). They noted that conifers have more mass or needle surface and therefore can hold a greater amount of water. In addition, the broad leaf form of the hardwood trees tend to cause the tiny drops to merge and form larger ones which will eventually drop off.

TABLE 1.1.   Median values of canopy interception as a percentage of annual or seasonal gross precipitation. Data from Helvey and Patric (1964), Patric (1966), and Rogerson and Byrnes (1968).

FOREST TYPE	NUMBER OF EVENTS	CANOPY INTERCEPTION (% OF PRECIPITATION)
Deciduous forest	10	13
Coniferous forest		
Rainfall only	11	22
Rain and snow	26	28
European data	9	35
North American data	27	27

3) INFILTRATION

Infiltration is the next process to reduce the amount of water available to surface runoff. Horton (1933) defined infiltration as the passage of water through the soil surface into the soil. He stated that there is a maximum rate at which the soil in a given condition can absorb water; this upper limit is known as the infiltration capacity. Horton developed an empirical relationship

$$f = f_c + (f_o - f_c)e^{-Kt} \ ,$$
(1.1)

in which f is the infiltration rate, f_c is the ultimate or steady state, f_o is the high initial rate, K is a constant, and t is the time elapsed since the beginning of the rain.

Different types of soil allow water to infiltrate at different rates. Rain falling on a gravelly or sandy soil will rapidly infiltrate and, provided the saturation zone is below ground surface, even heavy rain will not produce surface runoff. Similarly soil with a large clay content will resist infiltration and the surface will become covered with water even in light rains (Wilson, 1990). Figure 1.2 illustrates the high rates of absorption at the beginning of the rain, then a rapidly diminishing rate until a fairly constant ultimate rate is obtained (Foster, 1948). Some of the other factors that effect infiltration capacities include rain packing, swelling of colloids, antecedent conditions, inwashing, vegetal cover, land use, and season.

4) DEPRESSION STORAGE

Once the infiltration capacity exceeds the soils capacity to absorb water, the excess water fills all surface dips and hollows. Termed depression storage, these sites range from microtroughs to expansive flood plains. Though not a component in the hydrological cycle, depression storage is examined to illustrate the sequence leading up to surface runoff. Almost immediately after the beginning of rainfall excess, the smallest depressions become filled and overland flow begins. Most of this water in turn fills larger depressions, but some of it follows an unobstructed path to the stream channel. This chain of events continues, with successively larger portions of overland flow contributing water to streams, until such time as all depression storage within the basin is filled (Linsley et al., 1949).

Determining a basin's depression storage is very difficult to model. The volume of water in depression storage V_s, can be approximated by the equation

$$V_s = S_d \left(1 - e^{-KP_e} \right) , \qquad\qquad (1.2)$$

6
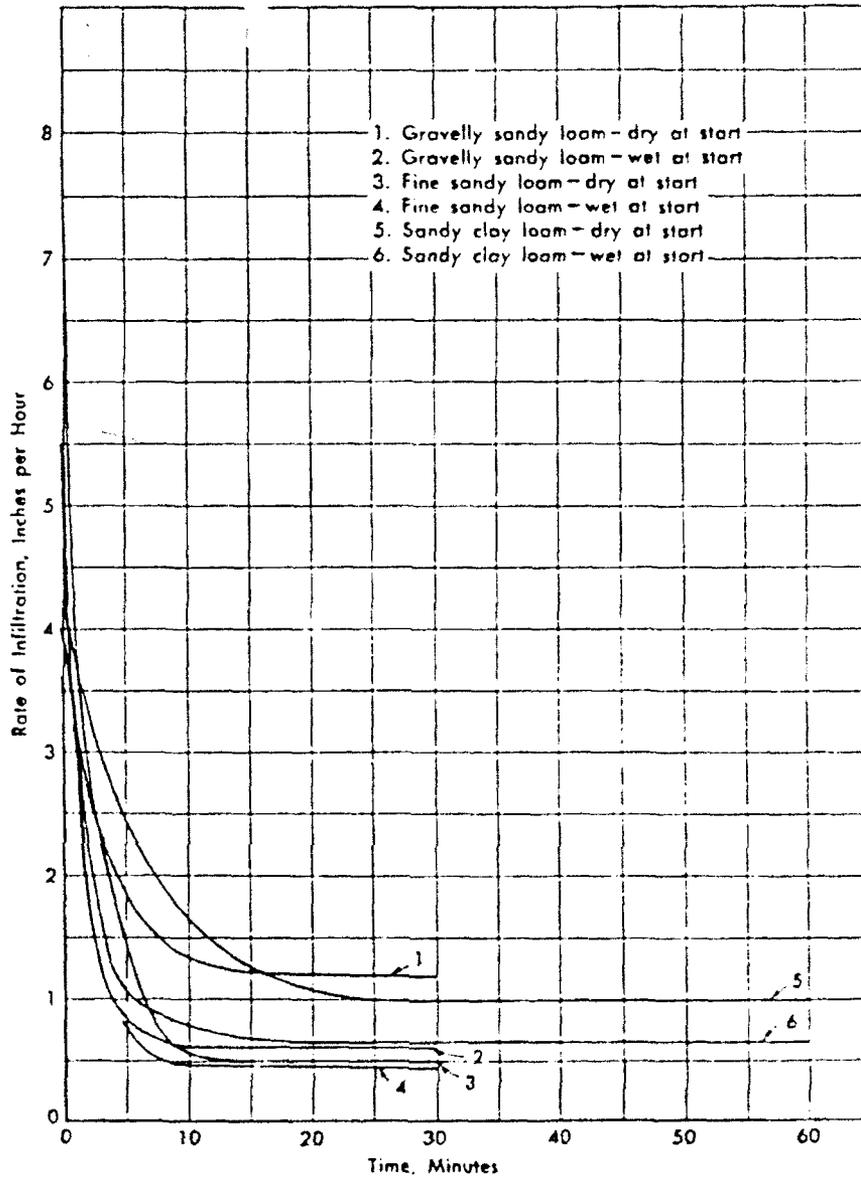
FIG. 1.2. Infiltration curves of Arizona soils, (Beutner *et al.*, 1953).

where S_d is the total basin's depression storage capacity, P_e is the accumulated rainfall excess, and K is a constant. Even with this relationship, the basin's depression storage capacity must be initially known. Depression storage does not contribute to storm runoff; the retained water will either evaporate or infiltrate into the soil.

5) EVAPORATION

Although not a key factor in the reduction of water during floods, evaporation plays a significant role after the storms have occurred. In most temperate climates the loss of water through evaporation is typically 600 mm per year from open water and perhaps 450 mm per year from land surfaces. In an arid climate, like that of Iraq, the corresponding figures could be 2000 mm and 100 mm, the disparity in this latter case being caused by the absence of precipitation for much of the year (Wilson, 1990).

Evaporation is the result of water molecules moving from the liquid phase to the vapor phase. The rate of change is directly proportional to the difference in vapor pressure between the water surface and the air. In addition, two other conditions are required to further this process: an energy input in the form of solar radiation and wind to replace the saturated air near the water surface with dry air.

Many empirical formulas are available to estimate the evaporation rate. One of the most common evaporation (E) equations is expressed in the form of Dalton's law:

$$E = (e_o - e_a)(a + bu) , \qquad (1.3)$$

where e_o is the vapor pressure at the water surface, e_a is the vapor pressure at some fixed level above the surface, u is the wind speed, and a, b are empirical constants.

The annual amount of water leaving a drainage basin as runoff varies from less than 10 percent of the yearly precipitation in hot deserts to more than 90 percent in the Cascade Mountains of Washington.

6) TRANSPIRATION

Transpiration is the loss of water from the cuticle or the stomatal openings in the leaves of plants. Water is vaporized within the leaf in the intercellular spaces and passes out of the stomata by molecular diffusion. The stomata are pores on the underside of a leaf (Dunne and Leopold, 1978). Because of the difficulty in differentiating the water losses of evaporation from that of transpiration, hydrologists usually group evaporation and transpiration losses together.

The combined evaporation and transpiration loss is called evapotranspiration (ET) and is a maximum if the water supply to both the plant and soil surface is unlimited. The maximum possible loss is restricted by meteorological conditions and is called potential evapotranspiration (Thornthwaite, 1948). Penman (1948) considered transpiration as a mechanism to bring water to the plant's surface at which time evaporation could take place. He also emphasized that potential evapotranspiration is largely controlled by weather, with vegetation and soil factors playing only a minor role.

7) GROUNDWATER FLOW

The previous hydrological processes reduced the available quantity of precipitation. Ground water flow, overland flow, and stream flow make up the three components that contribute to flood potential. The movement of water in the saturated subsurface layer, or phreatic zone plays an important role in the fluctuations of streamflow.

Wilson (1990) noted three factors that affect the flow of a liquid through a porous media:

1. the liquid - its density and viscosity,
2. the media through which the liquid moves,
3. the boundary conditions.

The amount of water stored in the voids between the rocks and soil is a function of the porosity. Table 1.2 shows some representative values for porosity for unconsolidated material. For a saturated zone, groundwater fills all the voids completely and porosity therefore becomes a direct measure of water storage volume. Part of this water cannot be removed by pumping or drainage because of the molecular and surface tension forces (Viessman *et al.*,1977).

TABLE 1.2. Representative values of porosity for unconsolidated materials. Porosity can be expressed in terms of percent volume or as a decimal fraction, as given here. From U.S. Geological Water Supply Papers.

UNCONSOLIDATED MATERIAL	POROSITY
Soils	0.30-0.50
Saprolite	0.01-0.50
Clays	0.45-0.55
Silt	0.40-0.50
Loess	0.40-0.55
Fine sand, old sediments	0.30-0.40
Fine sand, recent alluvium	0.45-0.52
Medium sand, old sediments	0.30-0.40
Medium sand, dunes	0.35
Coarse sand	0.30-0.35
Sand and gravel	0.20-0.30
Gravel	0.25-0.40
Glacial till	0.25-0.45

However, the amount of water available for streamflow is measured by the storativity of the aquifer. The storativity is the volume of water released from or taken into storage per unit area of aquifer for a unit change in head. In unconfined aquifers the storativity is called the specific yield. As the water table falls, water drains out of the larger pores, but the smaller pores retain water by capillary forces (Dunne and Leopold, 1978). The specific yield is usually calculated as the ratio of the volume of water draining out of the aquifer to the total volume of the aquifer

that is drained. Figure 1.3 shows the specific yields for a variety of materials. The specific yield depends not only on the porosity but also on the size of the individual pores. Thus, highly porous clay has very fine pores in which capillary forces can hold the water; the specific yield is low. In well-jointed, consolidated rocks the voids are so large that no significant capillary attraction withholds water from the stream or well (Dunne and Leopold, 1978).
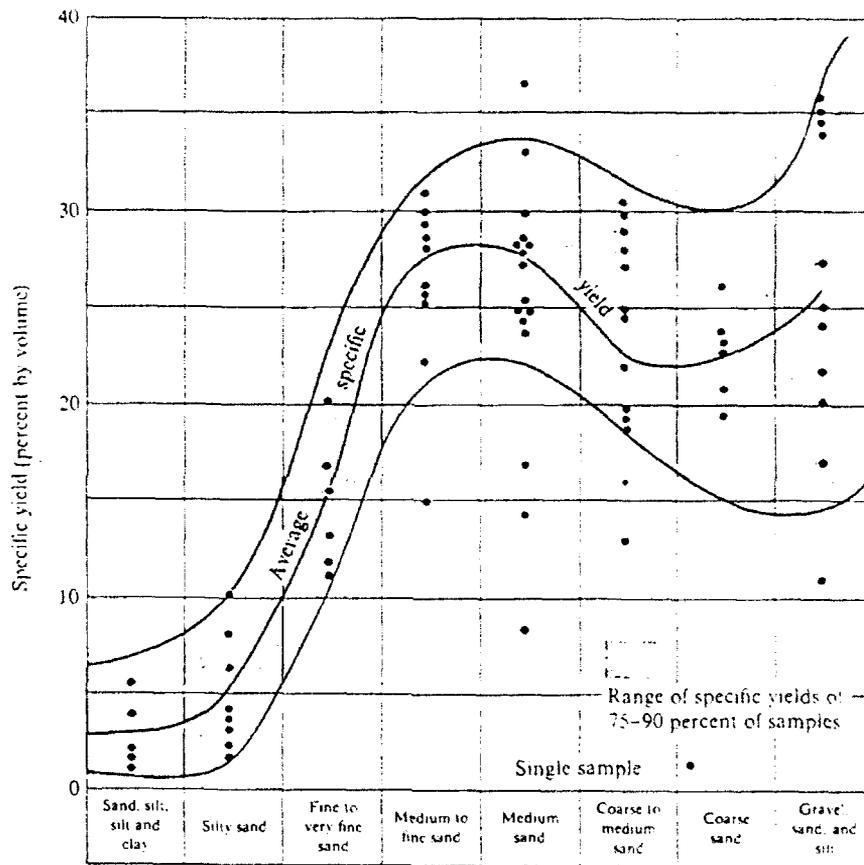
FIG. 1.3.   Specific yield and texture for alluvial materials of Pakistan (Kazmi, 1961).

In 1856, Henri Darcy described the equations governing groundwater flow in a confined aquifer. The fundamental hydrological principles he established is known as Darcy's law and states that the fluid flow through a porous media is proportional to the head loss and inversely proportional to the length of the flow path. Darcy's

law (see Figure 1.4) can be expressed as

$$Q = Au = wyK\left(\frac{\Delta h}{\Delta l}\right) \ , \tag{1.4}$$

where Q is the rate of flow ($\frac{m^3}{day}$);

A is the cross-sectional area of flow (m^2);

u is the mean flow velocity ($\frac{m}{day}$);

w is the width of flow (m);

y is the depth of flow (m);

K is the hydraulic conductivity;

Δh is the difference in head;

Δl is the distance between measuring points (m).
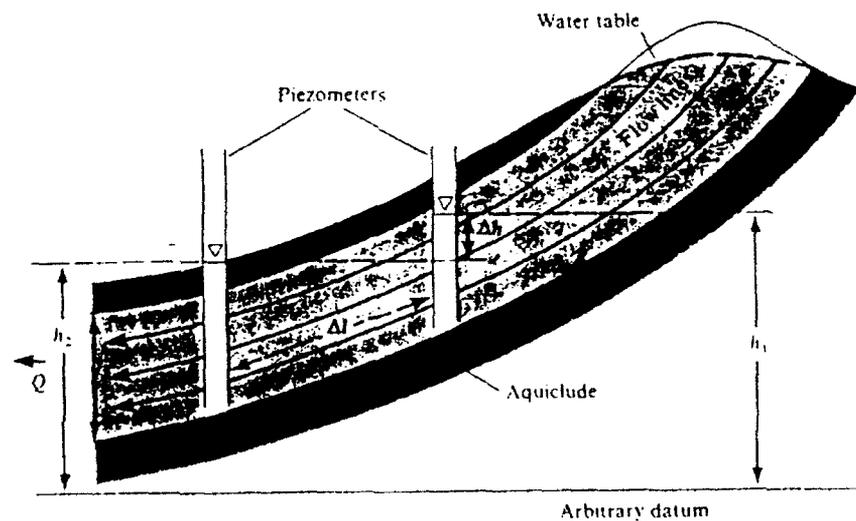
FIG. 1.4.   Flow in a confined aquifer. The piezometric gradient is $\Delta h/\Delta l$; aquifer thickness is y; flow lines are parallel to aquifer boundaries and equipotential lines normal to the boundaries (Dunne and Leopold, 1978).

The concepts for unconfined ground water flow were derived from Darcy's law by Jules Dupuit. He assumed that all flow lines are horizontal and of uniform velocity in any vertical section. In addition, the water table must be only slightly

12

inclined. The discharge per unit width (q) in any vertical section through the aquifer is given by the Dupuit approximation

$$q = \frac{k}{2x}(h_o^2 - h_1^2) \ ,$$ (1.5)

where h_o, h_1, and x are defined in Figure 1.5. It is significant to note in laboratory tests of more than 2000 rock samples under hydraulic gradients($\frac{\Delta h}{\Delta l}$) of 100 percent, the observed range of velocities was from a minimum of 1 foot in 10 years to a maximum of 60 feet per day (Stearns, 1927).
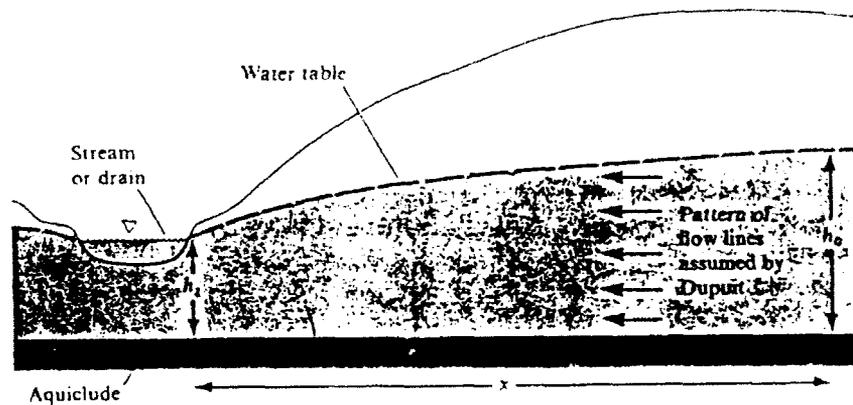
FIG. 1.5. Constant flow from a shallow horizontal aquifer (Dunne and Leopold, 1978).

8) RUNOFF

Runoff becomes the next component after interception, infiltration, evaporation, and surface storage processes have been subtracted from total precipitation (see Fig. 1.6). Because of the difficulty in differentiating surface runoff from subsurface runoff the two are usually lumped together as direct runoff for accounting purposes. Subsurface flow also known as interflow reflects the lateral movement of water through the upper soil zones to a stream. This contribution has a faster response time than groundwater flow and can be a significant part of stormflow

for very permeable soils (Freeze, 1972). One of the simplest ways for evaluating runoff potential is by plotting a graph of discharge versus time. This plot known as a hydrograph shows the volume of runoff produced, its peak rate, and the timing of contributions to the channel. A more thorough examination of runoff and hydrograph application will be explored in Section 3, Runoff Analysis.
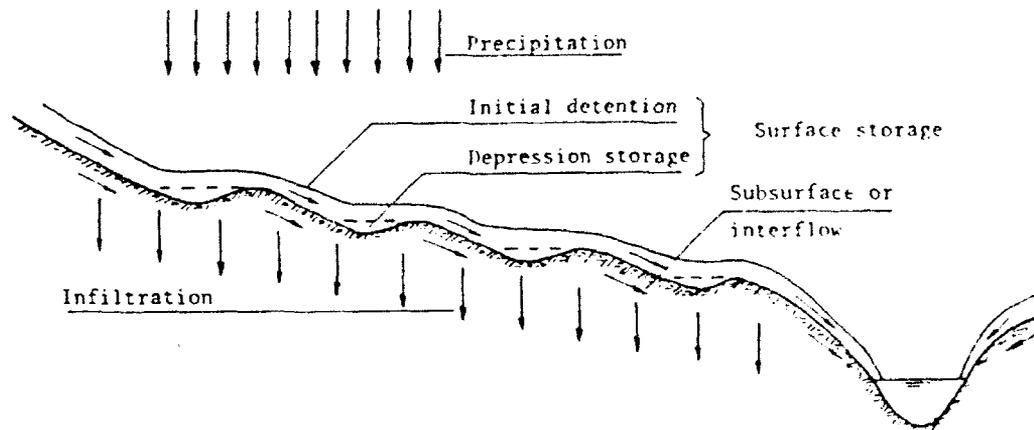
FIG. 1.6.   Distribution of uniform rainfall, (Bedient and Huber, 1988).

As previously stated, rainfall must first satisfy *soil and vegetal storage*, detention and interception requirements. After surface depressions are filled, surface water begins to spread down the slopes in thin films and little rivulets. This overland flow is significantly affected by surface tension and friction forces. Horton (1945) explained that as precipitation continues, the depth of surface detention increases, and it is distributed according to the distance from the outlet (see Figure 1.7). With an increase in depth or volume of supply, there is a corresponding increase in the rate of discharge. Therefore, the rate of outflow is a function of the depth of water retained on the surface.

Water flows the path of least resistance, yet this course is still filled with numerous obstructions. Each obstruction causes a finite delay until the water builds up enough (obtains sufficient head) to overcome the resistance. Horton (1935) noted that upon release, the stream suddenly speeds on its way again. Each time there is a

14
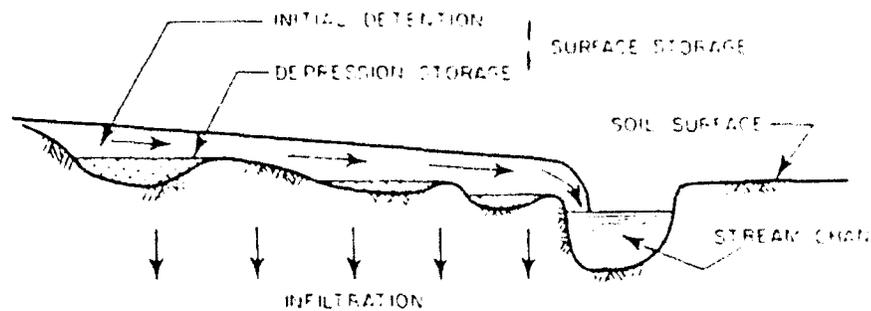
FIG. 1.7. Surface runoff phenomena (Gray, 1973).

merging of two or more streams, the water is accelerated still more in its downward path. The culmination of all these small contributions thus produces the basin's surface runoff hydrograph. After the excess rain ends, the water remaining in the area (surface detention) disappears progressively from the basin as a result of the combined action of surface runoff and infiltration.

Surface runoff is affected by a variety of factors. Most hydrologists look at runoff from the perspective of whether rainfall exceeds the infiltration capacity or if the infiltration capacity is not a constraint. Surface runoff often called Horton overland flow occurs once the soil's infiltration capacity has been exceeded. Arid to subhumid areas most frequently experience overland flow, especially if vegetation is thin. Cultivated regions, urban areas, and places where soils have been compacted improve the potential for surface runoff.

Volumes and peak rates of Horton overland flow vary with storm size and intensity, and with the factors that affect infiltration. Thus, great differences occur between regions and between storms. On catchments of less than one square kilometer, intense storms yield over 50 percent of the rainfall as overland flow, and in the larger storms the yield approaches 100 percent. For larger catchments, the peak runoff rate declines approximately with the square root of the drainage area. The lag between a burst of intense rainfall and the resulting hydrograph peak for this

runoff varies from a few minutes for individual hillsides to one-half hour for one-square-kilometer catchments and several hours at 100 square kilometers (Dunne, 1978).

Subsurface stormflow dominates in humid climates with dense vegetation. The vegetation tends to loosen up and till the upper soil layers enabling rainfall to infiltrate rapidly. In substantial subsurface flow regions, the upper permeable layers are situated on top of an impervious strata. Consequently, the water has a direct route to the stream channel. The steeper the hillslope, the quicker the hydrograph response to subsurface flow.

The volumes of subsurface stormflow are much lower than those from Horton overland flow. Studies generally indicate subsurface runoff less than 20 percent of rainfall. Optimal conditions can produce runoff rates of nearly 50 percent of rainfall accumulations. Most of the rain is stored in the soil and in the ground water zone and is released slowly to supply baseflow. By comparison with velocities of overland flow, subsurface stormflow is very slow. The highest rates measured 11 $\frac{m}{day}$ in a highly permeable sandy loam on a steep hillslope. Hydrograph peaks lag rainfall by 1 to 20 or 30 hours, even for small catchments, and the recession limbs are much flatter than those for Hortonian flow (Dunne and Leopold, 1978).

9) CHANNEL FLOW

Channel flow represents the drainage conduit for overland flow. The amount of water passing through a stream section is the product of the cross-sectional area and its velocity. Expressed by the equation

$$Q = AV \ , \tag{1.6}$$

where Q is the discharge in cubic meters per second; A, the area in square meters; and V, the average velocity in meters per second.

Water flowing in a channel is being pulled downhill by gravity. Counteracting the downhill force is the drag or resistance of the banks and bed, tending to retard the flow. Because; in general, the water neither accelerates nor decelerates but maintains an approximate constant velocity, the downhill component of gravitational force is equal to and opposite to the resisting force (Dunne and Leopold, 1978).

The formulas most used in computing open-channel stream flow make velocity a function of the slope of the water surface and the hydraulic radius, which is defined as the ratio between the area of a stream cross section and the channel portion covered or wetted by the water, called the "wetted perimeter." An experimentally determined coefficient for evaluating energy losses due to friction and turbulence caused by channel roughness.

One of the first stream velocity relationships was determined by the French engineer Chezy (1769),

$$V = C\sqrt{RS} \ , \tag{1.7}$$

where V is the velocity; C, a resistance coefficient that is large for smooth boundaries and small for rough ones; R, the hydraulic radius ($\frac{A}{WP}$); and S, the energy gradient, approximated by the water surface slope.

Another widely used stream velocity measurement formula was introduced by Manning (1889). Similar to Chezy's, the Manning formula is expressed as

$$V = \frac{1.486 R^{\frac{2}{3}} S^{\frac{1}{2}}}{n} \ , \tag{1.8}$$

in which V, R, and S are as previously defined and n, called the Manning resistance coefficient, is a determined roughness of the various boundaries.

River channels play a significant role in the storage and translation of flood waves. Flood routing techniques modify the flood wave as it continues downstream. These modifications form the basis for area flood control plans.

Runoff supplied to the channel moves downstream as a wave of increasing and then decreasing stream discharge. The flood wave itself is subjected to two processes that alter its character. The first process is translation, whereby the wave moves downstream without changing its shape. This tendency is associated with steep, straight mountain streams and desert washes during intense rainstorms, where flow velocities are high and remain relatively constant throughout the range of flood discharge.

The second process operating on the flood wave is pondage, whereby the wave is attenuated by storage within the channel and valley bottom. When a rapid pulse of water enters a true reservoir, it does not flow out or displace a similar amount of water immediately. Rather, most of the input is stored within the reservoir. As water flows in, it is stored, raising the water level progressively and causing the outflow to increase. But because some of the input must be stored to increase the output rate, the peak outflow rate cannot be as high as that of the inflow. When the inflow ceases or declines significantly, the water in storage then drains out slowly (Dunne and Leopold, 1978).

In most runoff scenarios, a combination of both transmission mechanisms take place in a stream. If the storm hydrograph were examined at several locations along a river section, the affects of translation and storage become apparent. Figure 1.8 shows a set of hydrographs from basins on the Sleepers River Experiment Watershed in northeastern Vermont. It illustrates the river's ability to damp the peak rate of runoff with increasing basin size. Each peak becomes successively attenuated and absorbed within the river system as the drainage area increases, even though the total discharge progressively increases.
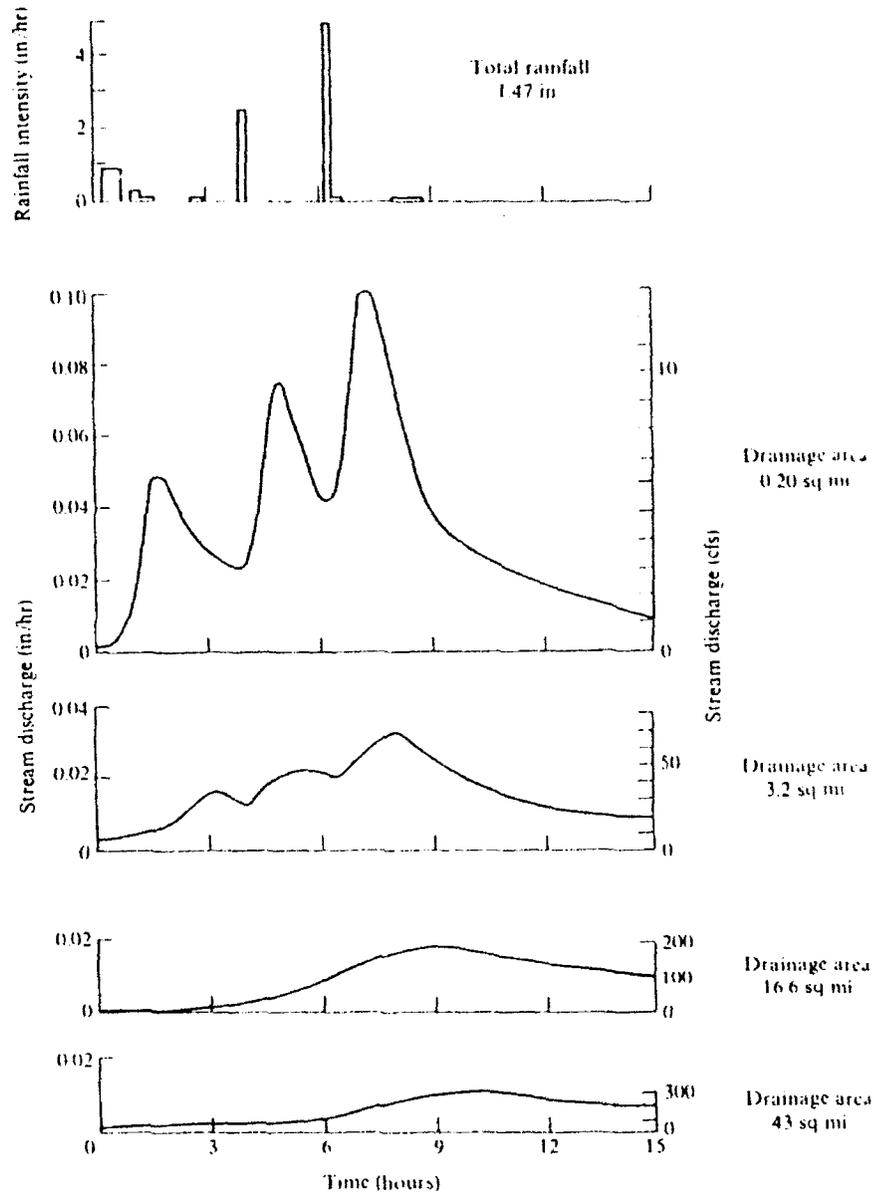
FIG. 1.8. Changes in hydrograph shape at a series of stations along the Sleepers River, near Danville, Vermont (Dunne and Leopold, 1978). Data from the Agricultural Research Service, U.S. Department of Agriculture.

3. Runoff Analysis

a. Components of the Hydrograph

A hydrograph is a continuous plot of instantaneous discharge versus time. It is made up of the combined contributions of surface runoff, base flow, interflow, and channel precipitation. The relative contribution of each component to the hydrograph is dependent on the rainfall rate, i, relative to the infiltration rate, f. In addition, interflow and groundwater movement depends on the soil moisture deficiency with respect to the field capacity, F, which is defined as the amount of water held in soil after excess gravitational water has drained (Horton, 1935). Figure 1.9 is used to illustrate the contribution of each component under various conditions.
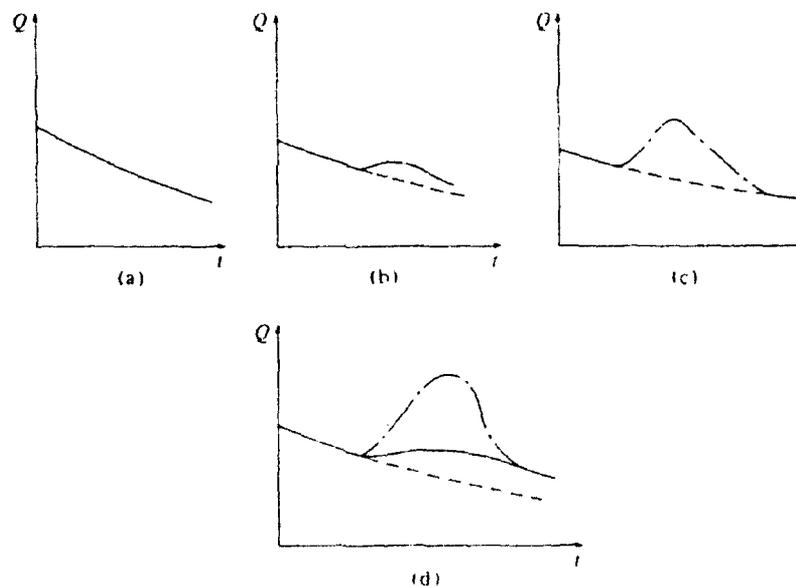
FIG. 1.9. Effect of the infiltration rate and soil moisture deficiency on hydrograph shape (Viessman et al., 1977).

Figure 1.9(a) depicts the flow of a permanent stream during a period between precipitation events. It is described as a base flow hydrograph since groundwater sustains the flow. If the graph is examined with respect to the infiltration rate and the soil's field capacity, the following inequalities can be used: $i < f$ and $F < S_D$.

No overland flow occurs since the infiltration rate is not exceeded. Furthermore, interflow and additional ground water contributions are nonexistent since the soil's field capacity is not reached. There will be a small discharge rise due to channel precipitation as will be the case in the other three examples.

The second illustration (Fig. 1.9(b)) again reflects a scenario with no overland flow since $i < f$. However, this time the soil's field capacity has been exceeded, $F > S_D$, thus enabling additional groundwater and interflow contributions to the hydrograph. Do to the nature of these flows, these contributions will be relatively small.

Figure 1.9(c) illustrates a case in which overland flow exists, $i > f$. The rainfall rate exceeds the infiltration rate thereby causing surface runoff. Because the soil's field capacity has not been reached, $F < S_D$, additional support by interflow and groundwater flow does not exist. This later condition can occur as a result of inwashing, rain packing, urbanization, and basin slope.

The last picture (Fig. 1.9(d)) represents the classic high intensity rainfall event ($i > f$ and $F > S_D$). All components of the hydrograph - overland flow, interflow, channel precipitation, and groundwater flow - contribute to outflow.

In most hydrograph analyses, interflow and channel precipitation are lumped together with surface runoff. The contributions to the three to the hydrograph are relatively rapid as compared to groundwater flow. Channel precipitation is the fastest and immediately adds to the outflow. Its contribution is usually only a small fraction of total flow. As pointed out by Linsley et al. (1949), the water surface area for most basins does not exceed five percent of the total area at fairly high stages.

Interflow is part of the subsurface flow which moves at shallow depths and reaches the surface channels in fairly short time periods. Its distribution is commonly characterized by a slowly increasing rate up to the end of the storm period,

followed by a gradual recession which terminates at the intersection of the surface flow hydrograph and the base flow hydrograph (Viessman *et al.*, 1977). Figure 1.10 shows the various contributions of each component.
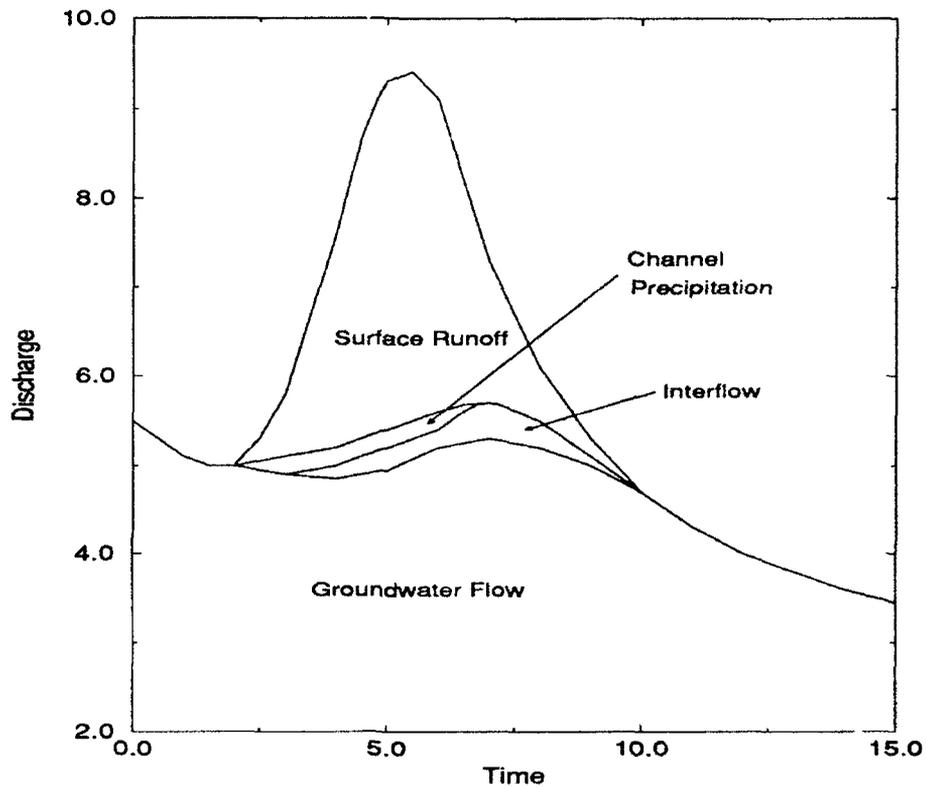
FIG. 1.10.   Components of the hydrograph.

The base flow component of the hydrograph results from the percolation of rainfall downward until it reaches the water table. Next, it flows toward streams as groundwater discharge. The actual effect of rainfall as additional groundwater flow may not be felt during the storm's lifetime. The time period of groundwater release may be measured in days for small basins and months or years for large drainage ones.

b. *Hydrograph Shape and Timing Characteristics*

The shape of the hydrograph for a single, short-duration storm has three distinct characteristics: a rising limb, a crest segment, and a recession limb. Figure 1.11 shows these hydrograph components for a uniform rainfall event. The inflection points separate the crest segment from the rising and falling limbs. The falling part of the hydrograph can be thought of as a combination of recession curves. The storage accumulations from surface runoff, baseflow and interflow will slowly deplete once rainfall ends. For small catchment areas, total contributions by groundwater flow, channel precipitation, and interflow are relatively small in comparison to the amount received by surface runoff.
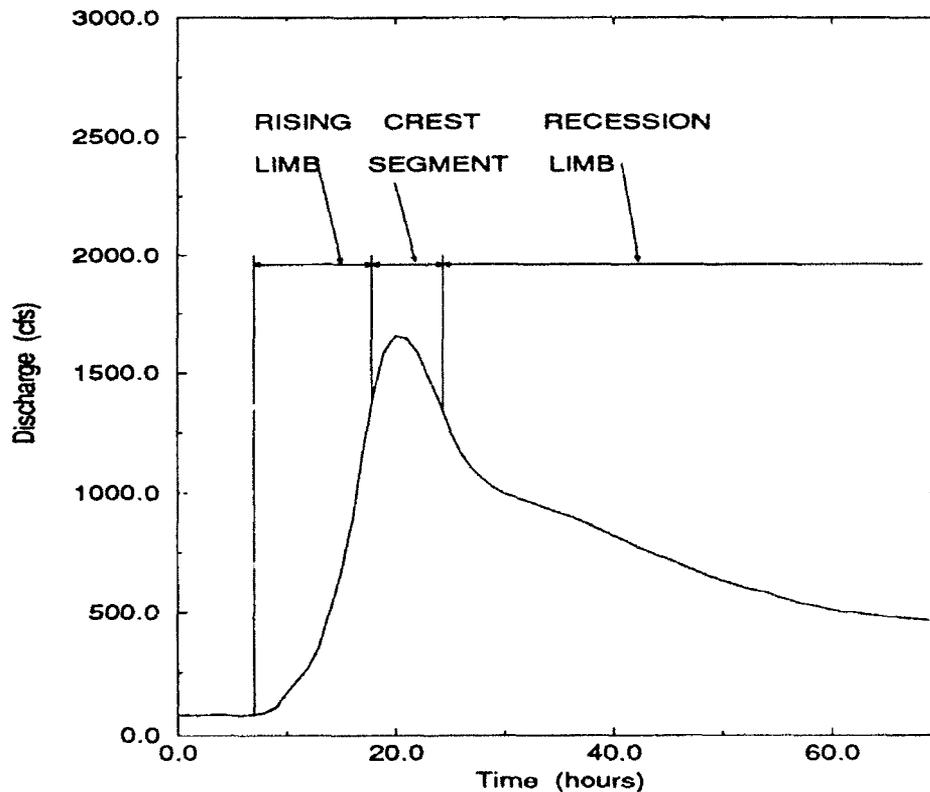
FIG. 1.11. Regions of the hydrograph.

Timing parameters are essential to understanding the relationship between rainfall and runoff. Figure 1.12 explores the terminology associated with a typical

storm hydrograph and a rainfall hyetograph. The following timing aspects are defined:

1. Lag to peak (L) : time from the center of mass of rainfall excess to peak of the hydrograph

2. Duration (D): length of time during which rain falls

3. Time base or Baselength (T_b): length of time of surface runoff

4. Time of rise (T_R): time from the start of rainfall excess to the peak
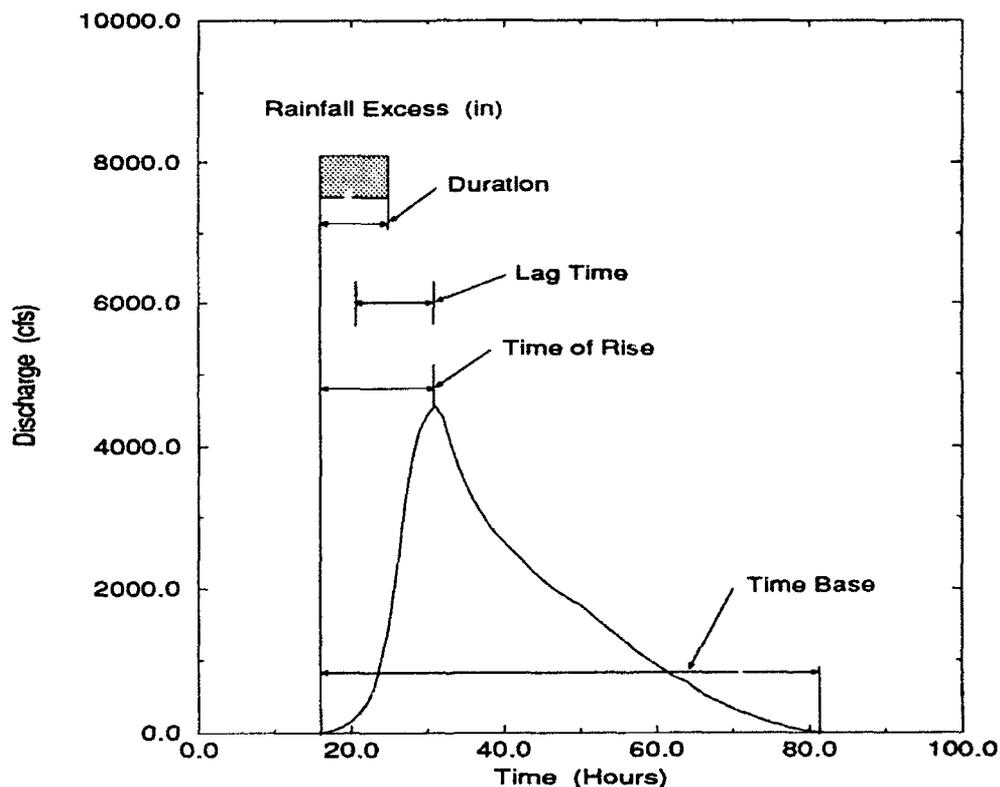
FIG. 1.12.   Terminology associated with the runoff hydrograph.

c. Factors Affecting Hydrograph Shape

The time distribution of runoff is determined by the physical characteristics of the basin, and the climatic factors. The rising limb and the peak are functions of history and rainfall intensity as well as of basin characteristics, while the recession limb is largely independent of the storm details producing runoff (Ward, 1967).

1) CLIMATIC FACTORS AFFECTING HYDROGRAPH SHAPE

The climatic factors which influence hydrograph shape and the runoff volume are

1. rainfall intensity and duration;
2. rainfall distribution over the basin;
3. direction of storm movement; and
4. type of precipitation and type of storm.

(i) *Rainfall Intensity and Duration.* Only if the rainfall intensity exceeds the infiltration rate will surface runoff occur. Rainfall intensity and duration govern the amount of runoff, the peak flow rate, and the duration of surface runoff for a given basin. For a constant rainfall duration, an increase in rainfall intensity will increase the peak discharge and the volume of runoff. Short time variations in intensity during a storm affect the hydrograph's shape for small basins, but generally they will have little noticeable effect on hydrographs from large basins (Gray, 1973).

Likewise, for a situation where intensity is constant, rainfall duration mainly determines the peak flow and time period of surface runoff. Further if a storm lasts long enough the entire basin will contribute to outflow. The peak flow will become the product of rainfall intensity and basin area. This scenario frequently happens for small basins; however, it rarely occurs for larger ones.

(ii) *Rainfall Distribution.* The areal distribution of rainfall significantly affects the hydrograph's shape. High intensity rainfall near the outflow point results in a rapid rising and falling hydrograph with a sharp peak. Greater rainfalls in the upper reaches of the basin produce a lower and broader hydrograph peak. Figures 1.13(a) and (b) illustrate the effects of localized rainfall on the streamflow hydrograph. If all other conditions remain constant throughout the catchment, a uniformly distributed rainfall will produce the minimum peak discharge. The more non-uniform the rainfall distribution the greater the peak discharge will be (Raudkivi, 1979).
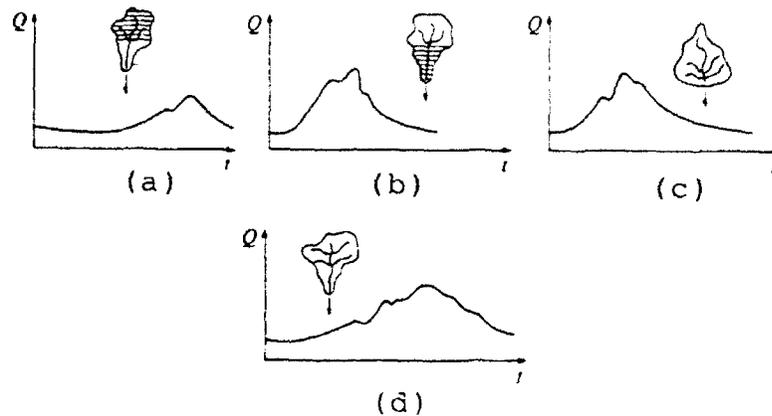
FIG. 1.13. Effects of precipitation and basin characteristics on hydrograph shape (Viessman *et al.*, 1977).

(iii) *Direction of Storm Movement.* The direction of storm movement along the basin affects both the peak outflow and the runoff duration. An elongated basin with the rain moving downstream will produce a much greater peak. Consequently, a storm moving up the basin will result in a faster runoff response but with a much lower peak and a longer time base.

(iv) *Type of Precipitation and Storm.* The nature of precipitation as either rain, snow, or sleet will drastically change the hydrograph's shape. A rainfall event will immediately produce a runoff response while the effect of a snowstorm may not be felt for months. The release rate of rainfall runoff is rapid as compared to the time required for snow to undergo a phase change and become runoff.

2) PHYSICAL FACTORS AFFECTING HYDROGRAPH SHAPE

The primary physical characteristics of drainage basins are its area, shape, elevation, slope, soil type, timing distribution, and peak discharge of runoff. The surface-runoff hydrograph represents the integrated effect of all the basin's physical characteristics and their modifying influence on the translation and storage of rain-

fall excess. The factors involved are numerous, some having a major bearing on the phenomena and others being of negligible consequence. It is difficult to cover the influence of each individual factor in detail. The effect of each factor may be obscured by the effect of another (Gray, 1973). The following list describes the basin's physical characteristics that hydrologists consider to have the main influence on hydrograph shape.

(i) *Drainage Basin Area.* The major effect of increasing the basin's area is a lengthening of the runoff duration. In addition, if runoff is expressed not as a total quantity for a basin but as a quantity per unit area ($\frac{ft^3}{s}$ per square mile) it is observed, that peak runoff decreases as the catchment area increases. This is due to the finite time taken by the water to flow through the stream channels to the outlet point and also to the lower average rainfall intensity as as storm size increases (Wilson, 1990).

(ii) *Drainage Density.* The drainage density, D_D, expresses the average length of streams per unit area within the basin

$$D_D = \frac{\sum L}{A_d} \ , \tag{1.9}$$

where $\sum L$ is the total length of streams in the drainage basin and A_d is the drainage area. Areas with high density are associated with high flood peaks, high sediment production, steep hillslopes, general difficulties in access, relatively low suitability for agriculture, and high development costs (Dunne and Huber, 1978).

Linsley *et al.* (1949) indicated that the values of drainage density ordinarily range from well below 1 mile/square mile in poorly drained basins, upward to 5 miles/square mile in exceptionally well drained basins. Since a well-drained drained basin reduces the distance water must flow overland, the corresponding reduction in time involved is reflected by a runoff hydrograph having a rapid time of concentration.

(iii) *Slope of the Drainage Basin.* The greater the drainage basin's slope, the faster storm runoff will travel. In addition, steep slopes are commonly associated will flash flood regions. These zones have high runoff peaks and fast response times. Infiltration rates typically decrease as slopes increase. On steep inclines, Vegetal cover is less dense and soil more compact and rocky, thereby improving runoff processes. A simple method to determine catchment slope is to describe the inclination between two points on the main stream. The standard points used in Britain are 10 and 85 percent of the main stream length from the basin origin. The velocity of overland flow, however, is difficult to quantify due to the complex nature of both the basin and the flow itself.

(iv) *Shape of the Basin.* The basin's shape is a key parameter in controlling the time distribution of outflow. Assuming that rainfall is evenly distributed over the basin, the hydrograph produced by a semicircular basin with the outflow point at the circle's center, will have a much faster time to peak than one produced by a long, narrow basin of equivalent size. Langbein (1947) summarized the effect by stating that a drainage basin whose drainage tributaries are compactly organized so that water from all parts of the basin has a comparatively short distance to travel, will discharge its runoff more quickly and reach greater flood crests than one in which the larger part of the basin is remote from the outlet. Most basins tend to be pear-shaped. Dooge (1956) reasoned that unless the basin's shape deviated from ovoid, the hydrograph's geometry remained consistent. Figures 1.13(c) and (d) show how basin shape effects the hydrograph's shape under uniform precipitation conditions.

d. Unit Hydrograph

The determination of runoff from precipitation measurements had its origins with hydrograph analyses. In 1932, Sherman conceived the idea of the unit hydro-

graph, as "basin outflow resulting from one inch (one centimeter) of direct runoff generated uniformly over the drainage area at a uniform rainfall rate during a specified period of time." The unit hydrograph concept has several assumptions limiting its usefulness in all rainfall-runoff scenarios (Johnstone and Cross, 1949):

1. For a given watershed, rainfall excesses of equal duration are assumed to produce surface runoff hydrographs with equivalent time bases regardless of the intensity of the rain.

2. For a given watershed, the magnitude of the runoff ordinates for a storm of a given duration are assumed directly proportional to rainfall excess volumes. Thus, twice the rainfall produces a doubling of the hydrograph ordinates.

3. For a given watershed, the time distribution of direct runoff from a given storm is assumed independent from antecedent or subsequent storm periods.

The unit hydrograph theory is predicated on the system being linear and time-invariant (Dooge, 1973). However, these assumptions are incorrect. The relationship between rainfall excess and surface runoff in a basin is nonlinear. Laboratory testing supports channel flow theory such that greater depths of water move faster and would therefore alter runoff response. Furthermore, antecedent conditions change the infiltration rate and depression storage resulting in a reduction of total rainfall. However, for most runoff models the linearity guidelines produce results consistent with those using nonlinear criteria.

The requirements to analyze runoff involve only two inputs: excess rainfall and the unit hydrograph. The simplicity in the input/output relationship enables runoff modeling with a minimum of calculations. The complexities of the hydrological cycle and each basin's physical characteristics are assumed fixed and inherently incorporated within the unit hydrograph. Therefore, the response of a linear basin to any rainfall excess input is directly proportional to the unit hydrograph. All aspects of the models physics and hydrology are replaced by the linear response

function. The unit hydrograph construction will be explored in the methodology section.

Most practical techniques of forecasting runoff from rainfall are based on either correlation techniques between observed volumes of rainfall and runoff or on the unit hydrograph method. The hydrograph method is a "black box" technique. It is therefore not a tool which will aid in the understanding and development of the physics involved (Raudkivi, 1979).

The unit hydrograph is most easily derived from the hydrograph of a single isolated rainfall. To be able to use the unit hydrograph to determine the runoff from different storms, the selection of the proper storm duration is important. Opinions vary widely depending on whether the basin is large or small. Linsley *et al.* (1949) cite that in practical applications, experience has shown that the time unit employed should approximate one-fourth of the basin lag time. They suggested that the effect of small differences in storm duration is not large and that a tolerance of $\pm$ 25 percent from the adopted unit hydrograph duration is accepted.

The United States Army Corps of Engineers (1948) found that values of unit-storm duration equal to about half of the basin lag time appear to be satisfactory. This criteria is used for basins of less than 100 square miles.

Once the hydrograph has been determined, estimating the runoff from rainfall excess can begin. From the unit hydrograph for any duration of uniform rain, the unit hydrograph for any other duration can be obtained. As the duration becomes shorter, the resulting unit hydrograph approaches an instantaneous hydrograph. The instantaneous hydrograph (IUH) is the hydrograph of runoff that would result if an inch of water were spread uniformly over an area and then allowed to runoff (Schaake, 1965).

From a mathematical perspective, the ordinates of the IUH represent the relative effect of antecedent rainfall intensities on the runoff rate at any instant of time.
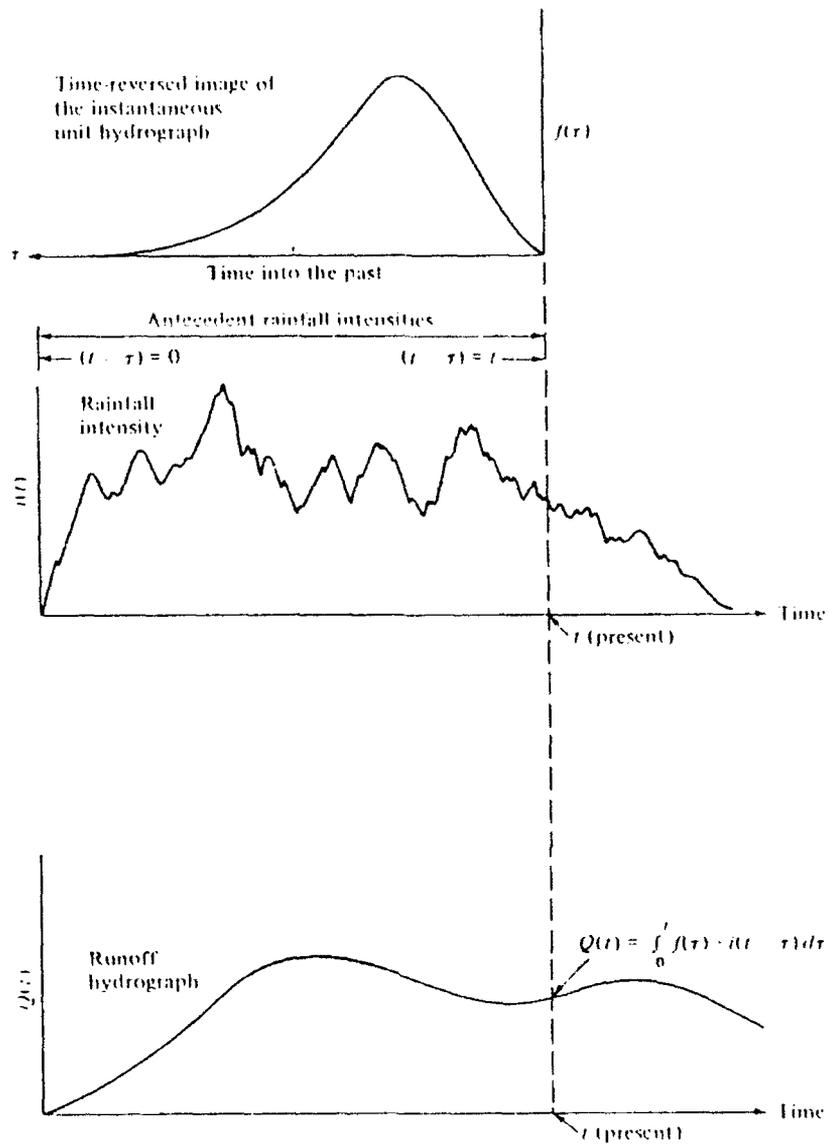
FIG. 1.14. Calculation of runoff rates with the instantaneous unit hydrograph (Schaake, 1965).

By plotting the IUH with time increasing to the left rather then to the right (see Fig 1.14), and then superimposing this plot over the excess rainfall hyetograph (plotted with time increasing to the right), the relative weight given to antecedent rainfall intensities is easily seen. The runoff rate at any time is computed as a weighted average of the previous rainfall intensities. The computed runoff hydrograph is the

weighted, moving average of the excess rainfall pattern and the weighting function is the time-reversed image of the unit hydrograph (Schaake, 1965).

The surface runoff rate can be expressed mathematically as

$$Q(t) = \int_0^t f(\tau)\, i\,(t-\tau)\, d\tau \; , \tag{1.10}$$

where $Q(t)$ = the surface runoff at time t

$\quad f(\tau)$ = the ordinate of the IUH at time τ

$\quad i(t-\tau)$ = the excess rainfall intensity at time $t-\tau$.

The variable τ represents time into the past so that time $t-\tau$ occur before time t. The limits of the integral allow τ to vary from the present time back through a duration equal to the hydrograph's baselength. The integral gives a continuous weighting of previous rainfall intensities by the ordinates of the IUH.

4. Measuring Storm Rainfall by Radar

The use of radar is a very common technique to evaluate rainfall accumulation as well as rainfall patterns. Radar scans are presentations of instantaneous back-scattered microwave energy. These depictions correspond to the number and sizes of water or ice scatterers within the viewing field. When precipitation particles are small with respect to the radar wavelength, the back-scattered power can be related to a rainfall rate.

a. Radar Measurement of Rainfall

Starting with the Probert-Jones form of the radar equation, the framework for estimating rainfall rates is as follows:

$$\overline{P_r} = \left[\frac{\pi^3 P_t\, G^2\, \theta^2\, h}{512\,(2\,ln\,2)\,\lambda^2} \right] \frac{|K|^2 Z}{r^2} \; , \tag{1.11}$$

where P_t = power output (mW)

r = distance to target (km)

G = antenna gain factor

θ = beamwidth of antenna (radians)

h = pulse length in space (cm)

λ = radar wavelength (cm)

Z = reflectivity factor $(\text{mm}^6\text{m}^{-3})$

$|K|^2$ = dielectric factor

P_r = back-scattered power (mW)

The radar equation relates the average back-scattered power to the radar reflectivity factor, Z. The assumptions include the following and form a basis for assessing the accuracy of weather radar measurements of rainfall rates (Battan, 1973).

1. The scatterers are homogeneous dielectric spheres, with diameters small compared to the wavelength (Rayleigh approximation).

2. The illuminated volume is filled with scatterers.

3. The radar reflectivity factor, Z, is uniform throughout the illuminated volume, i.e. homogeneous reflectivity.

4. The scatterers have the same dielectric constant; that is they are all water drops or ice spheres.

5. Multiple scattering is negligible.

6. The main lobe of the antenna beam pattern can be described adequately.

7. Microwave attenuation along the propagation path between the radar and the target is negligible.

8. The incident and back-scattered waves are linearly polarized.

9. The scatterers scatter isotropically.

The average back-scattered radar power from precipitation is proportional to the summation of the sixth power of drop diameters (D^6) illuminated by the radar beam; therefore the reflectivity factor is also defined by

$$Z = \sum ND^6 = \int_0^\infty N(D)D^6 dD \ , \qquad (1.12)$$

where N is the number of drops with diameter D per unit volume of atmosphere and $N(D)$ is the number of diameters between D and $D + dD$ per unit volume.

If vertical air motions are disregarded, the rainfall rate, R, is related to the diameter, D, by the following equation

$$R = \frac{\pi}{6} \int_0^\infty N(D)D^3 V_t dD \ , \qquad (1.13)$$

where $V_t(D)$ is the terminal velocity of a drop of diameter D. Spelhaus (1948) approximated the terminal velocity by

$$V_t = 1400D^{\frac{1}{2}} \ . \qquad (1.14)$$

Substituting the Marshall-Palmer (1948) exponential drop size distribution into equations 1.12 and 1.13 and using the relationship between V_t and D, the following empirical expression relating Z and R is obtained

$$Z = AR^b \ . \qquad (1.15)$$

This is a relationship between the radar reflectivity factor, Z, measured in $mm^6 m^{-3}$ and the rainfall rate, R, measured in mmh^{-1}. The constants A and b are empirically derived (Huebner, 1977).

The determination of Z is dependent upon the measurement of the scattered electromagnetic wave. Various methods are employed to measure the return power,

but large return variations exist between parcels within extremely short time periods. A radar processor is commonly used to determine average power returns over specific range increments.

b. *Sources of Error*

The numerous factors causing errors in the radar measurement of rainfall can be grouped into three broad categories: (1) estimating the radar reflectivity factor; (2) time and space averaging of substantial variations in reflectivity; and (3) variations in the $Z - R$ relationship and below-beam effects resulting from meteorological processes that modify the precipitation while it is falling (Brandes and Wilson, 1982).

1) ESTIMATING THE RADAR REFLECTIVITY FACTOR

Measurement accuracy of the average back-scattered power is dependent on the radar equipment. Even with careful calibrations, the task of averaging independent range and time samples produces errors. These inaccuracies can produce errors of approximately 10 percent of the rainfall rate (0.7 dB).

Another problem estimating the radar reflectivity factor can be attributed to a condition called "thunderstorm superrefraction" (Battan, 1973). In this case, the radar signal is lofted above and beyond the normal field of view due to a temperature inversion with decreasing moisture. The result is ground target returns from distant ranges.

Cohen and Smolski (1966) also identified the radome as a potential attenuator. When wet the radar wavelength can experience two way losses, those from signal transmission and reception, approaching 2 dB. Signal attenuation is a function of the water depth and radar wavelength.

2) Time and Space Averaging of Radar Measurements

Radar data are obtained by scanning in azimuth at a low elevation angle and making measurements at discrete range and angular intervals. Regardless of the $Z - R$ relationship used, this procedure results in time and space sampling errors that relate to storm element size, intensity, duration, and motion.

Signal averaging effectively smooths small scale radial and azimuthal variations. Radar components effectively restrict precipitation below this set size (resolution). These hydrometeors are not processed by the radar; they are however detected by rain gauges. The sampling differences between the two methods highlight the difficulty in correlating one with the other.

Further, the increased radar sampling volume and greater beam height at long ranges is usually not representative of that reaching the ground. The greater the distance from the radar, the wider the beam width. Thus the hydrometeors within these large volumes will vary considerably in size. An average value may differ markedly from point rain gauge measurements (Nemec, 1986).

The received signal power is inversely proportional to the square of the range to the target. Therefore it can be looked upon as another form of attenuation. As the beam propagates into space, the return signal is attenuated as the beam width increases with range. The radar pulse energy in the beam is dissipated much like the light waves in a flashlight beam (Nemec, 1986).

3) Variations in $Z - R$ Relationships and Below-Beam Effects

Because the return signal is influenced by drop size and is proportional to the sixth power of the hydrometeor's diameter, a considerably stronger signal is received from larger forms of precipitation. Consequently, studies have focused on drop size distribution as measured in stratiform rain, showers, and thunderstorms. Typically the $Z - R$ (Equation 1.15) coefficient increases and the exponent decreases with

convection intensity (Jones, 1955 and Fujiwara, 1965). Jones (1966) reduced radar errors from 62 to 43 percent by using storm specific $Z - R$ relationships.

Taking the analysis one step further, Atlas and Plank (1953) studied the evolution of the drop size distribution throughout a shower. They found that droplets initially had narrow spectra that shifted toward smaller sizes as the shower progressed. An examination of Texas thunderstorms showed relatively high number concentrations of large droplets during growth stages, when updrafts dominate, and large total droplet concentrations with smaller median diameters during declining or downward stages (Carbone and Nelson, 1978).

Many physical processes act to alter drop size distribution. Droplets often lose their sphericity and flatten as their size increases. Depending on the radar polarization, radar reflectivity may be enhanced or reduced several decibels, causing large errors in rainfall rate (Seliga and Bringi, 1976).

The rainfall process does not remain constant after each radar scan. Meteorological processes further alter precipitation before it reaches the ground. Studies noted that under certain conditions evaporation can reduce rainfall rates by 15 percent during a 300 meter fall. In addition, when horizontal wind speed and reflectivity gradients are large, precipitation drift below the elevated radar can be significant.

CHAPTER 2

METHODOLOGY

Flow in five drainage basins along the Alleghany River were chosen to verify runoff from several precipitation events. Using digitized radar reflectivity data from the NWS radar at Pittsburgh and unit hydrograph techniques, storm runoff and its timing characteristics are determined at each gauge station.

The runoff algorithm is a three step procedure: basin mapping and accumulation processing, unit hydrograph determination, and runoff/flood potential execution. The basin mapping and the unit hydrograph development are preparatory steps that must be accomplished only once for each basin.

1. Basin Description

The five drainage basins are situated in the southwest corner of Pennsylvania. Figure 2.1 shows the spatial relationship between the basins and the radar site. To illustrate the geomorphical diversity between basins and ultimately the universal application of unit hydrograph techniques, Tables 2.1 and 2.2 give a list of the basin's main physical characteristics These variables, to varying degrees, form the basis for the runoff response function. Each basin has a unique curve, mirroring the basin and channel network properties. The following definitions help clarify the nomenclature used in the tables:

1. Drainage area (AREA) is the area that contributes directly to surface runoff.

2. Main channel slope (SLOPE) is the difference in elevation at points 10 and 85 percent of the distance along the channel from the gauging
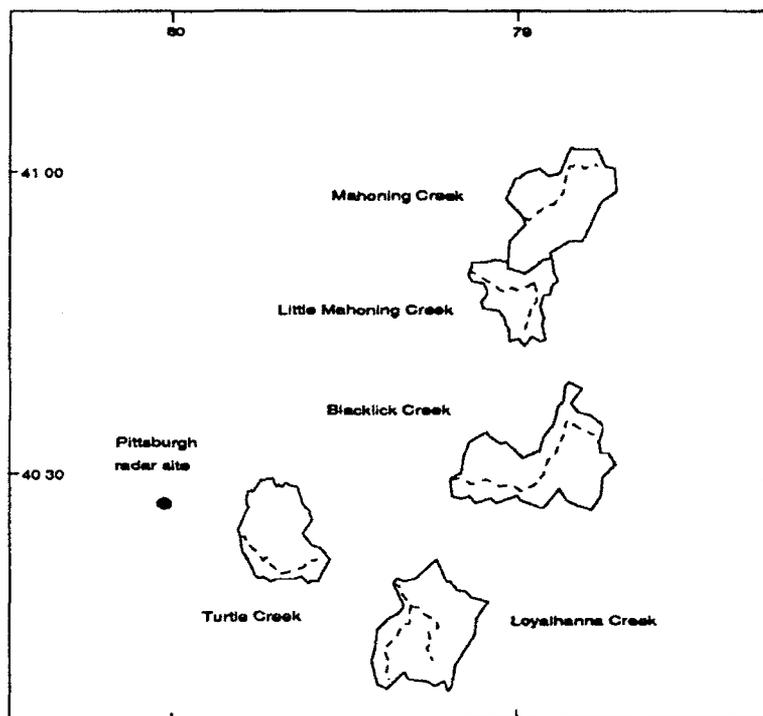
FIG. 2.1. Illustration of the five drainage basin locations relative to the Pittsburgh radar site. The dashed line shows the orientation of the main stream trunk

station to the basin's rim, divided by the distance between the two points.

3. Main channel length (LENGTH) is the length of the channel from the gauging station to the basin divide.

4. Mean base elevation (ELEVATION) is the average height, in feet, above National Geodetic Vertical Datum of 1929.

5. Forest cover (FOREST COVER) is the ratio of the forest cover, as shown on Geological Survey maps, to the drainage area.

6. Storage (STORAGE) is the percentage of the drainage area that includes lakes, ponds, and wetlands as shown on topographic maps.

2. Basin Mapping and Radar Data Processing

a. Basin Mapping

Outlining the basin is the first step of the mapping procedure. U.S. Geological Survey contour maps provide the most readily accessible source to identify each

TABLE 2.1.   Drainage basin characteristics from Wetzel and Bettandorff (1986).

BASIN	AREA (mi^2)	SLOPE (ft/mile)	LENGTH (miles)	ELEVATION (feet)
BLACKLICK CREEK	192.0	21.0	40.6	1780
LOYALHANNA CREEK	172.0	23.0	21.1	1730
TURTLE CREEK	55.9	21.0	15.1	1120
MAHONING CREEK	158.0	9.51	26.9	1570
LIL MAHONING CREEK	87.4	16.8	24.16	1550

TABLE 2.2.   Additional drainage basin characteristics from Wetzel and Bettandorff (1986).

BASIN	FOREST COVER (%)	ANNUAL PRECIPITATION (inches)	STORAGE (%)
BLACKLICK CREEK	47.0	46.0	0.10
LOYALHANNA CREEK	71.0	47.2	1.30
TURTLE CREEK	47.0	41.0	1.0
MAHONING CREEK	69.0	43.2	1.1
LIL MAHONING CREEK	44.0	44.3	1.00

basin. All water avenues filtering into the gauge site will be enclosed within the basin. Each gauge station marks the starting and completion point for the watershed.

The basin's perimeter is defined by drawing a line perpendicular from the gauge station through each contour line, up to the nearest peak. Subsequent lines are drawn perpendicular to the contour lines from elevation peak to elevation peak until the entire basin is outlined. To verify if the basin is correctly delineated, let an imaginary water drop fall within the basin's confines. The droplet will flow to the gauge station. If it does not reach the outlet point, reconfigure the basin.

b. Determine Active Radar Bins

Once the basin is outlined, radar reflectivity bins falling within the basin are identified. Methods to determine active radar bins include overlaying the basin with a radar bin grid (see Fig 2.2) or using trigonometric analysis. To be considered an active radar bin, the center point of each bin must fall within the basin. Those bins with only fractional areas within the basin must meet the above criteria. Repeat the procedure for all desired basins. Each basin will have a unique inventory of bins. No two distinct basins will share a radar reflectivity bin.

c. Radar Data Processing

Pittsburgh NWS RAdar DAta Processor, Version II (RADAP II) archived data provides the reflectivity information necessary to determine rainfall accumulations over each basin. The WSR-57 radar (see Table 2.3) used was part of a radar network to improve operational effectiveness of radar data through computer processing.
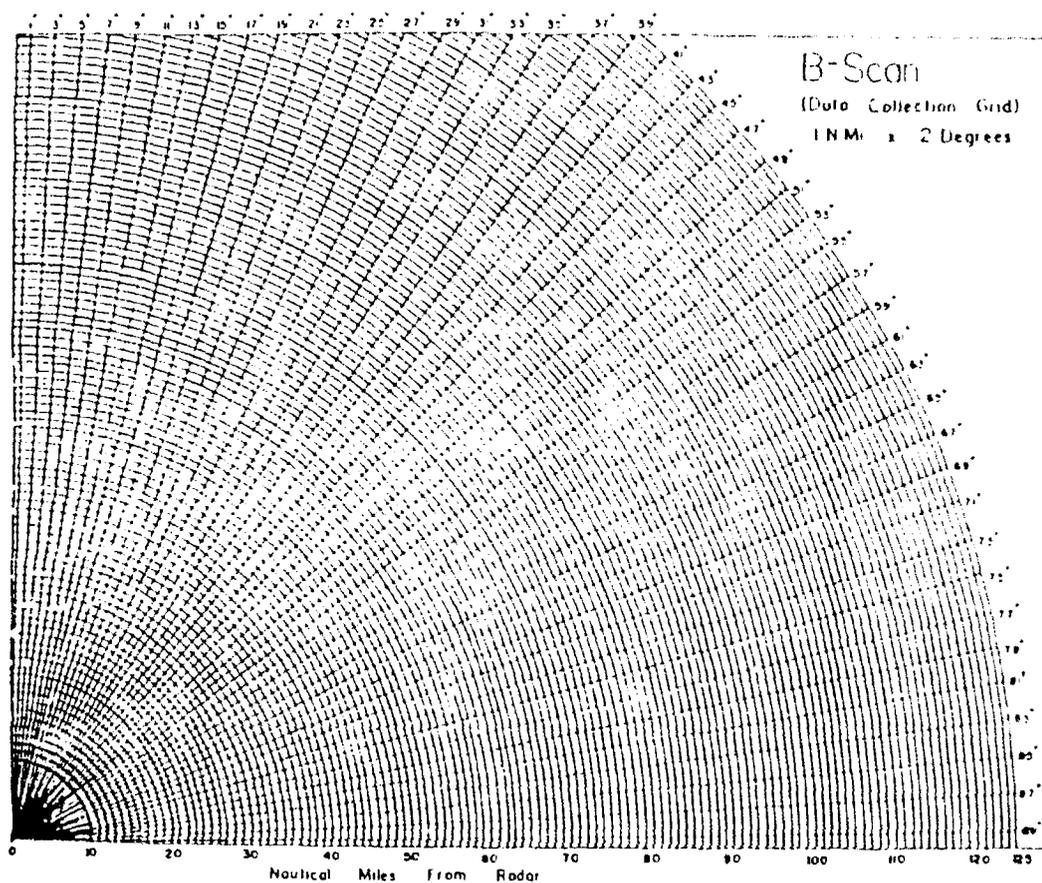
FIG. 2.2.   Diagram illustrating geometry of RADAP II data bin grid (McDonald and Saffle, 1989).

TABLE 2.3.   WSR-57 Radar Characteristics

Wavelength (cm)	10
Band	S
Frequency (Hz)	3000
Beamwidth (Deg)	2.2
Maximum Range (nm)	125

Based on the strength of the signal returned from the target, the radar receiver would estimate an equivalent reflectivity factor (in $mm^6 m^{-3}$). The reflectivity factor (Z) ranges from approximately 50 to 500,000 $mm^6 m^{-3}$. The receiver then calculates the logarithm of each estimated value of Z; the dynamic range of log Z is about 1.7

42

to 5.9. To further simplify data processing, the log Z is scaled upwards by a factor of 10 (10 log Z); these values are commonly referred to as dBZ values (McDonald and Saffle, 1989).

The RADAP II computer takes base elevation (0.5 degrees) observations every ten minutes. Each observation consists of 180 radials at ranges from 10 to 125 nm. The data are divided into 20,700 grid boxes, each which is 1 nm by 2 degrees of azimuth. Estimated radar rainfall rates are computed using the $Z - R$ relationship,

$$Z = 200\,R^{1.6}\ ,\qquad\qquad (2.1)$$

developed by Marshall and Palmer (1948). The data values range from 0 to 15 with each nonzero value representing a RADAP II category of radar reflectivity. Table 2.4 shows the hourly rainfall estimates and dBZ ranges of the RADAP II categories (Dragomir, 1990).

TABLE 2.4. Hourly rainfall estimates assigned to internal RADAP II levels from the RADAP II Operator's Manual, 1984.

INTERNAL RADAP LEVEL	HOURLY RAINFALL ESTIMATE	dBZ RANGE	STANDARD VIP LEVEL
1	0.03	18-24	1
2	0.07	25-29	1
3	0.15	30-34	2
4	0.29	35-37	2
5	0.45	38-40	3
6	0.58	41-42	3
7	0.75	43	3
8	0.91	44-45	3
9	1.15	46-47	4
10	1.49	48	4
11	1.82	49	4
12	2.46	50-52	5
13	3.48	53-54	5
14	4.50	55-56	5
15	4.50	57	6

3. Hydrograph Determination

a. Storm and Basin Selection

Viessman *et al.* (1977) cite that in developing a unit hydrograph, it is desirable to get as many rainfall records as possible within the study area to insure that the amount and distribution of rainfall over the watershed is accurately known. Preliminary selection of storms to use in deriving a unit hydrograph should be restricted to:

1. Storms occurring individually, that is simple storm structure.
2. Storms having uniform distribution of rainfall throughout the period of excess rainfall.
3. Storms having uniform spatial distribution over the entire watershed.

Several other restrictions are used as guidelines. The sizes of the basin should not exceed 1000 mi^2. One thousand acres is typically used as the lower limit; however, numerous physical factors define an appropriate response function. Studies indicate that direct runoff should range from 0.5 to 2.0 in. Finally, the duration of rainfall excess, D, should be approximately 20 to 30 percent of the basin lag time.

b. Separate Hydrograph

To determine the unit hydrograph for a drainage basin, it is necessary to separate outflow at the gauge site into two components: baseflow and surface runoff. During large storms, the maximum rate of discharge is just slightly affected by base flow, inaccuracies in separation are fortunately not important (Bedient and Huber, 1988). Several separation techniques have been devised but none are based on hydrological principles. Most hydrologists agree that whatever method is used, it must be employed consistently throughout the analysis.

The method used in this experiment required plotting the hydrograph. The separation is accomplished by joining a straight line from the beginning of surface
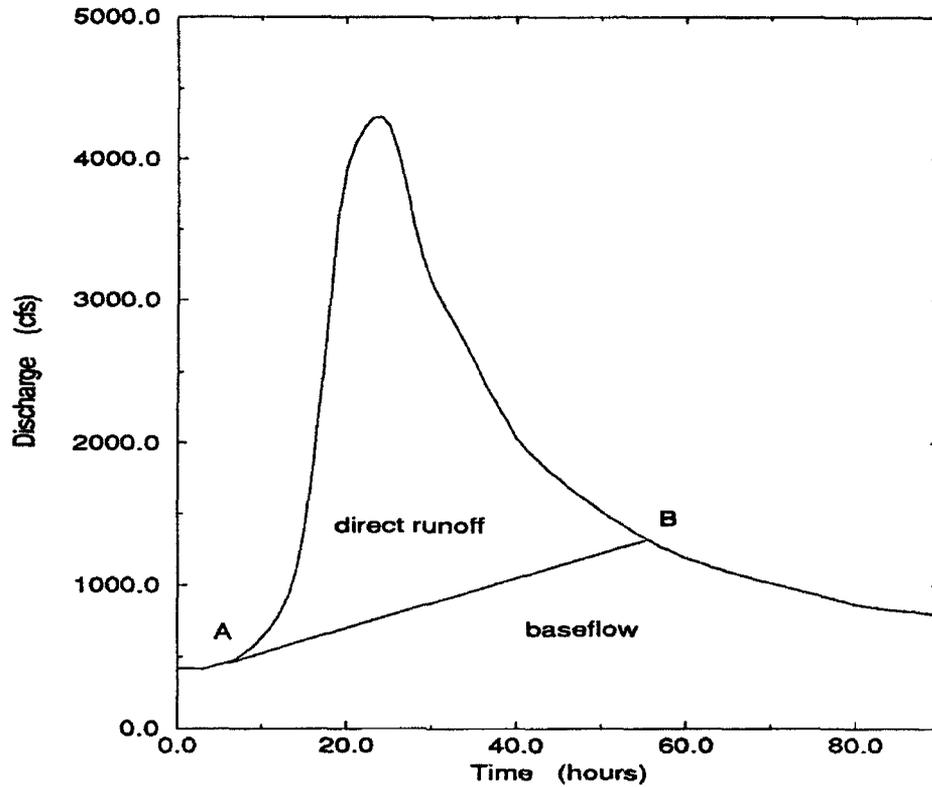
FIG. 2.3.   Illustration of baseflow/direct runoff separation.

runoff (pt. A) to a point on the recession limb representing the end of direct runoff (pt. B) (See Fig 2.3).

Usually, little difficulty is encountered in determining the start of the surface runoff; however, the break between the baseflow recession and direct runoff may be difficult to pinpoint. The recession limb of the hydrograph represents a series of depletion curves for the various components - baseflow, interflow, channel precipitation, and surface flow. It can be described mathematically as

$$Q_2 = Q_1 \, K^{-\Delta t} \, , \tag{2.2}$$

where Q_2 = the instantaneous discharge at time, t_2

Q_1 = the instantaneous discharge at time, t_1

K = the recession constant

Δt = the elapsed time, $(t_2 - t_1)$.

This equation produces a straight line when plotted on semilogarithmic paper (see Fig 2.4). Because of the effects of the different components of storage, the plot will be curvilinear having a series of line segments of different slopes (Gray, 1973). Each line segment's slope reflects the rate of decrease of discharge to the draining off process. The end of the direct runoff occurs at the beginning of the last curvilinear segment - the intersection of the baseflow recession curve with the total recession curve.
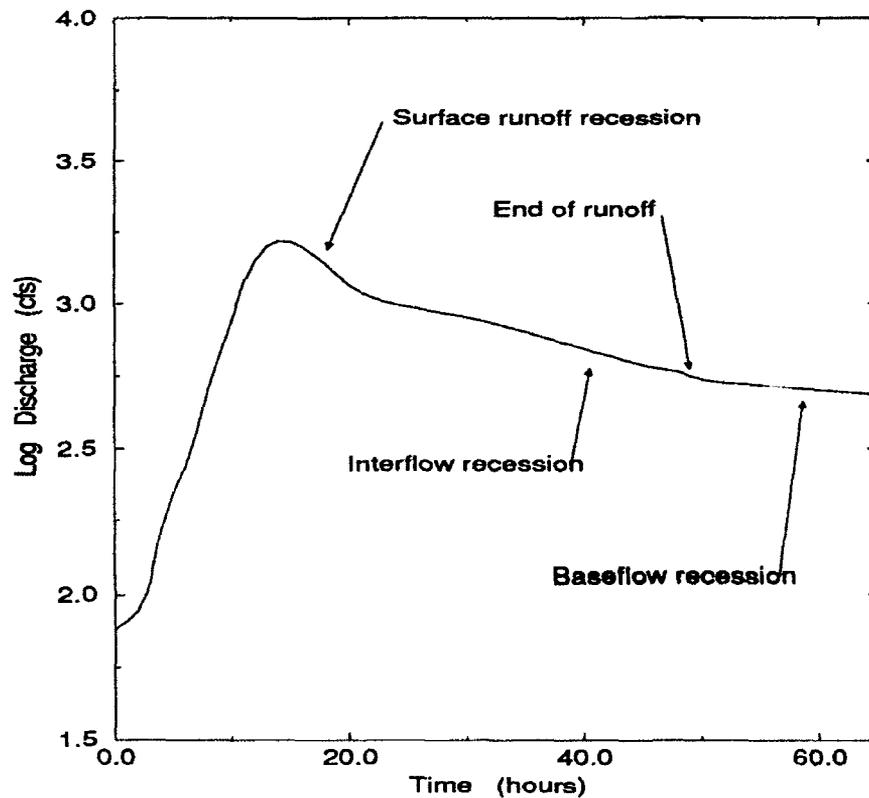
FIG. 2.4. Graphical method for determining the end of direct runoff.

c. Estimate Direct Runoff

After separating the direct surface runoff from the baseflow, plot the direct runoff ordinates. The area under the curve represents the total volume of runoff (see Fig 2.5). Area computations can be accomplished by planimeter, computer graphical techniques, or by using squared paper. The rainfall excess from the storm is calculated by dividing the total volume of direct runoff by the basin's area. This value can also be thought of as the equivalent depth of runoff spread uniformly over the basin (Shaw, 1988).
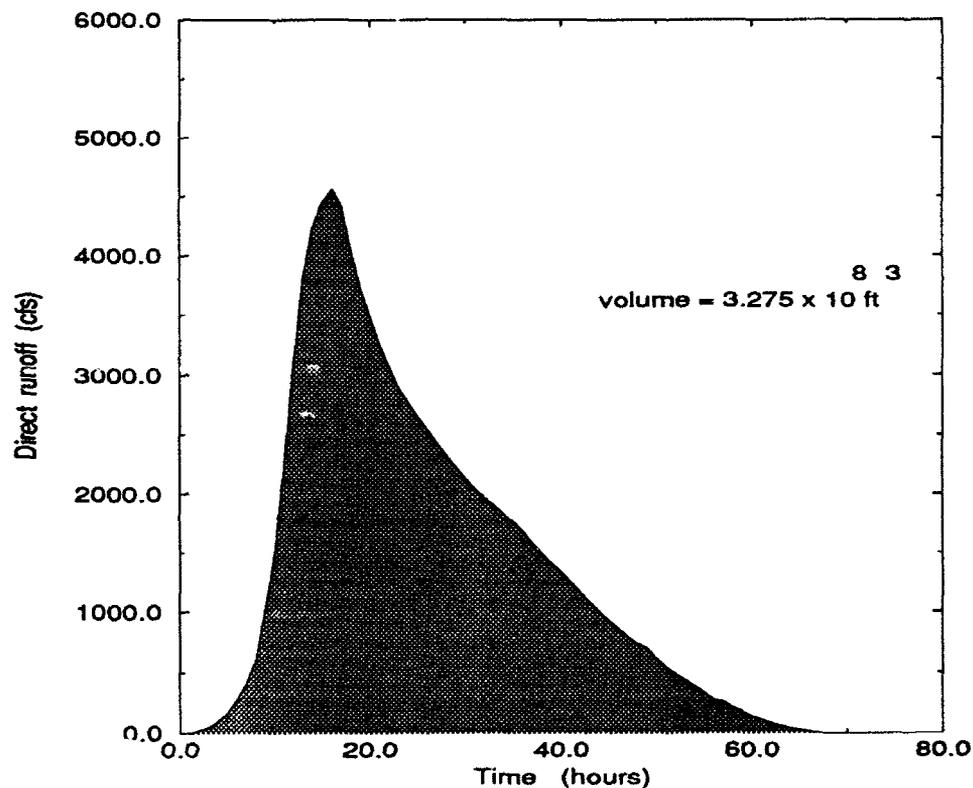
FIG. 2.5. Computation of direct runoff by integrating the area above the baseline separation line.

d. Infiltration Reduction

The rainfall excess describes that portion of total rainfall that becomes direct runoff. Using the rainfall hyetograph, convert total rainfall to effective rainfall by

applying the ϕ index infiltration method (see Fig 2.6). The ϕ infiltration method assumes that the total volume of storm period loss is distributed uniformly across the storm pattern. The volume of precipitation above the index line is equivalent to the runoff (rainfall excess). After calculating the part of the total rainfall that constitutes rainfall excess, determine the duration (D) of the rainfall excess.
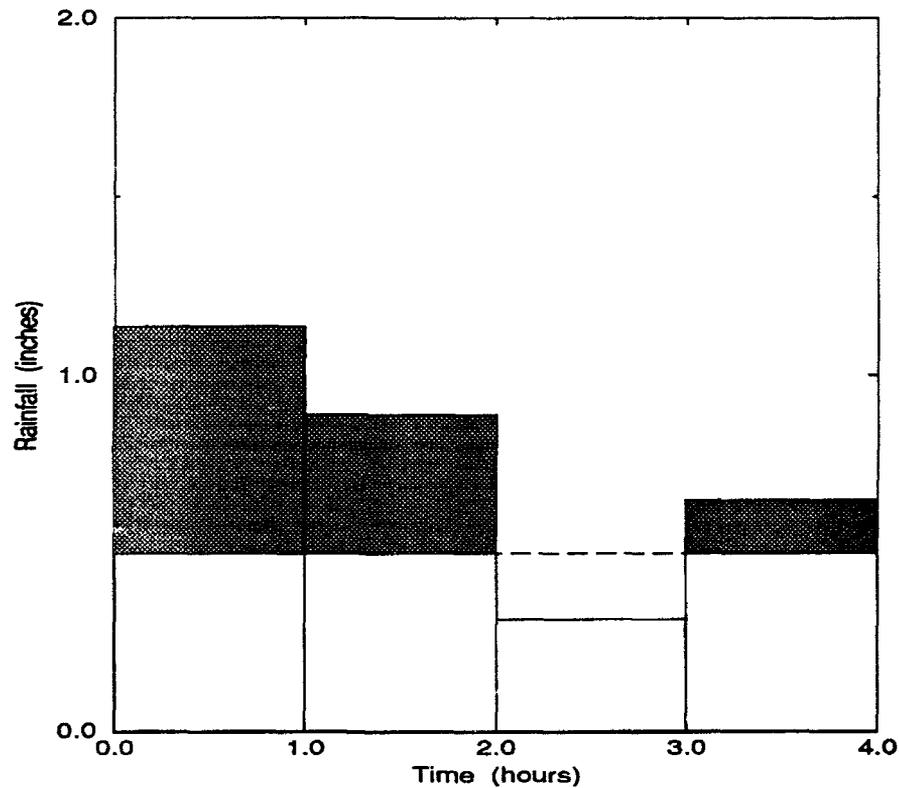
FIG. 2.6. Determination of rainfall excess (stippled area) using a ϕ rate infiltration rate (horizontal dashed line).

e. *Reduce to Unit hydrograph*

Divide the time axis of the hydrograph into convenient intervals. The interval duration most frequently used is hourly or some multiple of the radar scan period. The corresponding runoff ordinates to the time intervals are divided by the rainfall excess in inches (cm). Plot these results as a unit hydrograph for the basin.

48

f. Verify Result

Check the volume of the unit hydrograph. The area under the curve is equivalent to 1.0 inch over the entire basin's area. Graphically adjust the ordinates as necessary.

g. Repeat Procedure

Repeat the procedure for a number of storms that meet the criteria of section 3a. Obtain an average hydrograph for the basin (see Fig. 2.7). The average hydrograph may be constructed by taking the arithmetic mean of the peak flows and the times of rise. Using the previous two values as reference points, draw the hydrograph to match the general shape of the individual unit hydrographs.
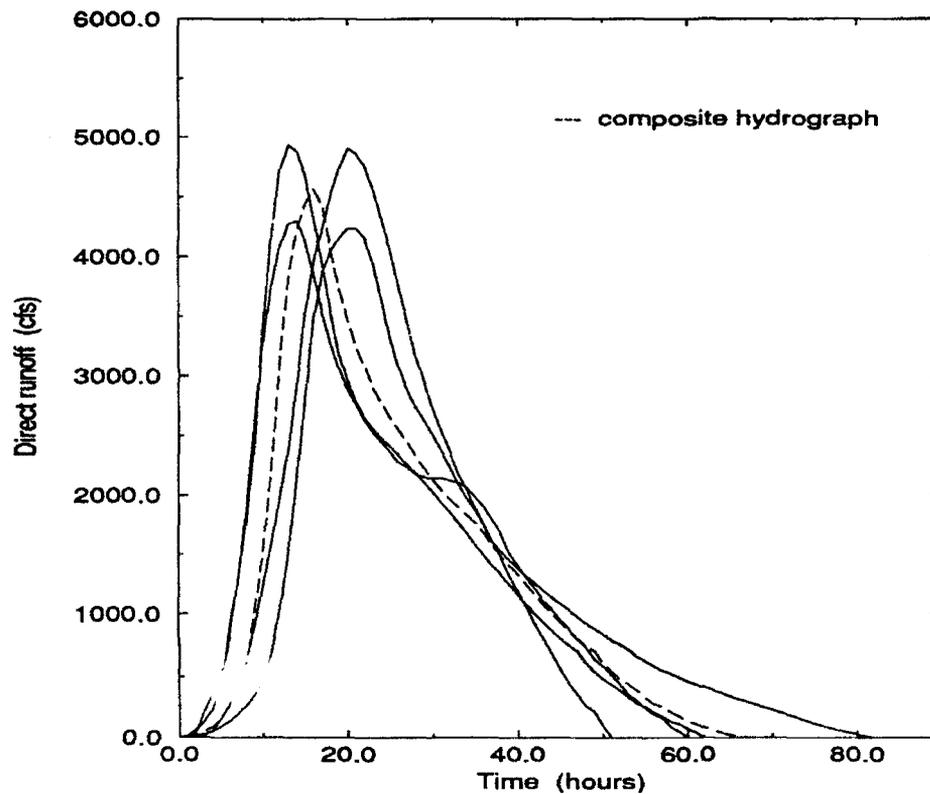
FIG. 2.7.   Derivation of a unit hydrograph from four storms.

4. Runoff Execution

Once the mapping and unit hydrograph procedures are completed, the actual execution of the runoff algorithm can begin.

a. Precipitation Processing

The first step in this procedure is to process the reflectivity data. Each scan is read by the computer, the reflectivity values are added together. Next, the reflectivity sum is divided by the total number of bins within each basin to get an average reflectivity value. The average basin reflectivity value is converted to an hourly rainfall accumulation using the corresponding reflectivity/rainfall relationships shown in Table 2.4.

Six hourly scans are processed to give one hourly rainfall estimate. Hourly estimates are used in this experiment because the available outflow data is measured on an hourly basis. Measurement intervals should be adapted to meet optimum experiment goals. Small basins (< 10 mi^2) have faster response functions and therefore may need shorter evaluation intervals.

b. Determine Rainfall Excess

After the rainfall accumulations are evaluated, these values are reduced by a constant infiltration rate. The resultant measurements reflect a rainfall excess for each time interval. Infiltration rates may be taken from basin geological survey reports or from averaging the portion of the hydrographs after the rainfall excess has been removed (see Fig 2.8). This value, a measure of the infiltration rate, reflects the difference between the total rainfall and the rainfall excess.

c. Apply Convolution Integral

The linear response of a basin to any rainfall input is proportional to the unit hydrograph. This proportionality can be generalized to compound storms as well
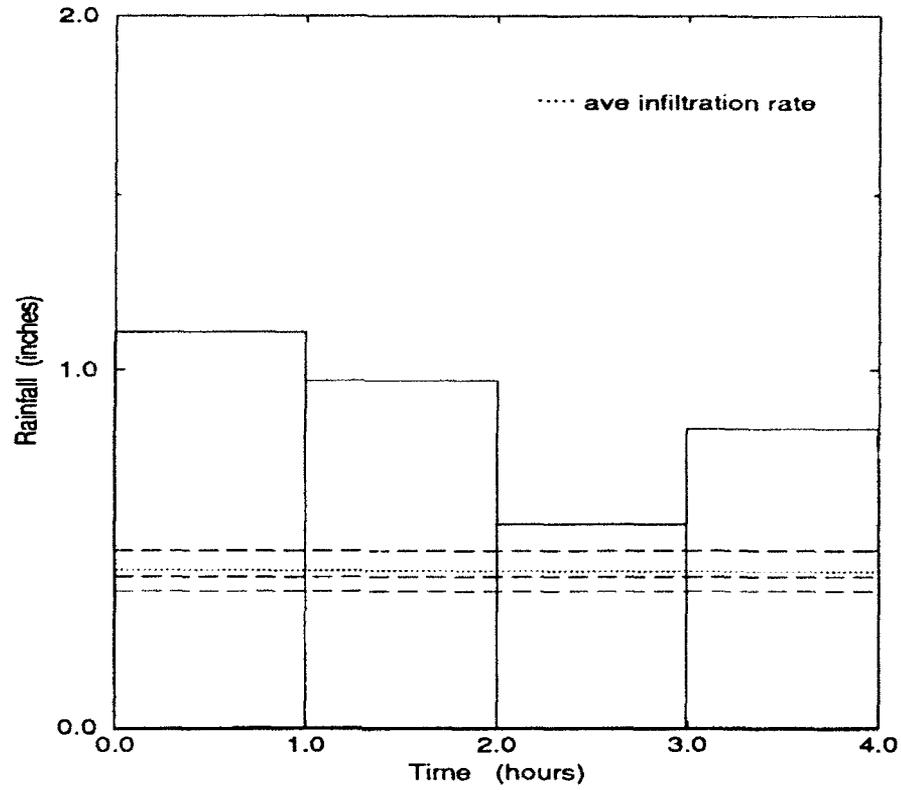
FIG. 2.8. Determination of basin infiltration rate by averaging the ϕ index loss rates from three storms.

as individual events. Figure 2.9 shows a compound storm extending over three time periods and the unit hydrograph. The storm hydrograph can be expressed by a series of equations representing the response function (h) ordinates and those of the rainfall excess (i):

$$i_1\, h_1 = Q_1$$

$$i_2\, h_1 + i_1\, h_2 = Q_2$$

$$i_3\, h_1 + i_2\, h_2 + i_1\, h_3 = Q_3 \qquad (2.3)$$

$$i_3\, h_2 + i_2\, h_3 + i_1\, h_4 = Q_4$$

$$i_3\, h_3 + i_2\, h_4 = Q_5$$

$$i_3\, h_4 = Q_6$$
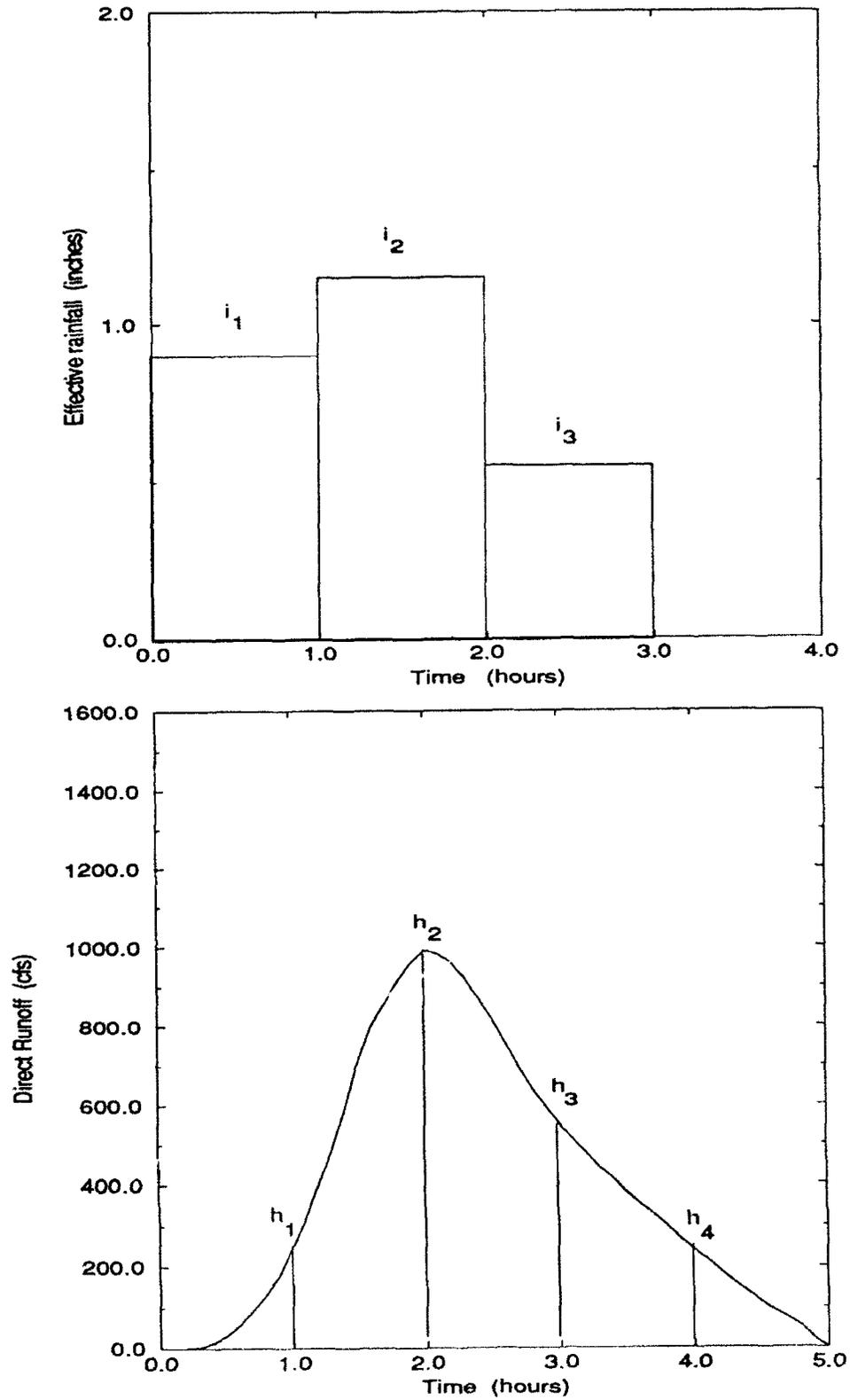
FIG. 2.9.   Determination of a storm hydrograph using rainfall excess and unit hydrograph inputs.

The relationship between the unit hydrograph, the rainfall excess, and the storm hydrograph time periods follows the form

$$n = j + i - 1 \ , \tag{2.4}$$

where n = the number of storm hydrograph ordinates

j = the number of unit hydrograph ordinates

i = the number of periods of rainfall excess

The system of equations can be expressed as

$$Q_i = \sum_{j=1}^{i} i_j \, h_{i-j+1} \ , \tag{2.5}$$

which is the discrete form of the convolution integral.

5. Flood Prediction

After summing the products of rainfall excess and basin response inputs, the stream flow hydrograph is plotted (see Fig 2.10) and flooding potential can be examined. To simplify the problem, hydrologists typically investigate the relationship between river height and discharge. River height or stage refers to the elevation of the water surface above some arbitrary datum (Dunne and Leopold, 1978). A rating curve can be developed if discharge is simultaneously plotted against the corresponding stage. Once this relationship is established, the river's threshold value is determined. Flood potential can be computed as

$$FLD - POTENTIAL = \left[\frac{RUNOFF + BASEFLOW}{THRESHOLD} \right] \times 100 \ , \tag{2.6}$$

where $FLD - POTENTIAL$ = probability of flood occurrence (%)

$RUNOFF$ = maximum predicted runoff ordinate (cfs)

$BASEFLOW$ = average baseflow rate for the basin (cfs)

$THRESHOLD$ = the river's maximum flow capacity (cfs).
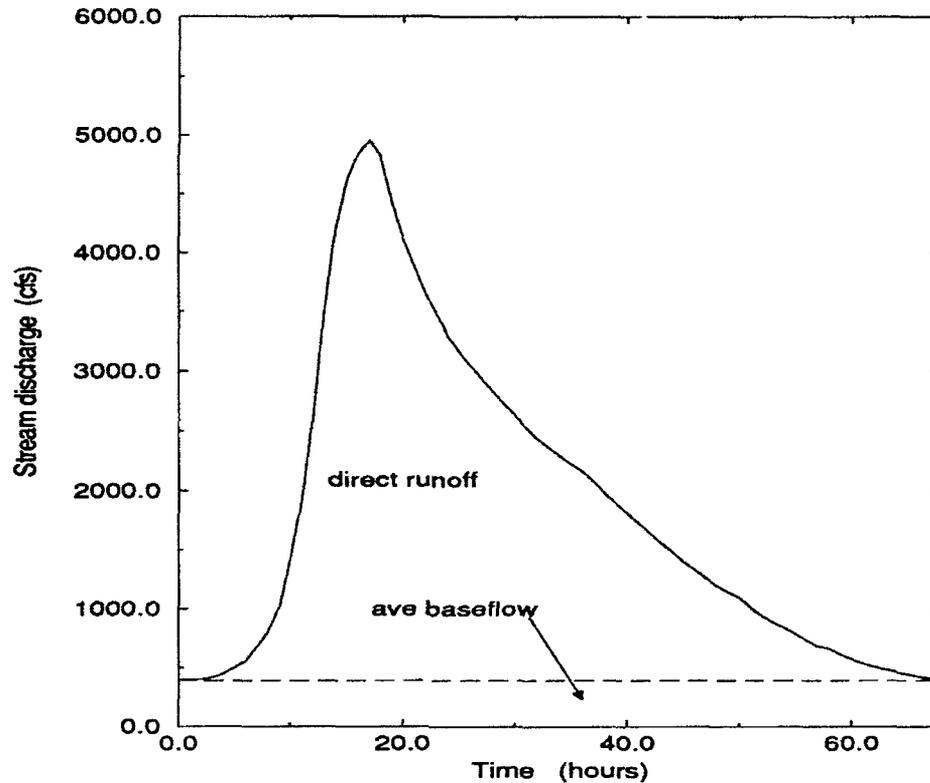
FIG. 2.10.   Forecasted stream flow hydrograph using a constant baseflow rate (400 cfs).

If the flood potential exceeds 100 percent, a flood near the gauging sta ion is likely (see Fig 2.11). Inferences about the flooding probability both upstream and downstream require careful examination. Basin thresholds vary and extending flood criteria to other locations should be done on a case by case basis.

Once the river's capacity has been surpassed, the flood time is computed. This time will be differentiated from the stream flow hydrograph (see Fig 2.11). If necessary, the flood inundation period can also be assessed. The duration is measured by subtracting the time the bank overflowed from the anticipated time the level will recede below the critical flow capacity.
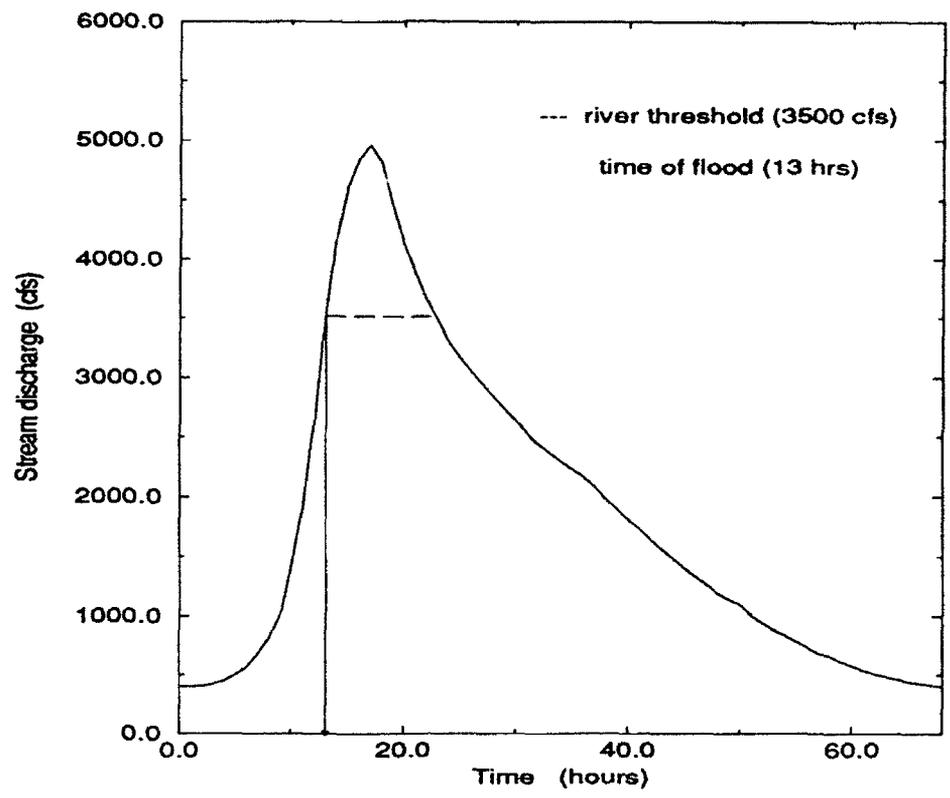
FIG. 2.11. Determination of flood time from the river's threshold capacity.

CHAPTER 3
ANALYSIS

Runoff analysis at the five watersheds is accomplished using the Pittsburgh RADAP II data, basin unit hydrographs, and Army Corps of Engineers discharge data. After the radar reflectivity data is processed into hourly accumulations, each rainfall increment is reduced by a constant basin infiltration rate. Next, the discrete form of the convolution integral (2.5) is applied. Unit hydrograph ordinates are multiplied by rainfall excess and lagged in sequence to produce the resulting storm hydrograph. All time increments of rainfall excess correspond to the duration of the unit hydrograph - one hour intervals.

The five unit hydrographs are plotted in Figure 3.1. Each response curve reflects the basin's unique behavior to one inch of uniformly distributed rainfall excess. The curves are composites from basin outflow data from 1986 - 1989. A minimum of four unit hydrographs were used to establish each basin's average unit hydrograph.

Examining the unit hydrograph plot, the volume of runoff for each basin is proportional to the area under each curve. Blacklick Creek (192 mi^2), has the greatest runoff volume (measured in million cubic feet (mcf)). Alternatively the smallest basin, Turtle Creek (55.9 mi^2), has the least runoff volume per rainfall input.

On the other hand, Turtle Creek (6247 cfs) has the highest runoff peak while Little Mahoning Creek (3953 cfs) has the lowest one. The runoff peak is the most significant hydrograph feature. The moment of greatest danger and maximum inun-
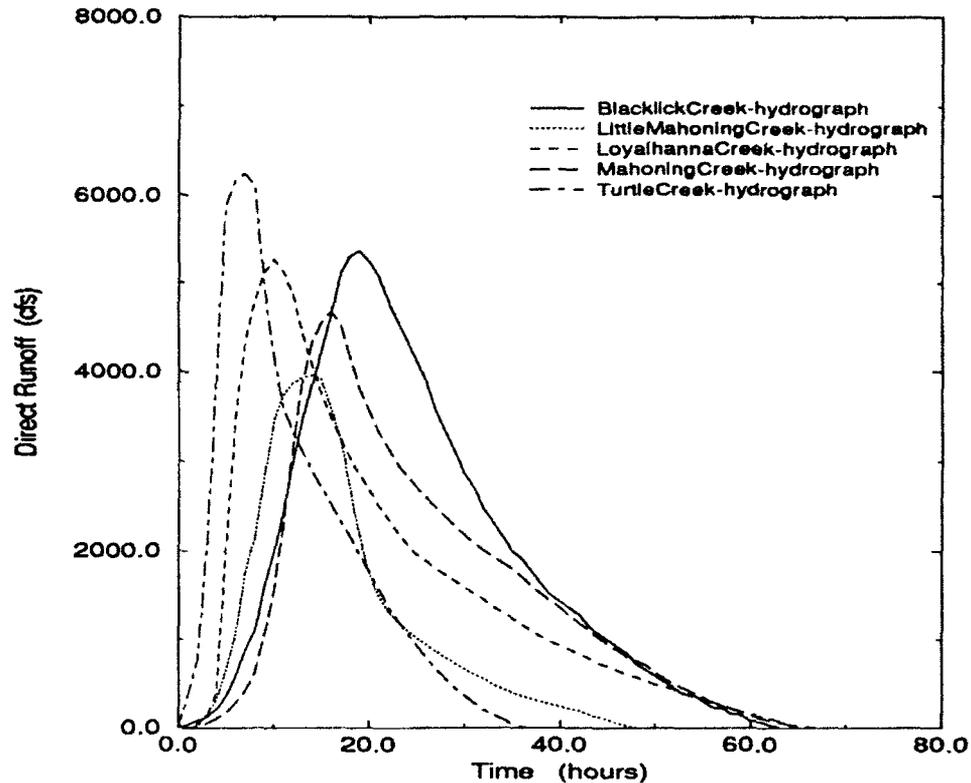
FIG. 3.1. A comparison of the five basin's unit hydrographs used in this experiment.

dation occurs at this point. Turtle Creek's sharp peak reflects the explosive nature of its runoff response. Flood potential will be most likely at this time also.

Even though Blacklick Creek has a larger basin area to contribute direct runoff, the discharge response function is spread over a longer time period. Subsequently the peak is less severe but if a flood should occur, duration of damage will most likely be longer. No generalized hydrological relationships should be drawn from these assessments. The comparisons are only highlighted for the purpose of seeing how close these pattern are maintained during the actual rainfall/runoff case studies.

The final timing parameter associated with the statistical likelihood of a flood is the *time of rise*. The duration from the runoff start to the peak discharge is critical in flood prediction. This is largely because people generally do not become concerned with flooding until actual flood conditions have been reached (Sheaffer,

1961). Again Turtle Creek (7 hrs) shows the must rapid or quickest time response to peak runoff. Blacklick Creek displays the slowest time of rise (19 hrs).

The accuracy of the unit hydrograph technique is explored through the aforementioned hydrograph characteristics in addition to a comparison of the track's shape. Usable radar reflectivity data for the Pittsburgh area is limited to March through October 1989. Because of the limited number of precipitation days, the sample size is too small to statistically generalize the technique results to all rainfall/runoff events. Samples should be as large as possible; in general, the larger the sample, the more representative it is likely to be. Minimum acceptable sample sizes depend on the type of research. For test case experimental research, 15 events per study is appropriate. Even large samples can lead to erroneous conclusions if they are not well selected (Gay, 1987).

The acceptability of the unit hydrograph technique will be measured by how well the predicted runoff parameters compare with the measured ones. The forecast and measured runoff (total discharge - baseflow) values are both scrutinized at the gauge stations. The hydrograph characteristics will be evaluated by the following two error analysis methods:

$$\epsilon = \tilde{r} - r \qquad (3.1)$$

and

$$\epsilon_r = \frac{\epsilon}{r} = \frac{\tilde{r} - r}{r} \qquad (3.2)$$

where ϵ = absolute error

$\tilde{r}$ = predicted variable

r = observed variable

ϵ_r = relative error

Equations 3.1 and 3.2 represent the absolute and relative errors, respectively, between the flood variables evaluated in this experiment. Hydrograph technique results will be examined on a basin by basin basis.

1. Blacklick Creek Hydrograph Analysis

Five radar recorded precipitation events in 1989 were used to verify runoff characteristics for the Blacklick Creek basin. Other radar precipitation producing events during the year over Blacklick Creek were unable to generate significant runoff. For this basin a minimum average internal RADAP level greater than 2 (0.07 in/hr) was needed to obtain a rainfall rate high enough to produce runoff once a constant infiltration loss was subtracted. A ϕ infiltration rate of 0.07 in/hr was used for the Blacklick Creek watershed.

The March 28 storm is the first and strongest precipitation producing event used for Blacklick Creek. Figure 3.2 shows the predicted and observed hydrograph tracks for the three hour precipitation input totalling 0.96 inches (see Table 3.1). The tracks are similar in shape with the exception of the predicted track's peak being skewed to the right and having a shorter time base.

TABLE 3.1. Rainfall characteristics for Blacklick Creek

Date 1989	Radar Rainfall (in)	Duration (hrs)	Basin Radar Coverage (%)
28 Mar	0.96	3	64
31 Mar	0.47	1	57
18 Apr	0.25	1	96
28 Jun	0.24	2	99
30 Jul	0.48	1	99
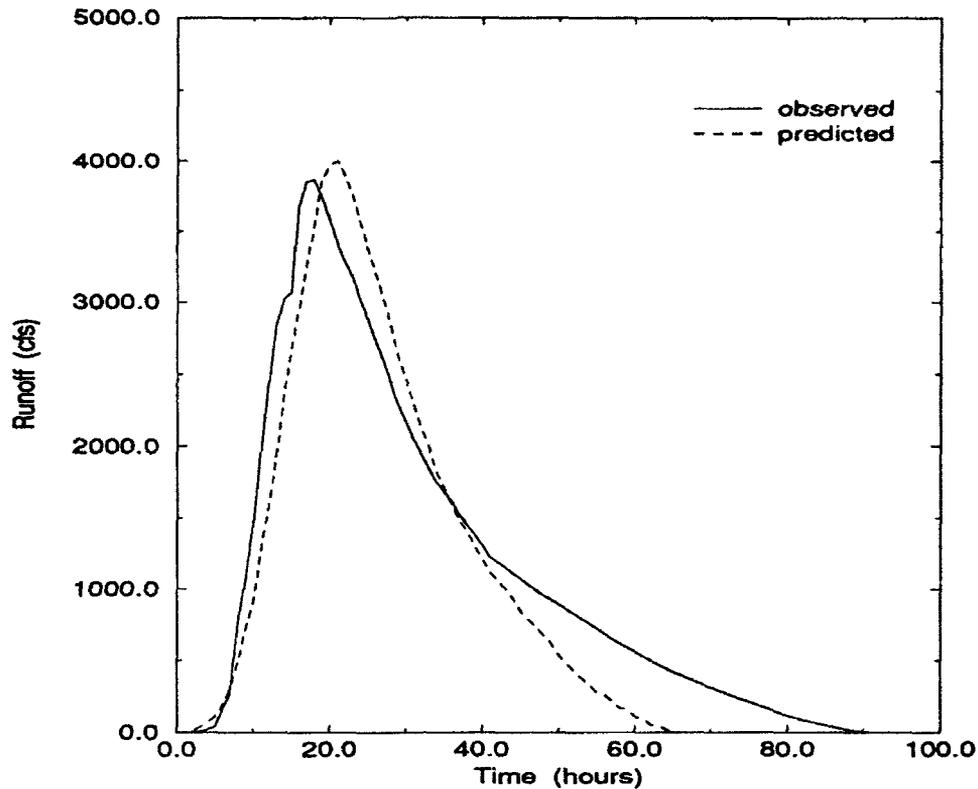
FIG. 3.2. Observed and predicted hydrograph tracks for Blacklick Creek, 28 March 1989.

Because of the shorter runoff duration, the predicted runoff volume is 12 % lower (see Table 3.2). The observed rainfall excess (total runoff volume divided by the basin area) of 0.85 inches compares favorably to the total radar determined rainfall (0.96 in) once the basin infiltration rate (0.07 in) is subtracted. As a result of the shorter time base, the predicted rainfall excess (0.74 in) is 12.9 % lower than the observed value (see Table 3.3).

An examination of peak outflow reveals the predicted maximum value (4002 cfs) is 133 cfs higher than the observed peak. The peak runoff difference accounts to a 3.4 % relative error (see Table 3.4). The times of rise for this event showed the faster response time for the observed track (18 hrs) as compared to the predicted one (21 hrs). As a whole the predicted track adequately paralleled the observed track with some minor deviations.

TABLE 3.2. Predicted and observed runoff volumes for Blacklick Creek.

Date 1989	Observed Runoff Volume (mcf)	Predicted Runoff Volume (mcf)	Absolute Error (mcf)	Relative Error (%)
28 Mar	378.1	332.1	-46.0	-12.2
31 Mar	179.8	175.5	-4.3	-2.4
18 Apr	149.3	77.9	-71.4	-47.8
28 Jun	56.5	44.2	-12.3	-21.8
30 Jul	270.4	180.2	-90.2	-33.3

TABLE 3.3. Predicted and observed rainfall excess for Blacklick Creek.

Date 1989	Observed Rainfall Excess (in)	Predicted Rainfall Excess (in)	Absolute Error (in)	Relative Error (%)
28 Mar	0.85	0.74	-0.11	-12.9
31 Mar	0.40	0.39	-0.01	-2.5
18 Apr	0.33	0.17	-0.16	-48.5
28 Jun	0.13	0.10	-0.03	-23.1
30 Jul	0.61	0.40	-0.21	-34.4

The next precipitation case study occurred three days later on March 31. The observed and predicted tracks are nearly identical (see Figure 3.3). A one hour radar rainfall accumulation of 0.47 inches produced an observed runoff of 179.8 mcf. The predicted runoff volume (175.5 mcf) equates to a 2.4 % relative error.

Due to the nearly identical pattern of the tracks, all the key characteristics will be consistent. The observed rainfall excess (0.40 in) perfectly matches the reduced
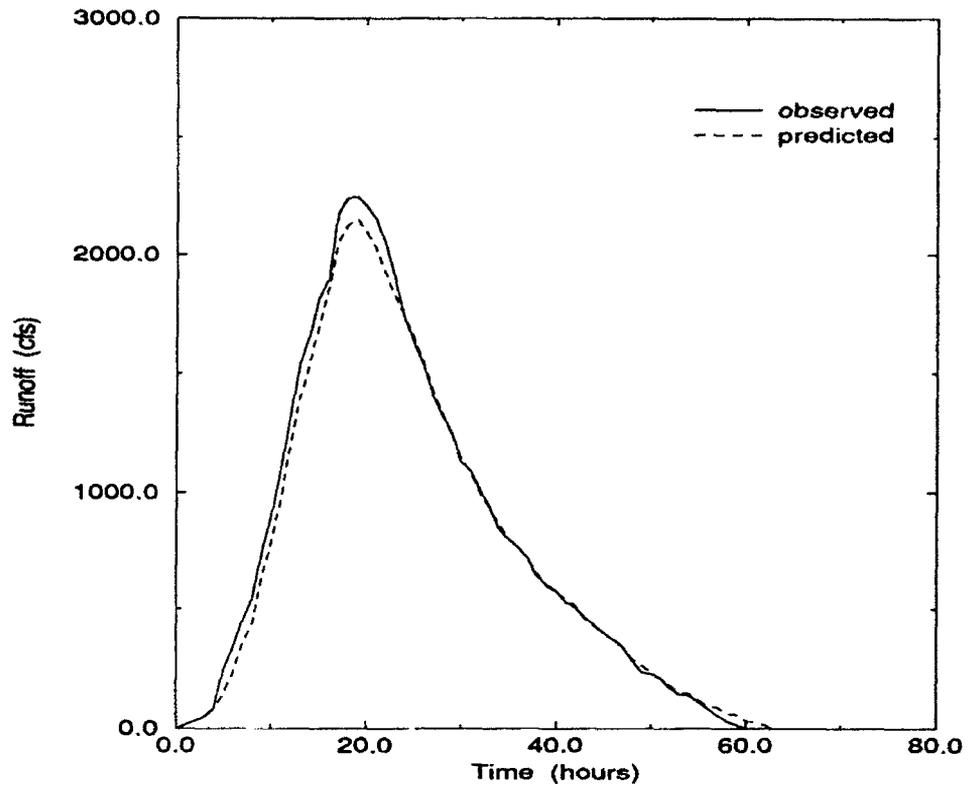
FIG. 3.3. Observed and predicted hydrograph tracks for Blacklick Creek, 31 March 1989.

TABLE 3.4. Predicted and observed peak runoff for Blacklick Creek

Date 1989	Observed Peak (cfs)	Predicted Peak (cfs)	Absolute Error (cfs)	Relative Error (%)
28 Mar	3869	4002	133	3.4
31 Mar	2244	2148	-56	-2.5
18 Apr	1519	967	-552	-36.3
28 Jun	619	533	-86	-13.9
30 Jul	3173	2202	-971	-30.6

radar rainfall accumulation (0.47 - 0.07 = 0.40 in) while the predicted rainfall excess was only one hundredth of an inch off (0.39 in).

TABLE 3.5. Predicted and observed times of rise for Blacklick Creek

Date 1989	Observed Time of Rise (hrs)	Predicted Time of Rise (hrs)	Absolute Error (hrs)	Relative Error (%)
28 Mar	18	21	3	16.7
31 Mar	19	19	0	0
18 Apr	22	19	-3	-13.6
28 Jun	34	20	-14	-41.1
30 Jul	21	19	-2	-9.5

The observed and predicted peak outflow compare favorably with each other. A difference of 56 cfs produced a −2.5 % relative error. Peak outflows occurred at the same time so that the time of rise for each track (19 hrs) was identical (see Table 3.6). Consequently both measurement errors were zero. Clearly, the predicted hydrograph matched the observed one to a high degree of accuracy.

April 18 marks the third precipitation event (see Figure 3.4). The hydrograph shapes are similar but the sizes are substantially different. In addition, the observed track has a saw tooth notch prior to the peak outflow. These shape characteristics are not evident with the predicted tract. Furthermore, the observed runoff is almost twice (47.3 %) the volume as the predicted quantity.

The observed rainfall excess is higher (by 0.08 in) than the radar determined rainfall accumulation - even without an infiltration rate reduction. Two error scenarios are possible: the radar underestimates the rainfall accumulation or the discharge data is in error. Blacklick creek had radar reflectivity returns in 96 % of the bins so coverage criteria was in agreement with unit hydrograph assumptions. The possibility of either conclusion must be based on additional events.
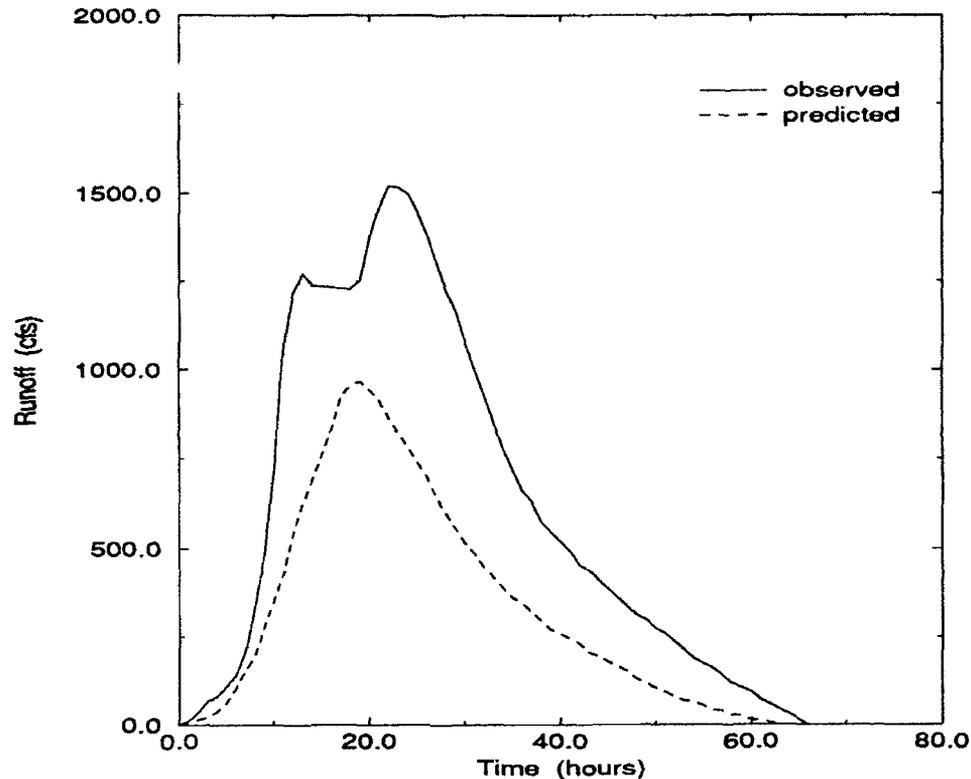
FIG. 3.4. Observed and predicted hydrograph tracks for Blacklick Creek, 18 April 1989.

Likewise, the observed peak outflow (1519 cfs) differed considerably from the predicted outflow (967 cfs). Also the time of rise for the observed track (22 hrs) occurred three hours later than the predicted track (19 hrs). The critical failure of the predicted tract is its underestimation of possible flood conditions. Even though the outflow was low, the error between hydrograph variables was considerable.

The fourth case study occurred on June 28 (see Figure 3.5). A general track description shows the predicted path is considerably skewed left of the observed track. Runoff volumes are comparatively low. The two hour radar rainfall accumulation of 0.24 inches does not follow the trend of the several rises and falls in the observed runoff. This could be the result of hourly rainfall averaging reducing usable radar rainfall reflectivities below the runoff criteria. In addition, smaller rainfall variations will be smoothed out in the convolution process.
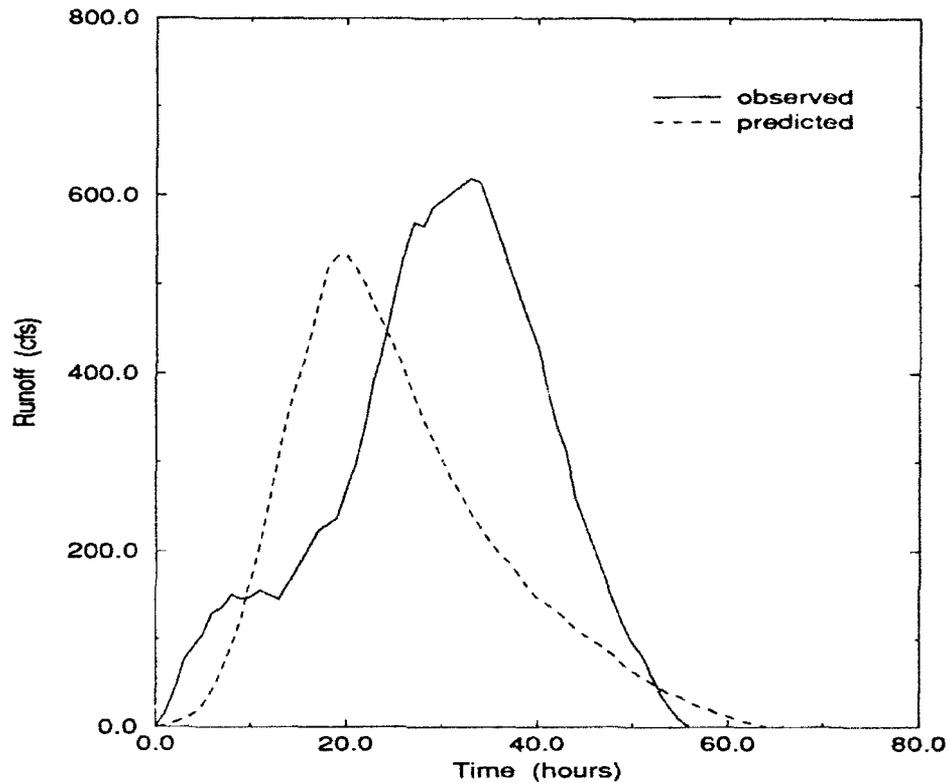
FIG. 3.5. Observed and predicted hydrograph tracks for Blacklick Creek, 28 June 1989.

The observed and predicted rainfall excesses are consistent (0.13 and 0.10 in respectively) with the reduced radar accumulation total (0.17 in). Also the observed peak runoff (533 cfs) is within reasonable expectation of the observed peak flow (619 cfs). Lastly, the observed time of rise (34 hrs) shows a wide disparity (14 hrs) with the predicted value (20 hrs). A −41.1 % relative error is too large for forecast requirements. Predicted variables have considerable variation at lower rainfall accumulation totals.

July 30 is the final date for the Blacklick Creek case study (see Figure 3.6). The hydrograph shapes are consistent although the predicted track underestimates the magnitude of the runoff. The relative error between the two runoff volumes is −33 %. Again as in the April 18 case study, the observed rainfall excess exceeded the total radar determined value. In this instance the difference is 0.13 inches. The radar

determined accumulation (0.48 in) falls close to the recommended depths for hydrograph analysis. However observed rainfall excess should not exceed radar derived values. A secondary rain gauge network would be helpful in verifying measurements.
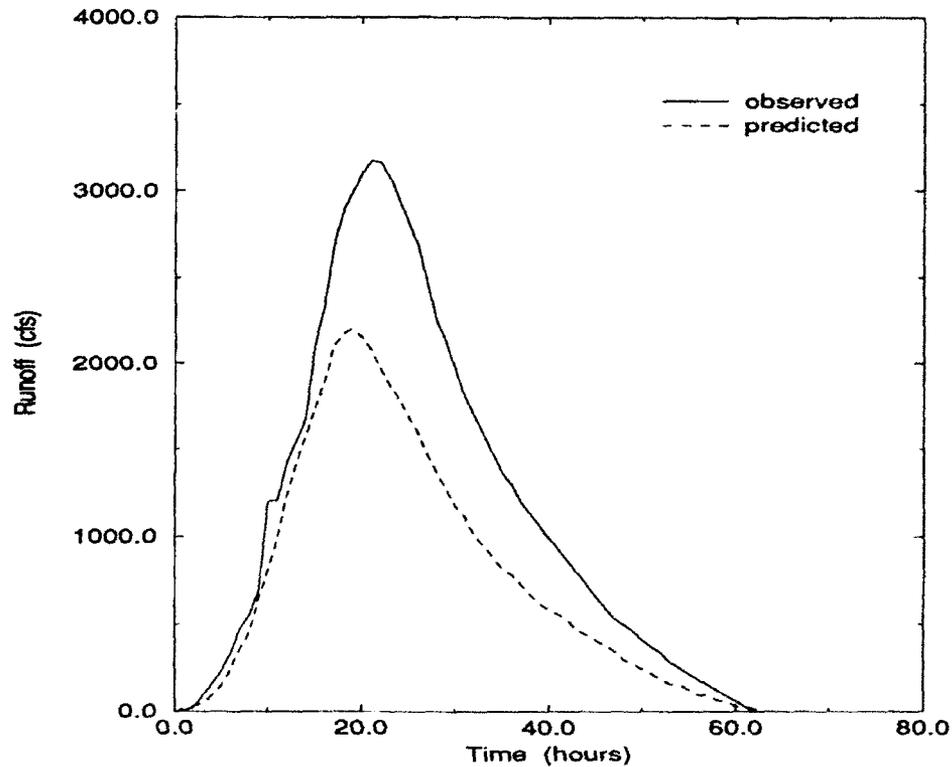
FIG. 3.6. Observed and predicted hydrograph tracks for Blacklick Creek, 30 July 1989.

As expected predicted peak outflow (2202 cfs) lagged maximum observed outflow (3173 cfs) by -30.6 %. However, the time of rise period for the two tracts was more consistent. The absolute error between the two tracks was only two hours. Examination of further Blacklick Creek events should concentrate on the possibility of a systematic radar rainfall underestimate.

2. Little Mahoning Creek Hydrograph Analysis

Little Mahoning is the next watershed to be analyzed. This basin case study contains the most precipitation events (7). An examination of the March 18 hydrographs (see Figure 3.7) reveals nearly identical paths for the first one-third of the track. Beyond that point the predicted track fails to identify a temporary leveling off segment and tends to taper off faster than the observed path. Radar bin coverage was 63 % (see Table 3.6).
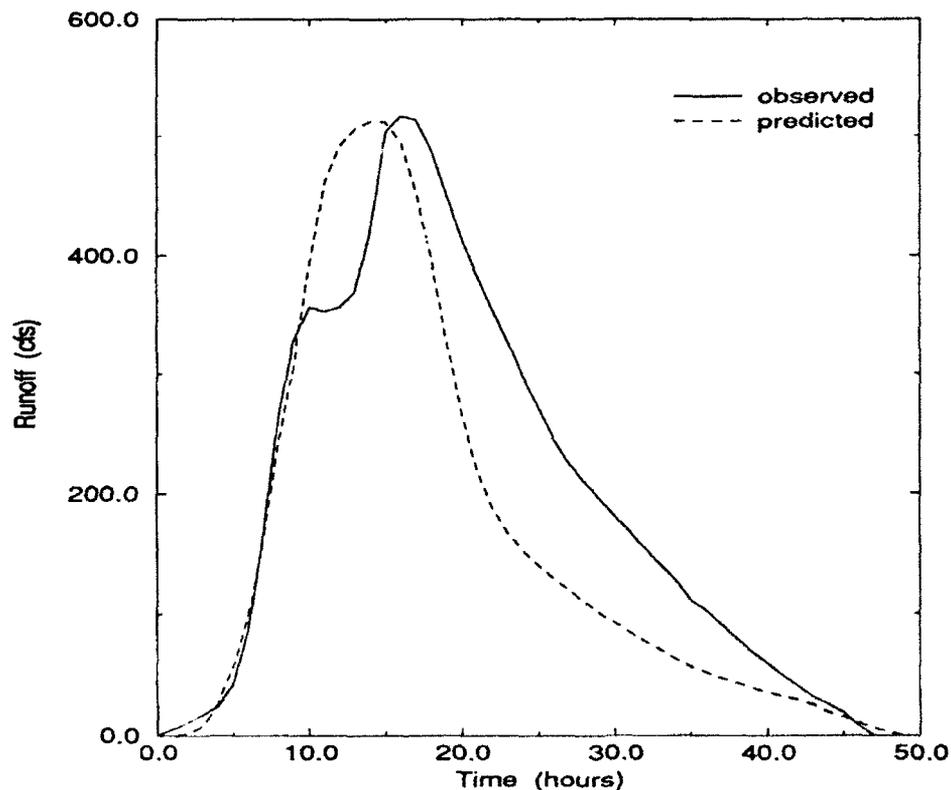
FIG. 3.7. Observed and predicted hydrograph tracks for Little Mahoning Creek, 18 March 1989.

TABLE 3.6.   Rainfall characteristics for Little Mahoning Creek

Date 1989	Radar Rainfall (in)	Duration (hrs)	Basin Radar Coverage (%)
18 Mar	0.23	2	63
28 Mar	0.90	2	66
30 Mar	0.53	2	61
31 Mar	0.47	1	86
15 May	0.19	1	100
27 Jun	0.32	1	69
19 Oct	0.11	1	100

The infiltration rate (0.05 in/hr) reduced radar accumulation (0.18 in) agrees with the observed (0.17 in) and predicted (0.14 in) rainfall excesses. However, the observed and predicted runoff volumes differed by 19 %. The peak runoff totals almost matched for the observed (517 cfs) and predicted (512 cfs) outflows. The relative error between the two peak values was -1.0 %.

Lastly, the observed time of rise was two hours later than the predicted one, corresponding to a −12.5 % relative error. A cursory glance indicates the two tracks are in approximate agreement. Outflow deviations; however, tend to be smoothed out with low rainfall totals. Fortunately flooding conditions rarely occur, if ever, with such small rainfall inputs.

March 28 is the next case study (see Figure 3.8). The hydrograph shapes are in complete agreement with one another. A two hour radar determined rainfall total of 0.90 inches was 0.06 inches lower than the observed rainfall excess value (0.96 in) before any infiltration rate reduction Observed and predicted runoff volumes were only 10.7 % apart.
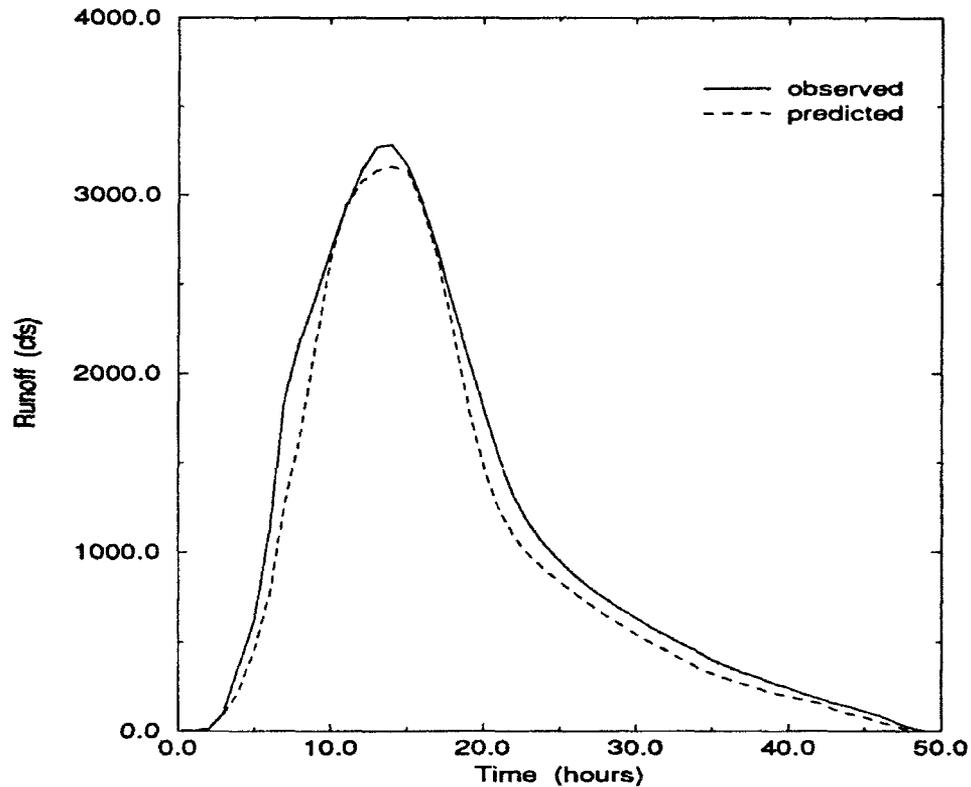
FIG. 3.8. Observed and predicted hydrograph tracks for Little Mahoning Creek, 28 March 1989.

In addition, the observed (3284 cfs) and predicted (3159 cfs) peak outflows showed only a small deviation. The times of rise for the observed and predicted tracks matched perfectly (14 hrs). This case study demonstrates the application of hydrograph methodology to accurately forecast runoff from moderate rainfall.

The next precipitation event occurred two days later on March 30 (see Figure 3.9). Again the observed and predicted hydrographs matched closely. This time the predicted track slightly overestimated the observed one. Past cases tended to underestimate runoff. Antecedent moisture conditions or prewetting may have played a factor in this reversal. The predicted runoff was 18.7 % higher than the observed runoff.

The other characteristics were in better agreement. The observed peak (3284 cfs) was 3.8 % higher than the predicted peak outflow (3159 cfs). Again the time

TABLE 3.7.   Predicted and observed runoff volumes for Little Mahoning Creek.

Date 1989	Observed Runoff Volume (mcf)	Predicted Runoff Volume (mcf)	Absolute Error (mcf)	Relative Error (%)
18 Mar	35.2	28.5	-6.7	-19.0
28 Mar	194.7	173.8	-20.9	-10.7
30 Mar	79.2	94.0	14.8	18.7
31 Mar	93.4	91.1	-2.3	-2.5
15 May	55.7	30.5	-25.2	-45.2
27 Jun	87.8	59.1	-28.7	-32.7
19 Oct	43.3	13.1	-30.2	-69.7

TABLE 3.8.   Predicted and observed rainfall excess for Little Mahoning Creek

Date 1989	Observed Rainfall Excess (in)	Predicted Rainfall Excess (in)	Absolute Error (in)	Relative Error (%)
18 Mar	0.17	0.14	-0.03	-17.6
28 Mar	0.96	0.85	-0.11	-11.4
30 Mar	0.39	0.46	0.07	17.9
31 Mar	0.46	0.45	-0.01	-2.
15 May	0.27	0.15	-0.12	-44.4
27 Jun	0.43	0.29	-0.14	-32.6
19 Oct	0.21	0.06	-0.15	-71.4

of rise durations matched (14 hrs). Being the second smallest basin (87.4 mi^2), hydrograph technique accuracy may improve with decreasing basin size.
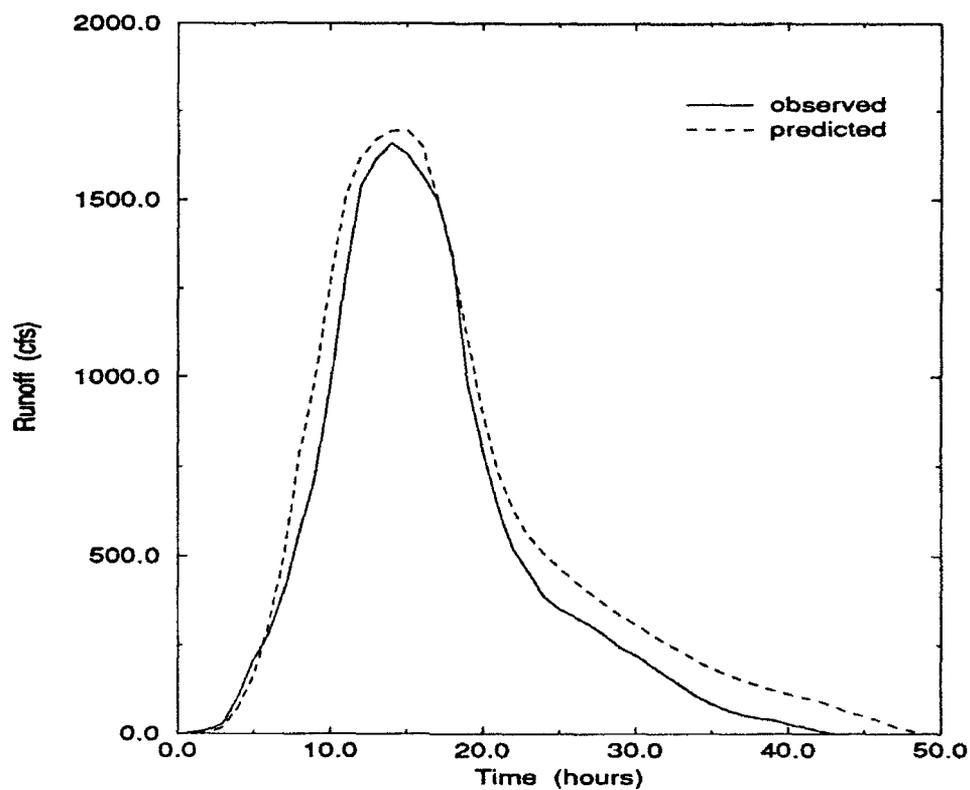
FIG. 3.9. Observed and predicted hydrograph tracks for Little Mahoning Creek, 30 March 1989.

TABLE 3.9. Predicted and observed peak runoff for Little Mahoning Creek

Date 1989	Observed Peak (cfs)	Predicted Peak (cfs)	Absolute Error (cfs)	Relative Error (%)
18 Mar	517	512	-5	-1.0
28 Mar	3284	3159	-125	-3.8
30 Mar	1658	1693	35	2.1
31 Mar	1792	1660	-132	-7.4
15 May	857	553	-304	-35.5
27 Jun	1272	1067	-205	-16.1
19 Oct	401	237	-164	-40.9
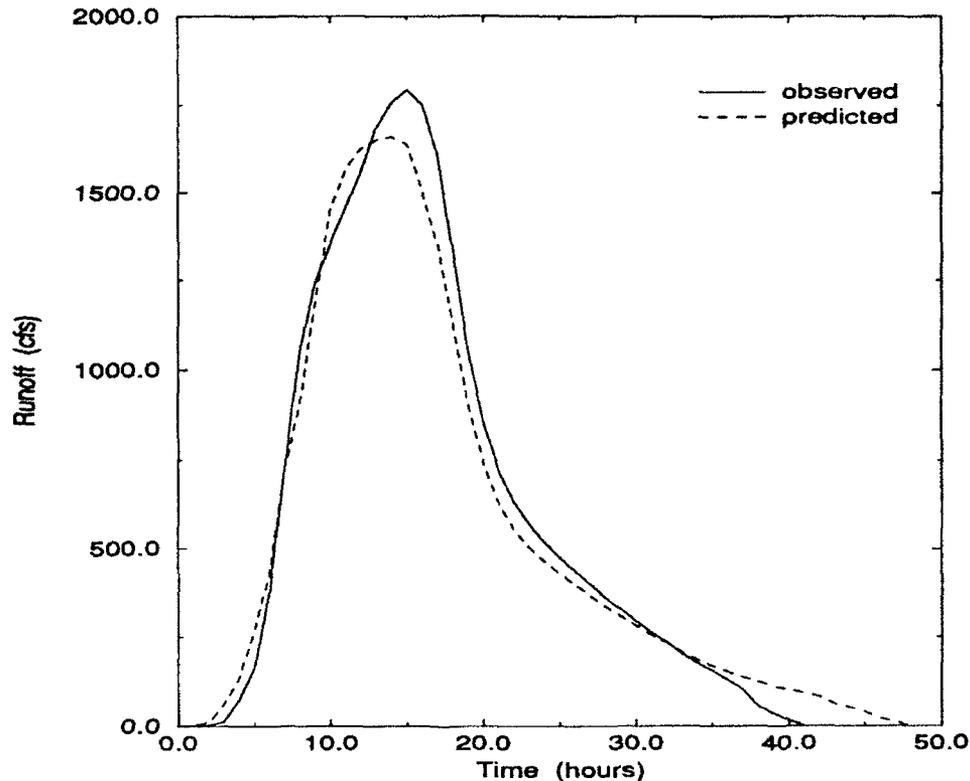
FIG. 3.10. Observed and predicted hydrograph tracks for Little Mahoning Creek, 31 March 1989

The fourth case study happened the following day, March 31 (see Figure 3.10). This hour long 0.47 inch downpour produced similar observed and predicted runoff responses. However, reduced radar rainfall accumulations (0.42 in) fell slightly below observed (0.46 in) and predicted (0.45 in) rainfall excesses. Total runoff volumes varied by only 2.5 %.

The observed peak (1792 cfs) was slightly higher than the predicted one (1660 cfs). The forecast time of rise (14 hrs) was one hour ahead of the observed period (15 hrs). All hydrograph variable results indicate strong agreement with each other.

The next precipitation event occurred on 15 May (see Figure 3.11). The hydrograph shapes are similar although the predicted track considerably underestimates the volume and peak outflows. Again the radar derived accumulation is small (0.19

TABLE 3.10. Predicted and observed times of rise for Little Mahoning Creek

Date 1989	Observed Time of Rise (hrs)	Predicted Time of Rise (hrs)	Absolute Error (hrs)	Relative Error (%)
18 Mar	16	14	-2	-12.5
28 Mar	14	14	0	0
30 Mar	14	14	0	0
31 Mar	15	14	-1	-6.7
15 May	17	14	-3	-17.6
27 Jun	13	14	1	7.7
19 Oct	19	14	-5	-26.3

in). The observed rainfall excess (0.27 in) was 0.12 inches higher than the predicted total (0.15 in).

Likewise, a runoff volume disparity of 45.2 % was measured. Peak outflow was underestimated by 35.5 %. Even the times of rise produced a relative error of −17.6 %. Results on low precipitation producing storms tend to vary considerably. The basin radar coverage indicated one hundred percent measurable precipitation reflectivities. Most of these reflectivities were small and may not of actually produced rainfall.

The sixth precipitation occurrence took place on June 27 (see Figure 3.12). It should be noted that radar returns ended before the second hump on the runoff track. Therefore hydrograph analysis will only concentrate on the first peak. Total runoff volumes and radar determined accumulations/observed rainfall excess comparisons will not be discussed.
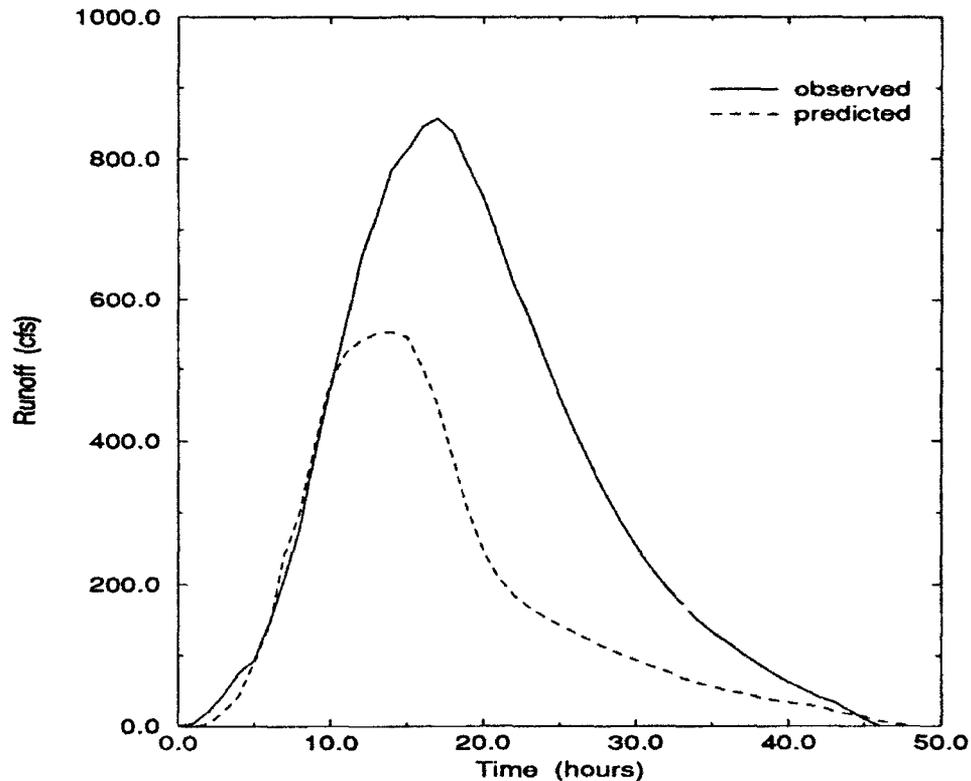
FIG. 3.11. Observed and predicted hydrograph tracks for Little Mahoning Creek, 15 May 1989

Again the predicted track appears to underestimate the observed outflow. The predicted peak (1067 cfs) is 16.1 % lower than the observed outflow (1272 cfs). Times of rise for both tracks are only one hour apart.

The last case study occurred on October 19 (see figure 3.13). Very little correlation exists between the two tracks. The 0.11 inch radar determined accumulation clearly underestimates the observed outflow. The reduced accumulation (0.06 in) strongly deviates from the measured rainfall excess (0.21 in). Again the pattern of underestimating the observed track is highlighted with low rainfall (< 0.25 in).

The disparity between the observed and predicted runoff volume was a staggering 69.7 %. The margin of error between the peak outflows was also large (40.9 %). Even the times of rise varied up to 26.3 %. The unit hydrograph response to small rainfall inputs does not produce substantial results.
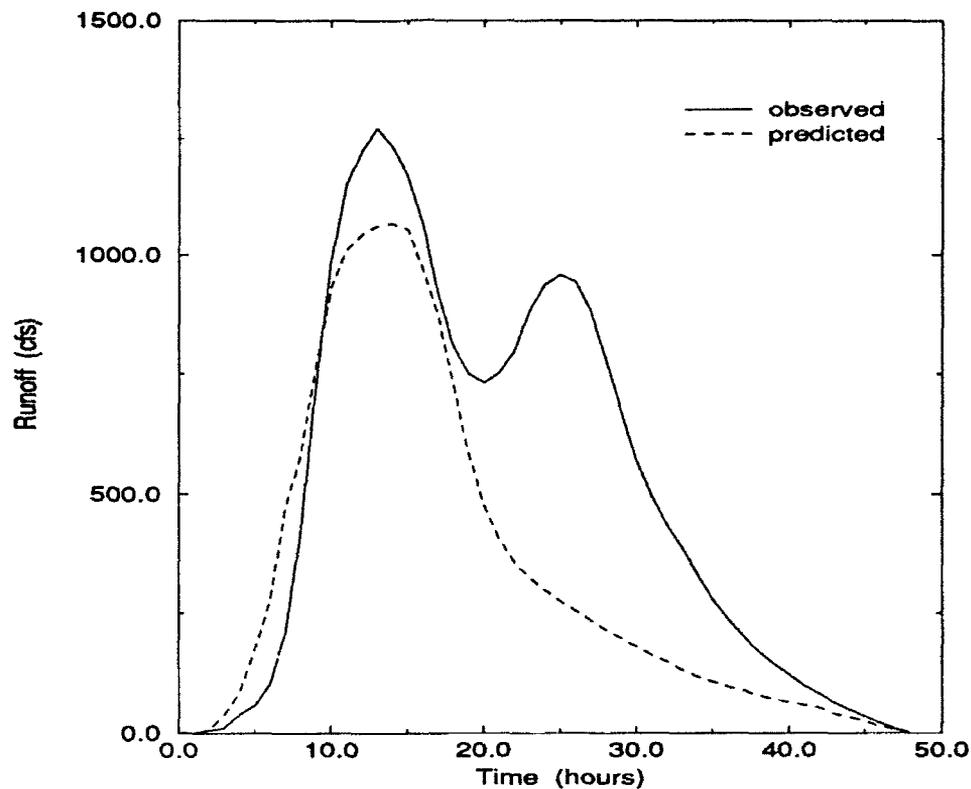
FIG. 3.12. Observed and predicted hydrograph tracks for Little Mahoning Creek, 27 June 1989.

3. Loyalhanna Creek Hydrograph Analysis

Loyalhanna Creek is the third test basin. It is the second largest (172 mi^2) and has the most forest coverage (71.0 %). The first precipitation event occurred on March 20 (see Figure 3.14). The observed track closely parallels the observed path even to the point of describing a subtle kink on the rising limb. The predicted track slightly overestimates the volume and peak runoff quantities. The radar determined rainfall accumulation was measured over a twenty hour stretch. Radar rainfall totalled 2.54 inches. The observed rainfall excess measured 1.20 inches, quite a difference from the radar determined value. But once each rainfall period is reduced by the 0.08 inch/hour infiltration rate, the excess rainfall values are only 6.7 % apart.

In addition, the predicted and observed runoff volumes compared quite well with only a 6.2 % difference separating the two quantities. Though the predicted
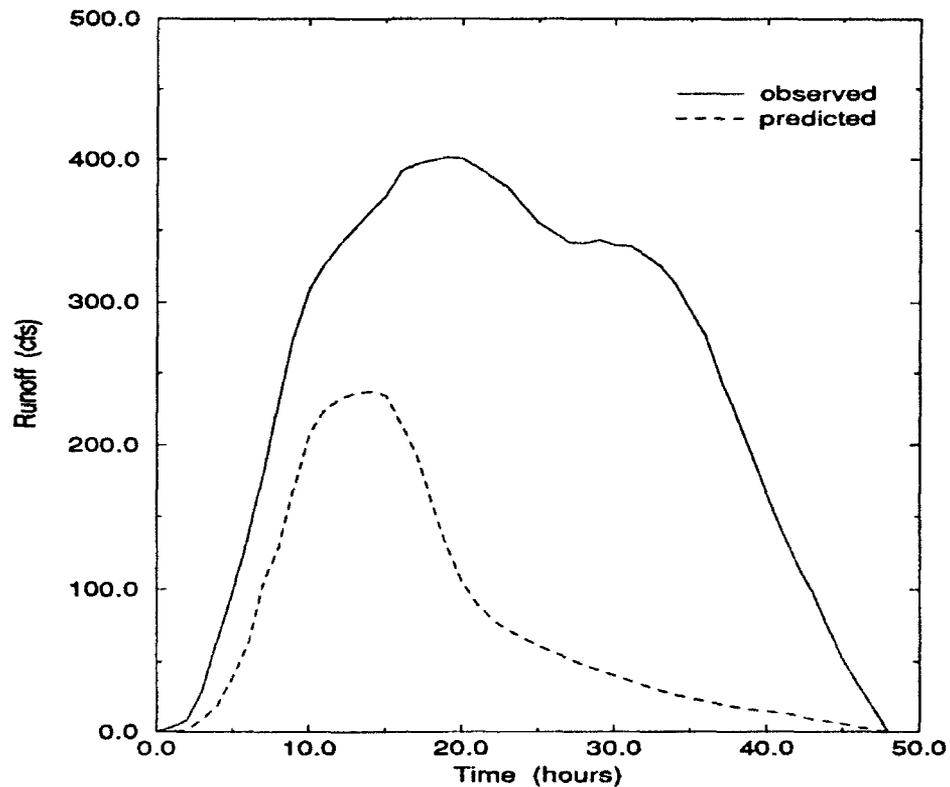
FIG. 3.13. Observed and predicted hydrograph tracks for Little Mahoning Creek, 19 October 1989.

peak runoff (5397 cfs) exceeded the observed quantity (4864 cfs) the relative error figured 11 %. Also the times to peak were both 25 hours. However radar bin coverage totalled only 36 % indicating several isolated cells were the cause of runoff.

March 25 is the next precipitation producing day (see Figure 3.15). The hydrograph shapes are similar in form. Variation near the downside of the observed crest were not identified on the predicted track. The predicted runoff volume exceeded the observed value by 27.9 %. As in the previous case, the rainfall total extended over a longer time span. The 0.71 radar accumulation was assessed over a 5 hour period. Reducing the hourly radar rainfall increments by the infiltration rate computes to a 0.31 inch rainfall runoff sum. This value is somewhat higher than the observed rainfall excess (0.23 in).
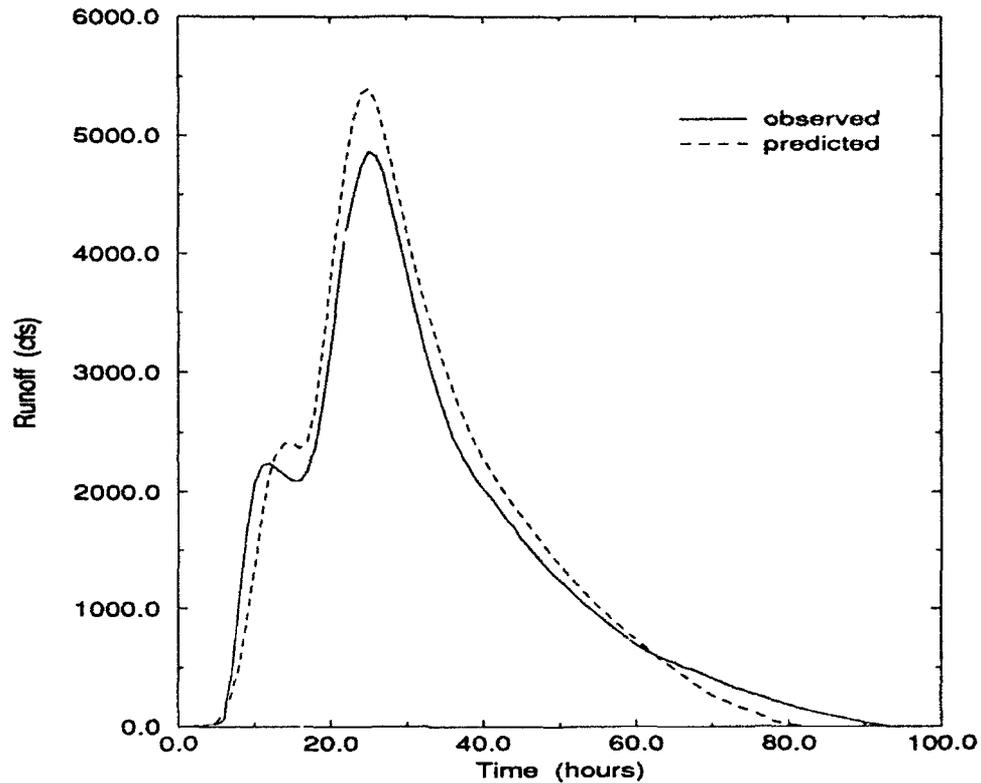
FIG. 3.14.   Observed and predicted hydrograph tracks for Loyalhanna Creek, 20 March 1989.

TABLE 3.11.   Rainfall characteristics for Loyalhanna Creek

Date 1989	Radar Rainfall (in)	Duration (hrs)	Basin Radar Coverage (%)
20 Mar	2.54	20	36
25 Mar	0.71	5	30
4 Apr	0.86	4	60
28 Jun	1.34	4	66
5 Jul	1.16	10	44

Further, predicted peak outflow (1549 cfs) surpassed the observed peak outflow (1402 cfs) by 10.5 %. Times of rise varied by three hours corresponding to a 33.3 % difference. Overall, forecast variables compared well within a reasonable margin.

FIG. 3.15.   Observed and predicted hydrograph tracks for Loyalhanna Creek, 25 March 1989.

TABLE 3.12.   Predicted and observed runoff volumes for Loyalhanna Creek.

Date 1989	Observed Runoff Volume (mcf)	Predicted Runoff Volume (mcf)	Absolute Error (mcf)	Relative Error (%)
20 Mar	486.1	516.1	3.0	6.2
25 Mar	93.9	120.3	26.4	27.9
4 Apr	179.7	161.4	-18.3	-9.8
28 Jun	325.0	393.2	68.2	21.0
5 Jul	249.4	168.0	-81.4	-32.6

The third case study occurred on 4 April (see Figure 3.16). The predicted hydrograph almost traced the observed runoff path. However the predicted track

underestimated the duration of the runoff by 14 hours. The radar accumulation totaled 0.86 inches over the four hour period. The reduced radar rainfall depth (0.42 in) compared favorably with the observed rainfall excess (0.45 in). Predicted and observed runoff volumes differed by only 9.8 %.
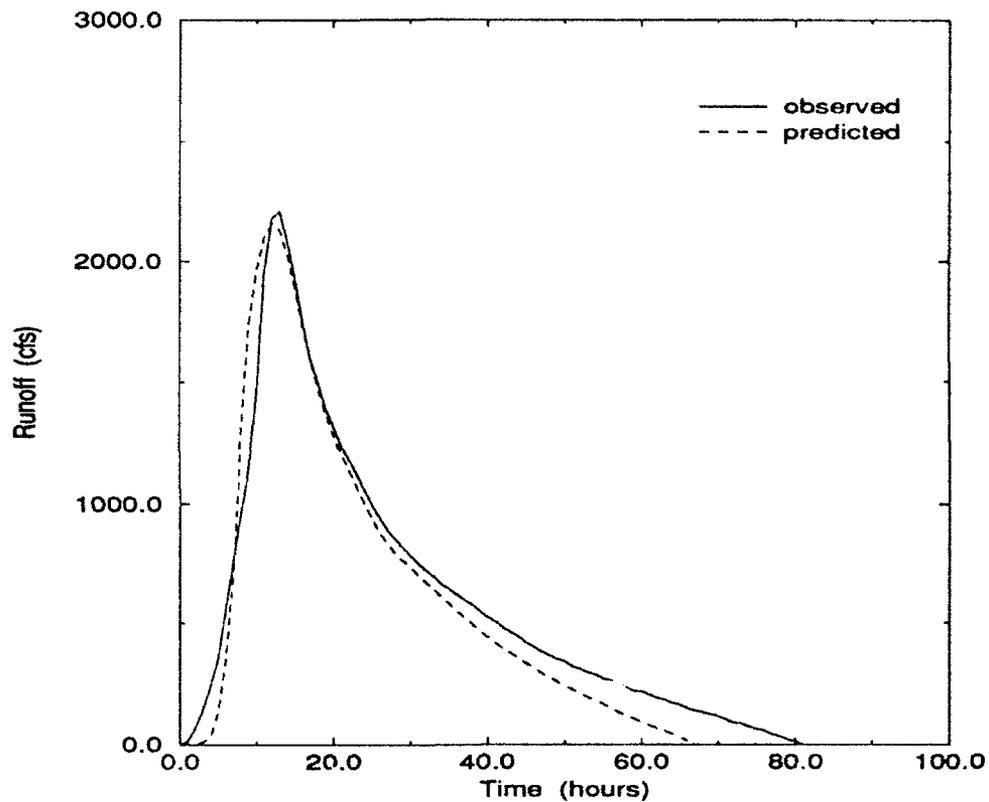
FIG. 3.16.   Observed and predicted hydrograph tracks for Loyalhanna Creek, 4 April 1989.

The difference between the observed (2211 cfs) and predicted (2158 cfs) peaks amounted to just 2.4 %. A high correlation also existed between the times of rise. The relative error between the two durations was −7.7 %. Rainfall quantities were

TABLE 3.13. Predicted and observed rainfall excess for Loyalhanna Creek

Date 1989	Observed Rainfall Excess (in)	Predicted Rainfall Excess (in)	Absolute Error (in)	Relative Error (%)
20 Mar	1.20	1.28	0.08	6.7
25 Mar	0.23	0.30	0.07	30.4
4 Apr	0.45	0.40	-0.05	-11.1
28 Jun	0.81	0.98	0.17	21.0
5 Jul	0.62	0.42	-0.20	-32.2

the highest for Loyalhanna Creek and hydrograph runoff tracks improved considerably with the increased depth.

June 28 was the next precipitation event (see Figure 3.17). Another high rainfall occurrence, precipitation totalled 1.34 inches over a four hour span. The predicted and observed hydrographs displayed strong resemblance especially with the rising limb and the baselength duration. The predicted track slightly overestimated the observed receding limb. As a result, the predicted volume exceeded the observed total by 21 %.

Reduced radar determined rainfall (1.03 in) overestimated actual rainfall excess (0.81 in) by 0.22 inches. Peak output volumes were nearly coincided. The observed maximum output (5343 mcf) surpassed the predicted total (5288 mcf) by 1 %. In addition, the times to peak outflow were identical. Both tracks reached their respective peaks after 11 hours of runoff. Again runoff characteristics show close agreement with significant precipitation totals.

The last case study occurred on 5 July (see Figure 3.18). A total of 1.16 inches were dispersed over a nine hour period. Radar bin coverage was only 44 %. The predicted and observed hydrographs have similar shapes but the predicted track

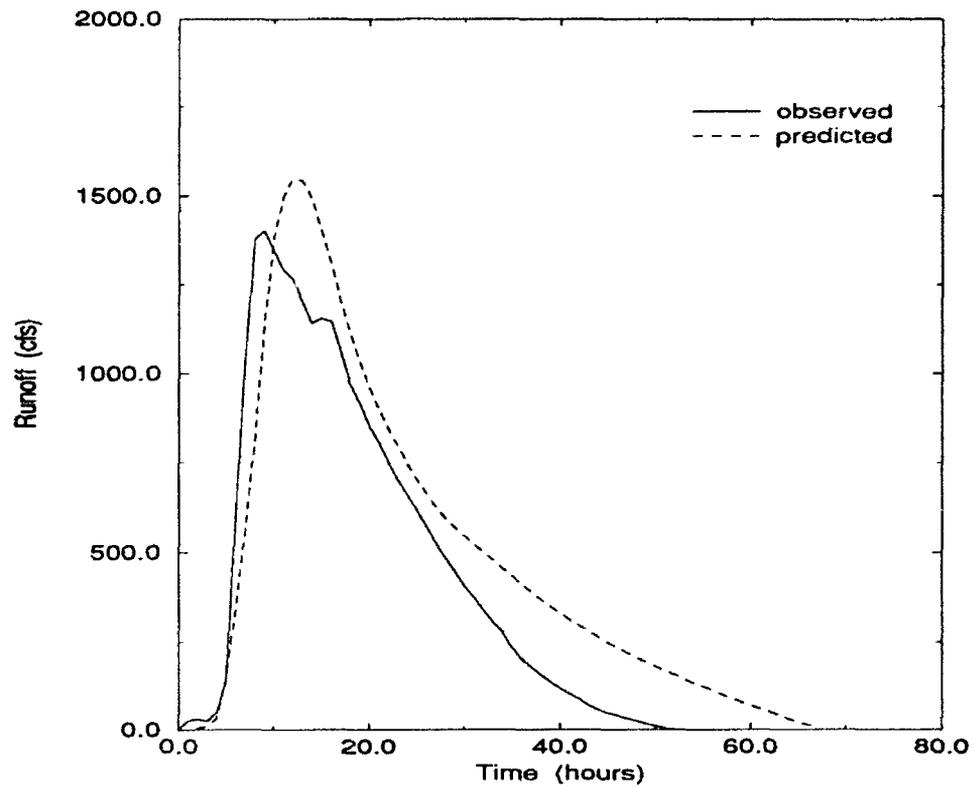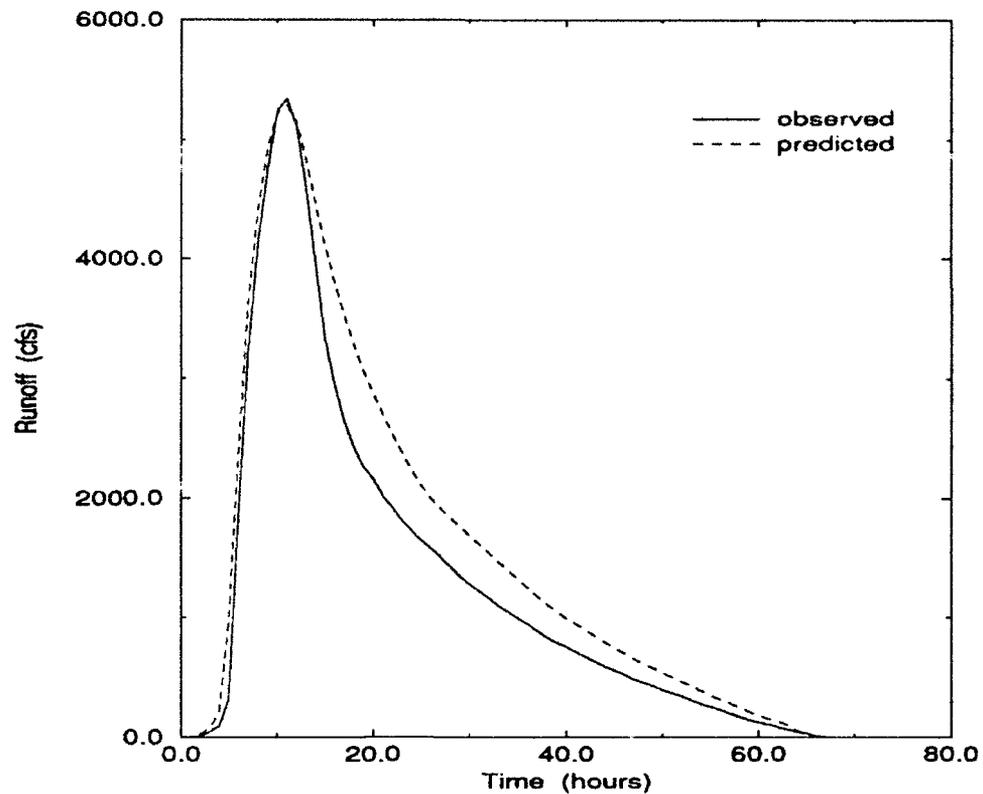FIG. 3.17. Observed and predicted hydrograph tracks for Loyalhanna Creek, 28 June 1989.

TABLE 3.14. Predicted and observed peak runoff for Loyalhanna Creek

Date 1989	Observed Peak (cfs)	Predicted Peak (cfs)	Absolute Error (cfs)	Relative Error (%)
20 Mar	4864	5397	533	11.0
25 Mar	1402	1549	147	10.5
4 Apr	2211	2158	-52	-2.4
28 Jun	5343	5288	-55	-1.0
5 Jul	2087	2086	-1	0.1

fails the duplicate the fine details in the measured flow. In addition, the predicted flow generally underestimates the observed outflow.

TABLE 3.15.   Predicted and observed times of rise for Loyalhanna Creek

Date 1989	Observed Time of Rise (hrs)	Predicted Time of Rise (hrs)	Absolute Error (hrs)	Relative Error (%)
20 Mar	25	25	0	0
25 Mar	9	12	3	33.3
4 Apr	13	12	-1	-7.7
28 Jun	11	11	0	0
5 Jul	11	14	3	27.3
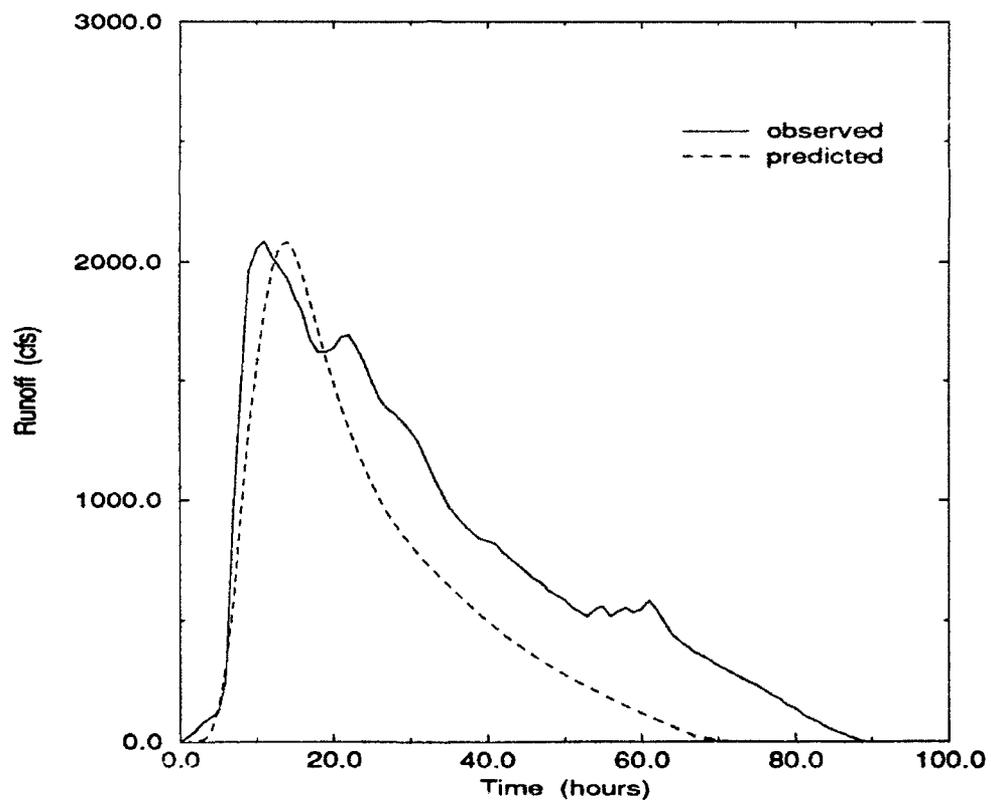
FIG. 3.18.   Observed and predicted hydrograph tracks for Loyalhanna Creek, 5 July 1989.

Runoff volume discrepancies reached 32.6 %. The infiltration reduced radar depth measured 0.44 inches, approximately 0.18 inches lower than the observed

rainfall excess (0.62 in). However, maximum outflow forecasting produced the best results out of all the case studies. The predicted peak (2086 cfs) reproduced the observed maximum outflow (2087 cfs) to within 1 cfs. The times to peak varied by over 27 %.

4. Mahoning Creek Hydrograph Analysis

Mahoning Creek is the fourth basin to be examined. It is 158 mile^2 and has the flattest slope (9.51 ft/mile). The first case study occurred on 18 March (see Figure 3.19). A one hour measured depth of 0.22 inches produced a predicted track that underestimated the majority of the observed hydrograph with the exception of the final portion of the receding limb.
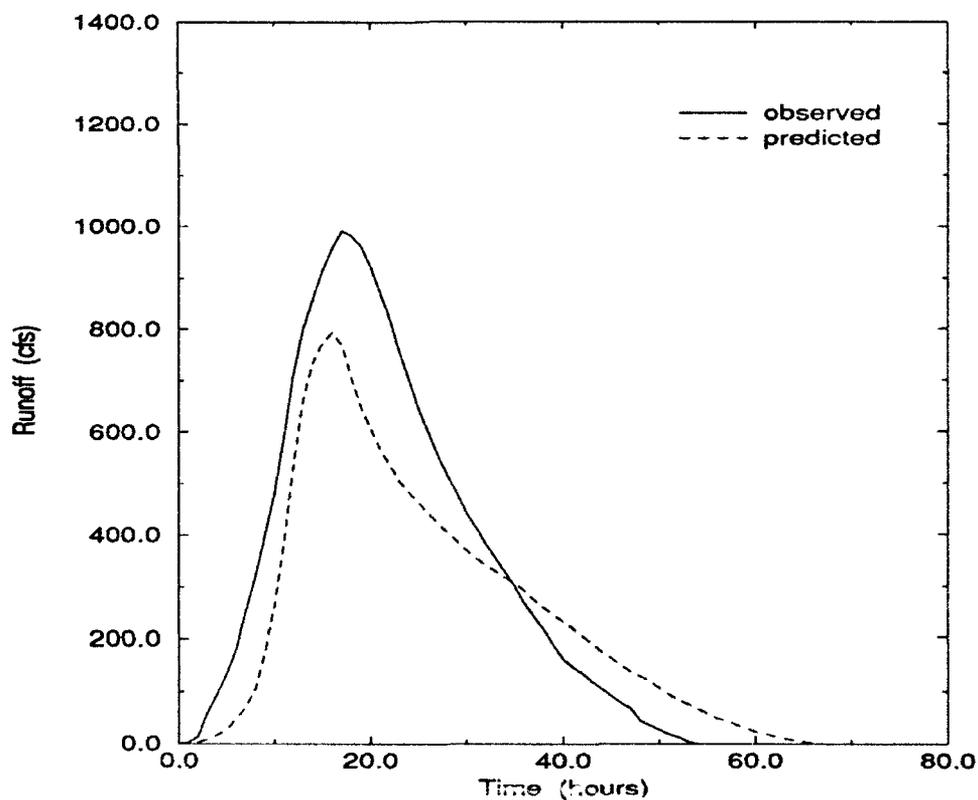
FIG. 3.19. Observed and predicted hydrograph tracks for Mahoning Creek, 18 March 1989.

The observed runoff volume exceeded the predicted sum by 16 %. An infiltration rate of 0.05 in/hr reduced the radar derived total to 0.17 inches. The observed rainfall excess (0.20 in) slightly surpassed this quantity. The predicted peak (793 cfs) also underestimated the observed peak (992 cfs) by 20.1 %. The times of rise matched closely. The predicted peak (16 hrs) differed by one hour from the observed peak time (17 hrs).

TABLE 3.16. Rainfall characteristics for Mahoning Creek

Date 1989	Radar Rainfall (in)	Duration (hrs)	Basin Radar Coverage (%)
18 Mar	0.22	1	54
15 May	0.27	2	99
24 Jun	1.27	10	66
27 Jun	0.29	1	84
28 Jun	0.11	1	85

The second case study on 15 May closely parallels the first one in many respects (see Figure 3.20). Again the predicted track underestimates the observed one. Like the previous case the radar derived rainfall (0.27 in) is small. In addition, a rainfall perturbation on the observed track is not illustrated in the forecast path.

The observed rainfall excess (0.23 in) exceeds the reduced radar determined total (0.17 in). Furthermore, the observed peak crests at 988 cfs nearly 21 % higher than the predicted peak (783 cfs). The times of rise are similar. The predicted peak (17 hrs) occurs one hour after the observed time (16 hrs). The tendency to underestimate the observed hydrograph frequently exists with low rainfall resulting in wide variations in total runoff volume, rainfall excess, and peak outflow.

FIG. 3.20. Observed and predicted hydrograph tracks for Mahoning Creek, 15 May 1989.

TABLE 3.17. Predicted and observed runoff volumes for Mahoning Creek.

Date 1989	Observed Runoff Volume (mcf)	Predicted Runoff Volume (mcf)	Absolute Error (mcf)	Relative Error (%)
18 Mar	75.0	63.0	12.0	-16.0
15 May	84.7	61.6	-23.1	-27.3
24 Jun	333.7	315.5	-18.2	-5.5
27 Jun	111.0	87.3	23.7	-21.4
28 Jun	53.9	22.3	-31.6	-58.6

June 24 is the next case study (see Figure 3.21). This time the rainfall is considerably greater (1.27 in). According, the hydrograph follow similar paths

especially highlighted by the closeness in the two rising limbs. The predicted path slightly underestimates the crest and the duration of the time base. Runoff volumes correspond well. The observed runoff volume exceeds the predicted one by 5.5 %.
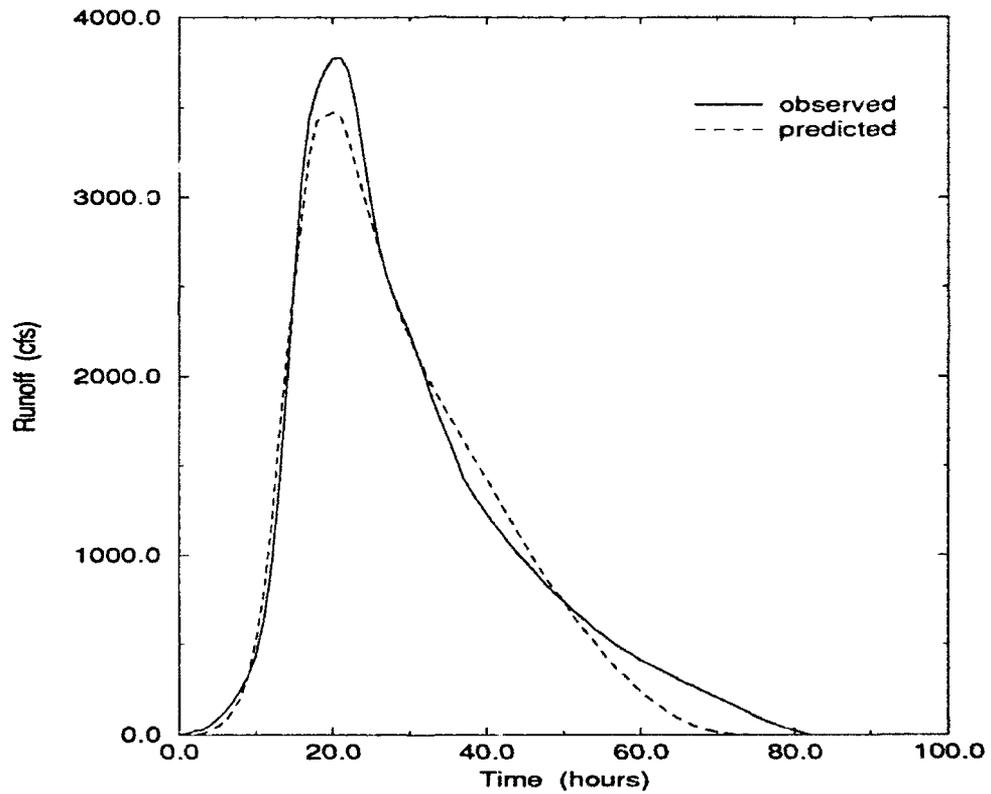
FIG. 3.21. Observed and predicted hydrograph tracks for Mahoning Creek, 24 June 1989.

TABLE 3.18.   Predicted and observed rainfall excess for Mahoning Creek

Date 1989	Observed Rainfall Excess (in)	Predicted Rainfall Excess (in)	Absolute Error (in)	Relative Error (%)
18 Mar	0.20	0.17	-0.03	-15.0
15 Mar	0.23	0.16	-0.07	-30.4
24 Jun	0.91	0.86	-0.05	-5.5
27 Jun	0.30	0.24	-0.06	-20.0
28 Jun	0.15	0.06	-0.09	-60.0

The predicted peak (3472 cfs) lagged the observed peak (3778 cfs) by 8.1 %. The observed time of rise (21 hrs) exceeded the predicted duration by one hour. As a whole, variable results show close agreement.

The fourth precipitation event took place on 27 June (see Figure 3.22). Hydrograph shapes compare with each other but the size of the observed track is larger. The radar derived rainfall (0.29 in) is small and when reduced by the infiltration rate (0.05 in/hr) underestimates the observed rainfall excess (0.30 in). Likewise, the runoff volume is underestimated by 21.4 %.

In addition, the observed runoff peak (1493 cfs) surpasses the predicted peak (1120 cfs) by 25 %. Again the times to rise match closely. For the fourth consecutive time, the duration difference was one hour corresponding to a 6.7 % relative error. The possibility of an adjustment or compensation for low rainfall generated depths should be explored.

The last case study occurred the next day on 28 June (see Figure 3.23). The radar rainfall is very small (0.11 in). There is very little semblance between the two plots. Prewetting conditions do not appear to play any role in the runoff hydrograph. Runoff volumes were underestimated by 58.6 %.
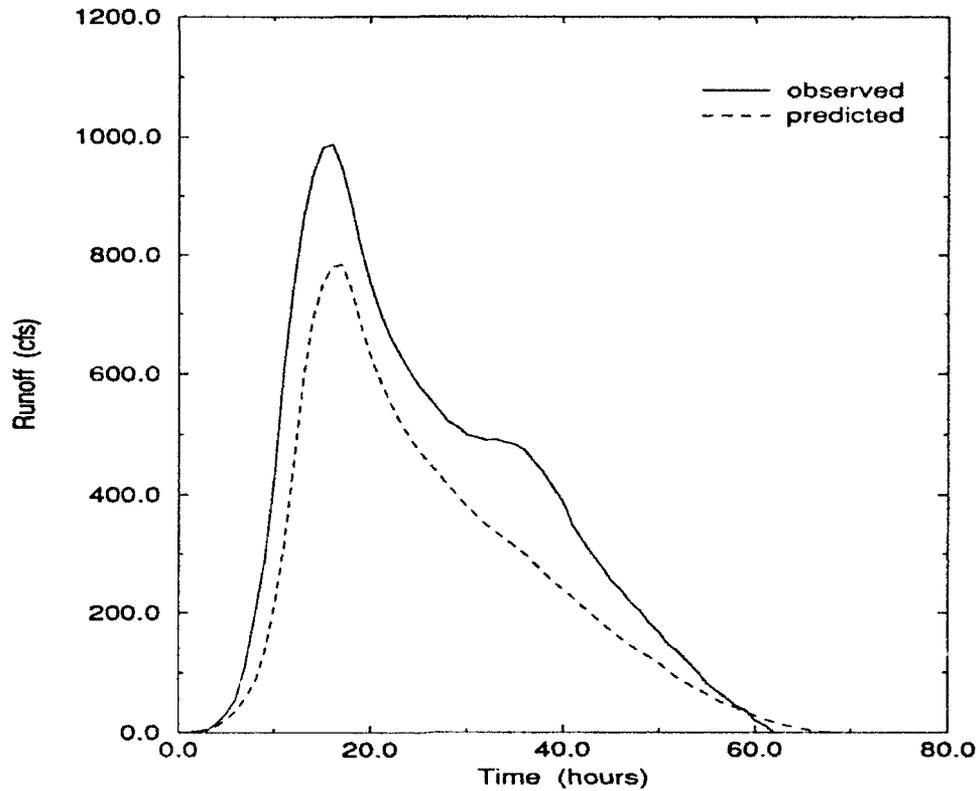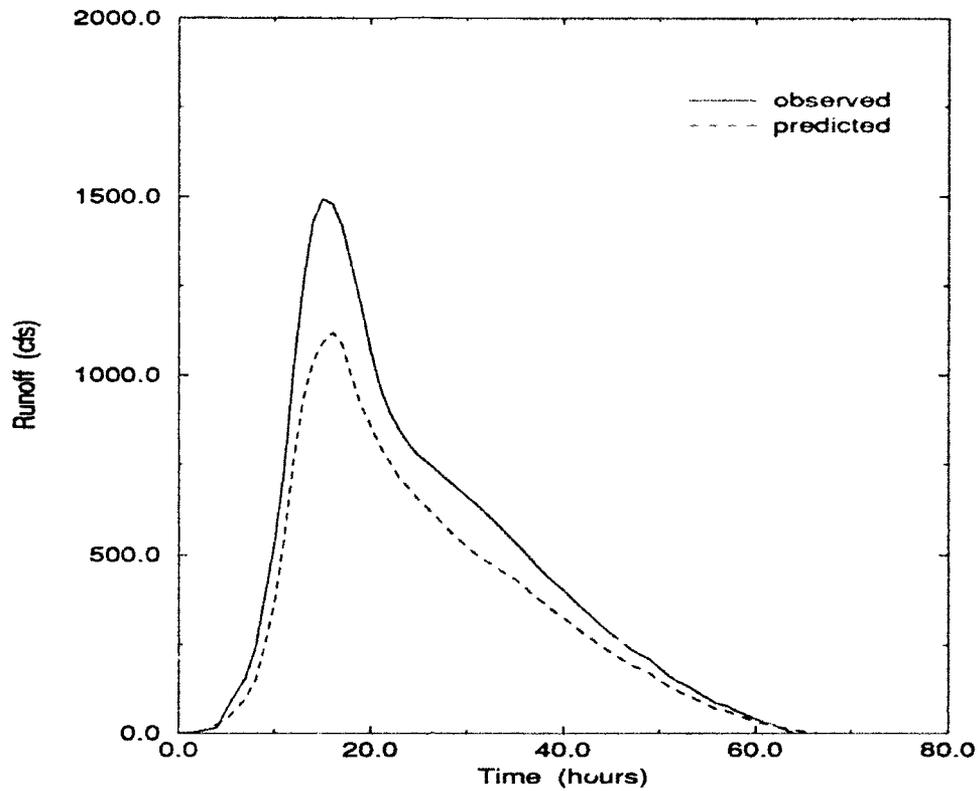
FIG. 3.22. Observed and predicted hydrograph tracks for Mahoning Creek, 27 June 1989.

TABLE 3.19. Predicted and observed peak runoff for Mahoning Creek

Date 1989	Observed Peak (cfs)	Predicted Peak (cfs)	Absolute Error (cfs)	Relative Error (%)
18 Mar	992	793	-199	-20.1
15 May	988	783	-205	-20.7
24 Jun	3778	3472	-306	-8.1
27 Jun	1493	1120	-373	-25.0
28 Jun	435	280	-155	-35.6

The observed rainfall excess (0.15 in) surpassed the radar reduced depth (0.06 in) by 0.09 in. Peak runoff disparities were also outstanding. Peaks varied by

TABLE 3.20.   Predicted and observed times of rise for Mahoning Creek

Date 1989	Observed Time of Rise (hrs)	Predicted Time of Rise (hrs)	Absolute Error (hrs)	Relative Error (%)
18 Mar	17	16	-1	-5.9
15 May	16	17	1	6.3
24 Jun	21	20	-1	-4.8
27 Jun	15	16	1	6.7
28 Jun	32	16	-16	-50.0
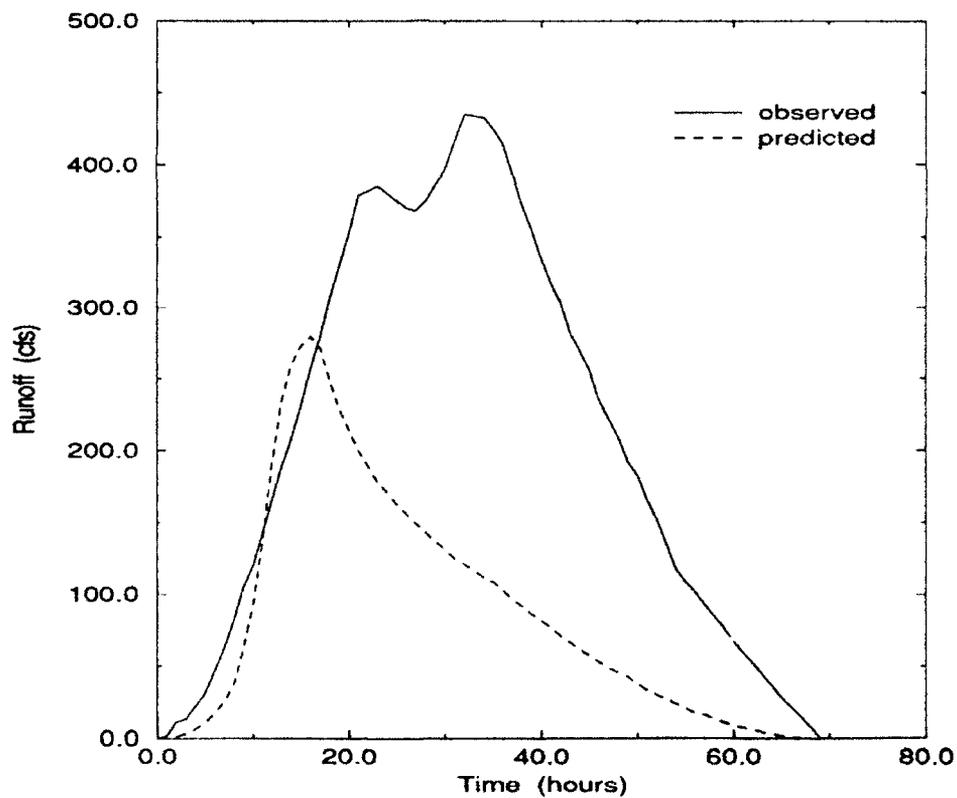
FIG. 3.23.   Observed and predicted hydrograph tracks for Mahoning Creek, 28 June 1989.

35.6 %. However, the most striking difference occurred will the times of rise. The observed rise peaked 16 hours after the predicted time of rise.

5. Turtle Creek Hydrograph Analysis

Turtle Creek is the last basin to be analyzed. It is the smallest watershed (55.9 mile^2). The first case study took place on 18 March (see Figure 3.24). Approximately 1.04 inches covered the basin over a two hour span. The shape of the predicted hydrograph matches the observed path with the exception of the overestimated recession limb. The predicted runoff volume exceeded the observed quantity by 18.8 %.

FIG. 3.24. Observed and predicted hydrograph tracks for Turtle Creek, 18 Mar 1989.

An infiltration rate of 0.05 in/hr reduced the radar rainfall depth to 0.94 inches. The observed rainfall excess measured 0.77 inches. The peak observed runoff (6187 cfs) for this event totalled the most for any basin. The predicted peak flow (5838 cfs) lagged the observed by 5.6 %. The times of rise for this event both equaled

TABLE 3.21. Rainfall characteristics for Turtle Creek

Date 1989	Radar Rainfall (in)	Duration (hrs)	Basin Radar Coverage (%)
18 Mar	1.04	2	82
31 Mar	0.66	1	95
18 Apr	0.14	1	96
17 Jun	0.28	3	100

seven hours. The time of rise shows a very fast response to the rainfall input. Flood potential would need to be carefully monitored.

The second precipitation event occurred on 31 March (see Figure 3.25). Again a large quantity of water (0.66 in) was dropped in a short period (one hour). Hydrographs compare favorably with one another. The predicted track slightly underestimates the observed path and is somewhat skewed to the left. In addition, the reduced radar determined rainfall (0.61 in) is 0.14 inches lower than the observed rainfall excess.

The observed runoff volume (209.7 mcf) exceeded the predicted volume (171.8 mcf) by 18.1 %. The observed peak outflow (4367 cfs) also surpassed the predicted flow (3810 cfs) by 12.8 %. The time of rise was one hour faster with the predicted peak (7 hrs) than for the observed track (8 hrs).

The next runoff case study took place on 18 April (see Figure 3.26). The predicted and observed hydrographs resemble one another only in a broad sense. The forecast track greatly underestimates the observed one. Also, several irregularities in the observed track are smoothed out in the predicted path.

Furthermore, the predicted runoff volume underestimates the observed volume by 68.2 %. Only 0.14 inches of rain were measured by the radar. When reduced by the infiltration rate (0.05 in/hr), the decreased or effective rainfall (0.09 in) vastly
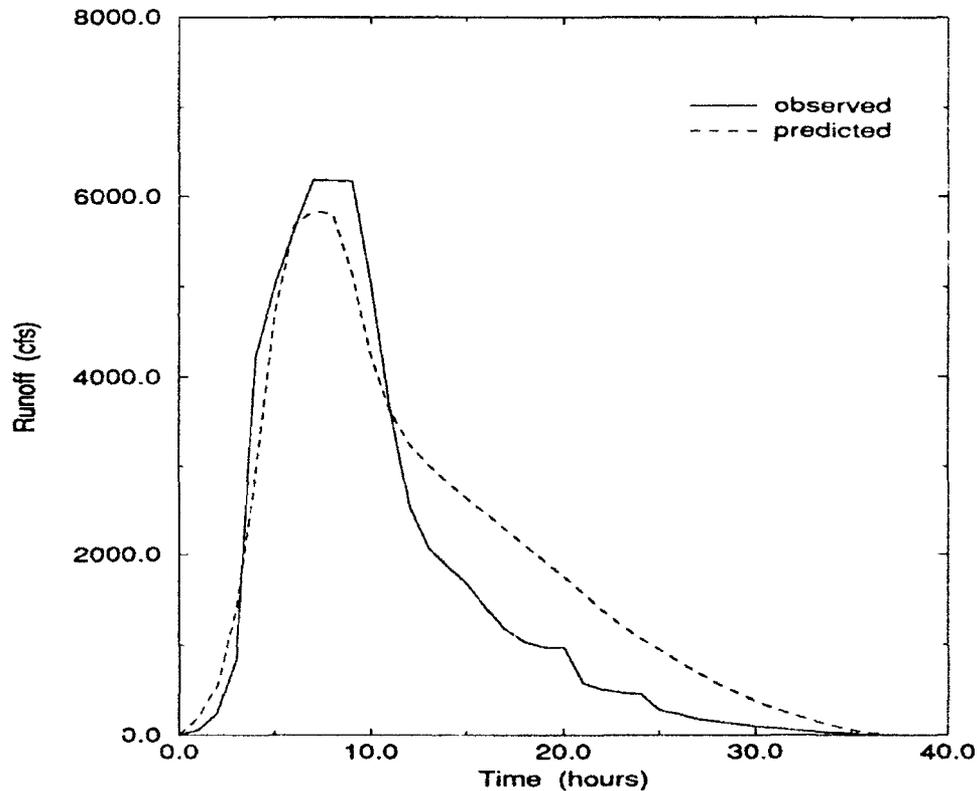
FIG. 3.25. Observed and predicted hydrograph tracks for Turtle Creek, 31 Mar 1989.

TABLE 3.22. Predicted and observed runoff volumes for Turtle Creek.

Date 1989	Observed Runoff Volume (mcf)	Predicted Runoff Volume (mcf)	Absolute Error (mcf)	Relative Error (%)
18 Mar	217.1	257.8	40.8	18.8
31 Mar	209.7	171.8	-37.9	-18.1
18 Apr	80.1	25.5	-54.6	-68.2
17 Jun	40.4	39.5	-0.9	-2.2

underestimates the observed rainfall excess (0.28 in). Peak outflow is another badly forecast characteristic. A -53.3 % relative error marked the difference between the observed (1203 cfs) and predicted (562 cfs) peaks. The times of rise exhibited only

FIG. 3.26. Observed and predicted hydrograph tracks for Turtle Creek, 18 April 1989.

TABLE 3.23. Predicted and observed rainfall excess for Turtle Creek

Date 1989	Observed Rainfall Excess (in)	Predicted Rainfall Excess (in)	Absolute Error (in)	Relative Error (%)
18 Mar	0.77	0.92	0.15	19.5
31 Mar	0.75	0.61	-0.14	-18.7
18 Apr	0.28	0.09	-0.19	-67.9
17 Jun	0.14	0.14	0.0	0.0

a one hour differential. This case exemplifies the forecast problems of low radar rainfall measurements.

TABLE 3.24. Predicted and observed peak runoff for Turtle Creek

Date 1989	Observed Peak (cfs)	Predicted Peak (cfs)	Absolute Error (cfs)	Relative Error (%)
18 Mar	6187	5838	-349	-5.6
31 Mar	4367	3810	-557	-12.8
18 Apr	1203	562	-641	-53.3
17 Jun	1249	867	-382	-30.6

The final precipitation input occurred on 17 Jun (see Figure 3.27). Approximately 0.28 inches of rain were measured over a three hour period. Again, as in the previous case, the fine details of the observed plot were damped out. The observed runoff rise at 26 hours probably was smoothed out by hourly radar reflectivity averaging. This problem appeared to be more common with low rainfall depths. The predicted track also rose faster than the observed one. A more accurately depicted infiltration rate with a steep initial absorption curve would correct the discrepancy. However, the problem appears to be a: ' 'ated case.

In this instance, the reduced radai . ,th (0.14 in) equaled that of the observed rainfall excess (0.14 in). Likewise, the runoff volumes were similar. The relative error between the observed runoff volume (40.4 mcf) and the predicted one (39.5 mcf) accounted to −2.2 %. The peak runoff, however, varied by 30.6 %. Turtle Creek had another fast response time. The time of rise for the predicted track took eight hours, underestimating the observed period by one hour.
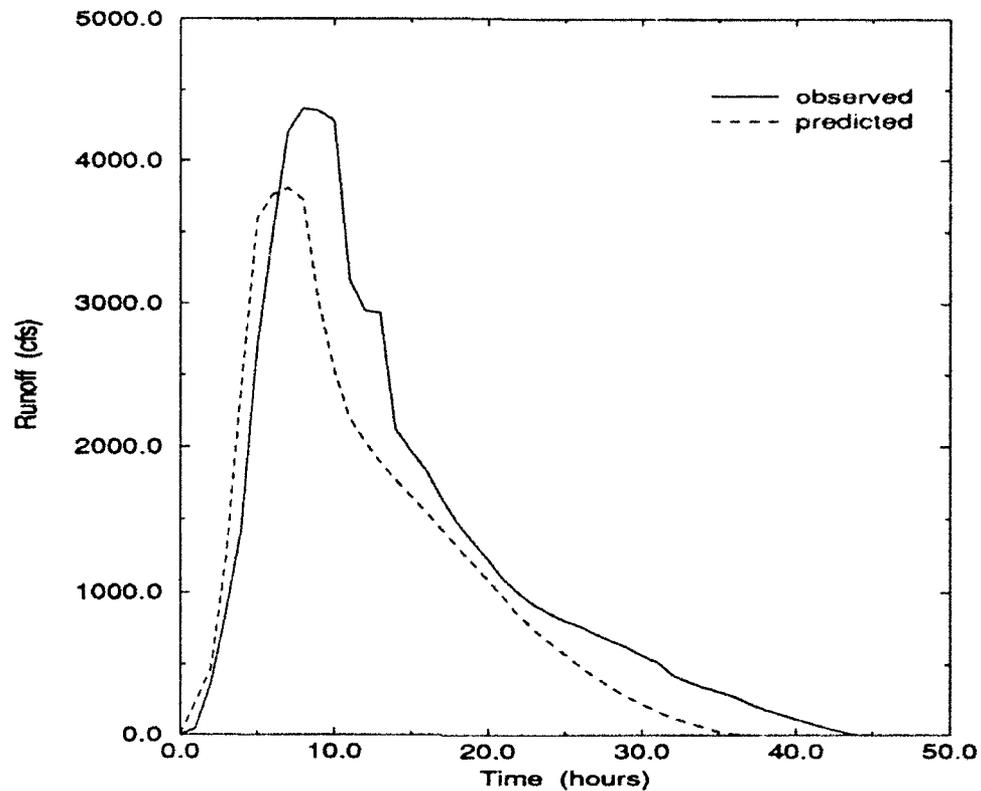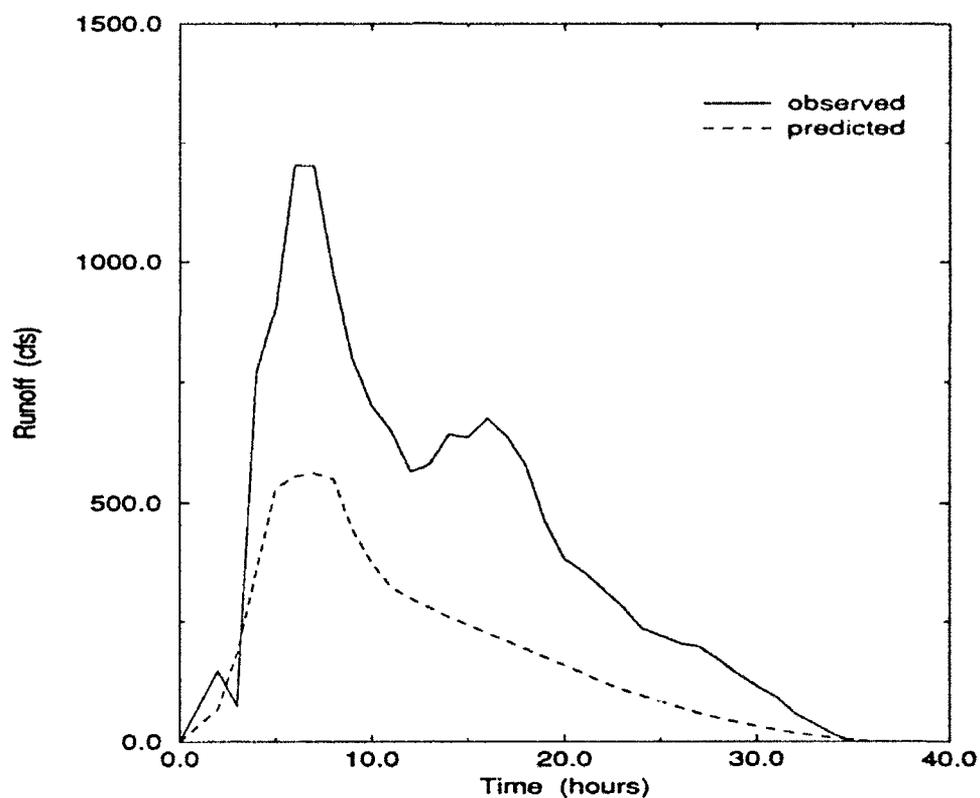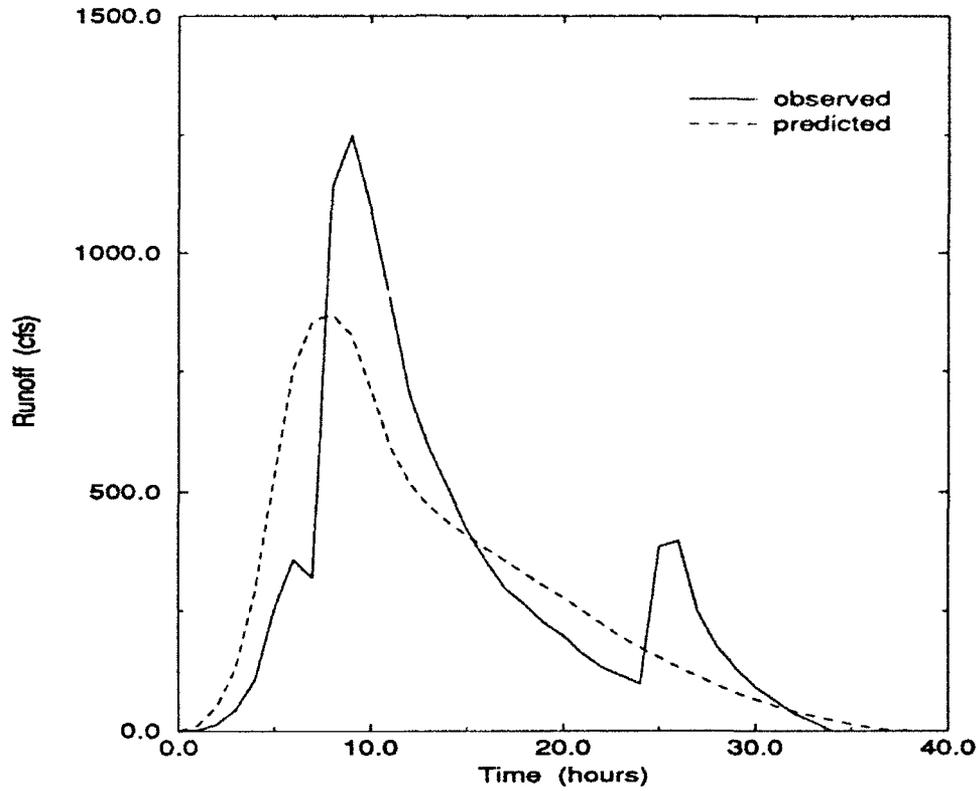
FIG. 3.27.   Observed and predicted hydrograph tracks for Turtle Creek, 17 June 1989.

TABLE 3.25.   Predicted and observed times of rise for Turtle Creek.

Date 1989	Observed Time of Rise (hrs)	Predicted Time of Rise (hrs)	Absolute Error (hrs)	Relative Error (%)
18 Mar	7	7	0	0.0
31 Mar	8	7	-1	-12.5
18 Apr	6	7	1	16.7
17 Jun	9	8	-1	-11.1

CHAPTER 4
CONCLUSIONS

Rainfall-runoff behavior can be analyzed by a variety of techniques including linear and nonlinear mathematical models. A simple and easy to apply linear approach is the unit hydrograph method. Basin runoff can be measured by combining unit hydrograph theory with radar derived precipitation accumulations. In extreme runoff scenarios, the method can be used to forecast flood conditions. Furthermore, hydrograph application is flexible and can be adapted to a wide variety of watersheds.

Successful runoff modeling can be traced to three distinct areas: unit hydrograph response curves, correct employment of hydrograph assumptions, and radar rainfall accounting. A failure in any one of the three categories will lead to erroneous results. Foremost, runoff prediction relies an accurate response curves. A large amount of discharge data is necessary to ensure a representative basin response function. Each watershed is assumed to have a unique runoff pattern. Consequently, predicted runoff is based on outflow following a similar pattern time after time.

Next, several assumptions must be adhered to obtain maximum results. The most important require rainfall to have uniform spatial and temporal distribution. In addition, rainfall excess should range from 0.5 to 2.0 inches. A comparison of the eight most dissimilar hydrographs revealed an average radar derived rainfall of only 0.23 inches. In contrast, the mean radar basin coverage for these examples totalled 96.8 %. The results suggest that hydrograph performance is more closely linked to quantity of rainfall excess then to basin's rainfall spatial distribution.

Finally, areal and temporal radar accumulations must reflect storm precipitation. Areal averaging and hourly averaging of six minute radar observations may not always be representative of the basin environment. Smaller basins and shorter convolution time steps may be necessary to improve runoff accuracy. In this experiment, observed runoff volumes consistently exceeded radar based accumulations, even without allowing for an infiltration rate.

Four criteria were used to evaluated the predicted runoff hydrograph with the observed one: overall shape, time of rise, peak outflow, and total runoff volume. The following list highlights the results from the five basins using the runoff algorithm.

- Hydrograph accuracy increased with increasing rainfall.

- Radar derived accumulations underestimated total rainfall especially during light precipitation. To compensate, infiltration rates used in this experiment were two to three times lower than those measured for similar soil type.

- The convolution procedure damped out irregularities in the observed runoff track. This problem was further magnified by areal and temporal radar reflectivity averaging.

- For all 26 cases, the time of rise was the easiest hydrograph characteristic to predicted (87 %).

- The forecast accuracy for the peak outflow and total runoff volume were 82.9 % and 74.0 % respectively.

- The basin (Turtle Creek) with the shortest unit hydrograph time of rise also had the shortest observed and predicted times of rise.

- For case studies with radar derived accumulations over 0.50 inches, the peak runoff became the most accurate forecast variable (94.5 %).

- Forecast accuracy also improved for the other two variables within this rainfall category. The accuracy rate jumped to 90.7 % and 83.5 % for the time of rise and runoff volume.

REFERENCES

Bedient, P.B., and W.C. Huber, 1988: *Hydrology and Floodplain Analysis*. Addison-Wesley Publishing Comp., New York, 34–180.

Brandes, E.A., and J.W. Wilson, 1982: Measuring storm rainfall by radar and rain gage. *Instruments and Techniques for Thunderstorm Observation and Analysis*, McGraw-Hill Book Comp., New York, 171–180.

Chezy, 1769, referred to in Rouse, H., and S. Ince, 1957: *History of Hydraulics*. Iowa Institute of Hydraulic Research, State University of Iowa.

Delleur, J.W., and A.R. Rao, 1973: Some extensions of linear systems analysis in hydrology. *Floods and Droughts: Proceedings of the Second Symposium in Hydrology*, Water Resources Publ., Fort Collins, 117.

Dragomar, J.H., 1990: A method to compare RADAP II radar rainfall to IFLOWS in real time. *NWS Eastern Tech. Attach. No. 90-8B*, 1–3.

Dunne, T., and L.B. Leopold, 1978: *Water in Environmental Planning*. W.H. Freeman and Comp., New York, 105–256.

Foster, E.E., 1948: *Rainfall and Runoff*. MacMillan Comp., New York, 293–314.

Gay, L.R., 1987: *Educational Research: Competencies for Analysis and Application*. Merrill Publishing Comp., Columbus, 113–119.

Gray, D.M., 1973: *Handbook on the Principles of Hydrology*. Water Information Council., Huntington, N.Y., Sect 7.

Horton, R.E., 1933: The role of infiltration in the hydrological cycle. *Trans Am. Geophys. Union*, 14, 446–460.

Horton, R.E., 1935: Surface runoff phenomena, part I: analysis of the hydrograph. Horton Hydrological Laboratory, Voorhees, N.Y., 45–80.

Horton, R.E., 1945: Erosional development of streams and their drainage basins: hydrological approach to quantitive morphology. *Bul. Geol. Soc. Amer.*, **56**, 275–370.

Huebner, G.L., 1977: Radar meteorology class notes. Texas A&M Unv., College Station.

Kreyszig, E., 1988: *Advanced Engineering Mathematics*. John Wiley and Sons, New York, 943.

Langbein, W.B., 1947: Topographic characteristics of drainage basins. *U.S. Dept Interior, Geological Water-Survey Paper 968-C*, 125–155.

Leyton, L., E.R.C. Reynolds, and F.B. Thompsom, 1967: Rainfall interception in forest and moorland. *Forest Hydrology*, Pergamon Press, Oxford, 163–177.

Linsley, R.K., M.A. Koler, and J.L.H. Paulhus, 1949: *Applied Hydrology*. McGraw-Hill Book Comp., New York City, N.Y., 102–450.

Manning, R., 1889: On the Flow of water in Open Channels and Pipes. *Trans. Inst. Civil Engrs.,Ireland*, **20**, 161–207.

Marshall, J.S. and W.M. Palmer, 1948: The distribution of raindrops with size. *J. Meteor.*, **5**, 165–166.

Patric, J.H., 1966: Rainfall interception by mature coniferous forests of southeast Alaska. *Journal of Soil and Water Conservation*, **21**, 229–231.

Penman, H.L., 1948: Natural evaporation from open water, bare soil and grass. *Proceedings of the Royal Society of London*, Series A, **193**, 120–145.

Raudkivi, A.J., 1979: *Hydrology: An Advanced Introduction to Hydrological Processes and Modelling*. Pergamon Press, New York, 198.

Schaake, J.C., 1965: Synthesis of the Inlet Hydrograph. *Tech. Rept. No. 3, Dept of Sanitary Eng. and Water Resources* John Hopkins Unv., Baltimore 56–60.

Sheaffer, J.R., 1961: Flood-to-peak Interval: Papers on Flood Problems. *Univ. of Chicago, Dept. of Geog. Res. Pap.*, **70**, 95–113.

Shaw, E.M., 1988: *Hydrology in Practice*. VNR International., London, 299–314.

Spilhaus, A.F., 1948: Drop size intensity and radar echo of rain. *J Meteo.* **6**, 161–164.

Stearns, N.W., 1927: Laboratory tests on physical properties of water bearing materials. *U.S. Geol. Survey Water-Supply Paper 596.*

Sutcliffe, J.V., 1975: *Flood Studies Report, Hydrology Studies Volume 1.* Whitefriar Press Ltd., London, 160–167.

Thornthwaite, C.W., 1948: An approach toward a rational classification of climate. *Geographic Review*, **38**, 55–94.

Viessman, W. Jr., J.W. Knapp, G.L. Lewis, and T.E. Harbaugh, 1977: Introduction to Hydrology, Harper and Row Publ., New York, 111–113.

Ward, R.C., 1967: *Principles of Hydrology.* McGraw-Hill Ltd., New York, 309–348.

Ward, R., 1978: *Floods: A Geographical Study.* Halsted Press, New York, 2–27.

Wetzel, K.L., and J.M. Bettandorff, 1986: Techniques for estimating streamflow characteristics in the eastern and interior coal provinces of the United States. *U.S. Geol. Water-Supply Paper 2276.*

Wilson, E.M., 1990: *Engineering Hydrology.* MacMillan Education Ltd., London, 23–170.

BIOGRAPHICAL SKETCH

Captain Russell A. K.tzman was born on June 11, 1960, in Ridgewood, New Jersey. He graduated from Sparta High School in 1978 and went on to attend Tulane University where he received a Bachelors of Science degree in engineering. In May of 1984, he was commissioned an officer in the United States Air Force. He worked for 18 months as a Wing Weather Officer at Little Rock Air Force Base, Arkansas. Subsequently transferred to Keesler Air Force Base, Mississippi, he flew as an Aerial Reconnaissance Weather Officer for the 53d Weather Reconnaissance Squadron. During this period, he penetrated forty-eight named typhoons and hurricanes. He later enrolled in the FSU meteorology program in January 1991 to begin his graduate studies.